NASA Contractor Report 3772

The Nonlinear Viscoelastic Response of Resin Matrix Composite Laminates

C. Hiel, A. H. Cardon, and H. F. Brinson

GRANT NCC2-71
JULY 1984

NASA

NASA Contractor Report 3772

The Nonlinear Viscoelastic Response of Resin Matrix Composite Laminates

C. Hiel, A. H. Cardon, and H. F. Brinson
Virginia Polytechnic Institute and State University
Blacksburg, Virginia

Prepared for
Ames Research Center
under Grant NCC2-71

National Aeronautics
and Space Administration

Scientific and Technical Information Branch

1984

ACKNOWLEDGEMENTS

The authors are indebted to the contributions of many individuals who have helped make this work possible. Special acknowledgement is appropriate for the financial support of the National Aeronautics and Space Administration through Grant NASA-NCC 2-71 and the authors are deeply grateful to Dr. H. G. Nelson of NASA-Ames for this support and for his many helpful discussions.

Financial support provided by The Free University of Brussels, VUB and the Belgian National Science Foundation (F.K.F.O.) is also greatly appreciated and hereby acknowledged.

The assistance of Andrea Bertolotti, Kiera Sword, David Fitzgerald and Catherine Brinson, together with the fast and excellent typing of Mrs. Peggy Epperly, proved to be invaluable throughout this work.

TABLE OF CONTENTS

Chapter 1

DISCUSSION OF SIGNIFICANCE AND SCOPE OF THE UNDERTAKEN STUDY

1.1 Introduction

Research and development in advanced composites technology and design procedures has advanced to a point where these materials can now meet the challenge of highly demanding aerospace, automobile and other structural applications. Performance payoffs in the form of weight savings, component integration and a five-fold maintenance reduction as compared to metal design have been demonstrated (Forsch [1]) and contribute to the overall picture of an attractive marketable product.

However, resin matrix composites have moduli and strength properties which are viscoelastic or time dependent. As a result there is a need for methods by which short term test results can be used to predict long term results.

The current effort is part of a continuing cooperative NASA-Ames - VPI&SU research program directed towards the development of an accelerated strength and stiffness characterization procedure which generates the design data and the confidence levels, needed to insure structural integrity for any projected lifetime. This process is greatly complicated by a number of environment exposure variables

such as temperature, moisture*, UV and space radiation, high vacuum and many others. An example of a typical thermal profile for an air carrier given by Ripley [2] is given in Fig. 1.1. Any attempt to handle such variables by overdesign will penalize the economical features mentioned above as a knockdown factor will seriously limit the full weight reduction potential of advanced composites.

1.2 Previous Efforts

An accelerated characterization, which is schematically given in Fig. 1.2, has been developed and documented by Brinson et al. [4-13]. A fair amount of experimental support has been accumulated, based on elements of linear viscoelasticity by Yeow [5]. Nonlinear viscoelasticity came into this picture when Griffith [7] potentially identified this behavior as the reason for a serious underprediction of creep rupture data for $[90/\pm60/90]_{2s}$ laminates. The prediction was based on a linear incremental lamination theory developed by Yeow [6]. As a result, a study of nonlinear viscoelastic characterization procedures was performed by Griffith [7] which led towards a valid graphical Time-Temperature-Stress Superposition (TTSSP) principle for the generation of modulus master curves.

Dillard [9] developed a non-linear viscoelastic incremental lamination theory and found reasonable correlation between his predictions and experiments. Because of the limited experimental data

---

*It has been shown that moisture pickup is generally reversible. When combined with thermal spikes, however, this phenomenon can create irreversible damage as shown by Adamson [3].

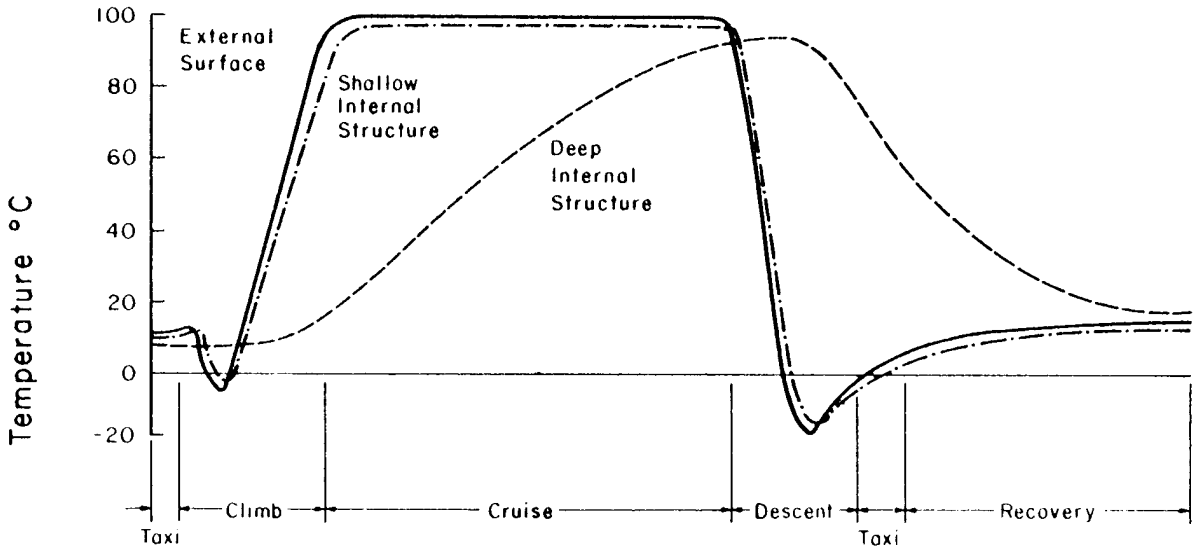

Fig. 1.1 Typical Thermal Profile for a Supersonic Air Carrier - Ripley [2], 1971.

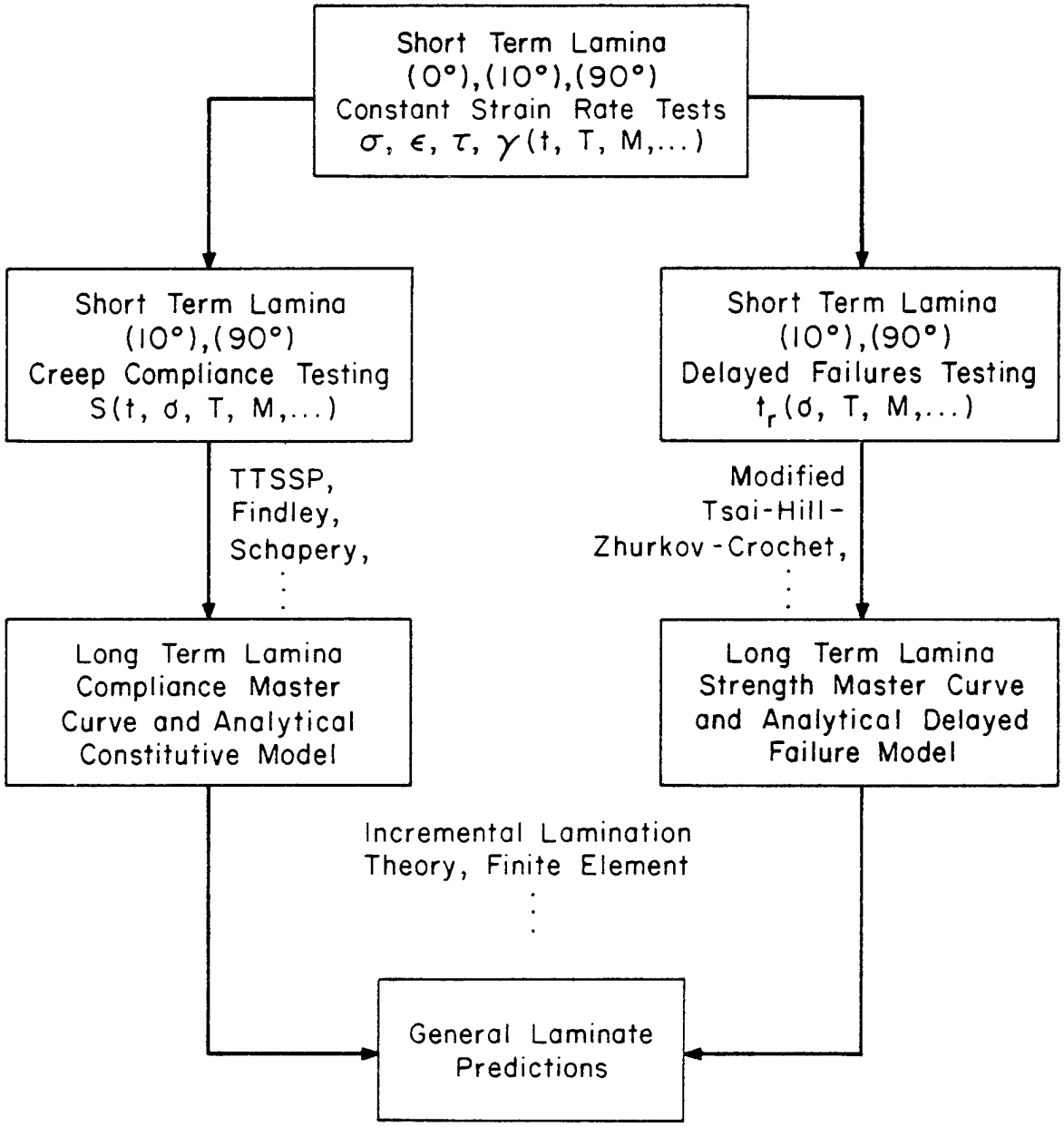

Fig. 1.2 Accelerated Characterization Method for Laminated Composite Materials.

available from the work of Griffith, Dillard used a semiempirical nonlinear viscoelastic model due to Findley to represent lamina compliances.

1.3 Objectives and Outline of the Present Study

The objective of the current study was to cast the graphical TTSSP method into an analytical form. It was believed that the analytical framework developed by Schapery in a series of publications could be adapted for this purpose. A literature review on nonlinear viscoelastic constitutive equations is given in Chapter 2, while the thermodynamic basis and the derivation of the Schapery model are the subjects of Chapter 3.

An effort to relate viscoelastic deformation and failure on an energy basis is developed in Chapter 4. This allows an immediate transfer of any modulus master curve into a strength master curve as depicted in Fig. 1.2.

Chapter 5 concentrates solely on 934 neat resin properties and on the discussion of obtained experimental results thereto.

Master curves for transverse and shear properties of T300/934 as obtained through the Schapery analysis are discussed in Chapter 6.

Results on creep rupture for $[90]_{8s}$ and $[60]_{8s}$ lamina, based on the energy criterion (Chapter 4), together with a comparison of an incremental lamination theory prediction with experimental results on $[90/\pm45/90]_{2s}$ are discussed in Chapter 7.

A general discussion and conclusions are given in Chapter 8.

Chapter 2

INELASTIC TIME-DEPENDENT MATERIAL BEHAVIOR

2.1 Introduction

The purpose of this chapter is to produce a brief literature overview on research in nonlinear viscoelasticity. The majority of publications explain how to deal with magnitude nonlinearities, i.e. they account for the stress dependence observed on creep compliance versus time as illustrated in Fig. 2.1.

A much smaller number of articles also account for intermode nonlinearity (nonlinear interaction between different components of the stress tensor) and almost invariably use a single mechanical invariant, namely the octahedral stress. In this respect it should be mentioned that data generated by Cole and Pipes [14] shown in Fig. 2.2 indicate the extent of stress interaction in off-axis unidirectional boron-epoxy coupons. These experimental results show that inelastic behavior is not a monotonic function of fiber orientation. Similar behavior has been observed for graphite-polyimide off-axis coupons by Pindera and Herakovich [15]. They indicate that the inclusion of residual thermal stresses and axial stress interaction at the micromechanics level are necessary in order to predict the correct trends in the shear response of off-axis specimens.

An almost never mentioned type of nonlinearity is interaction nonlinearity, i.e. nonlinear interaction between events (i.e. load application or release) occurring at different times.

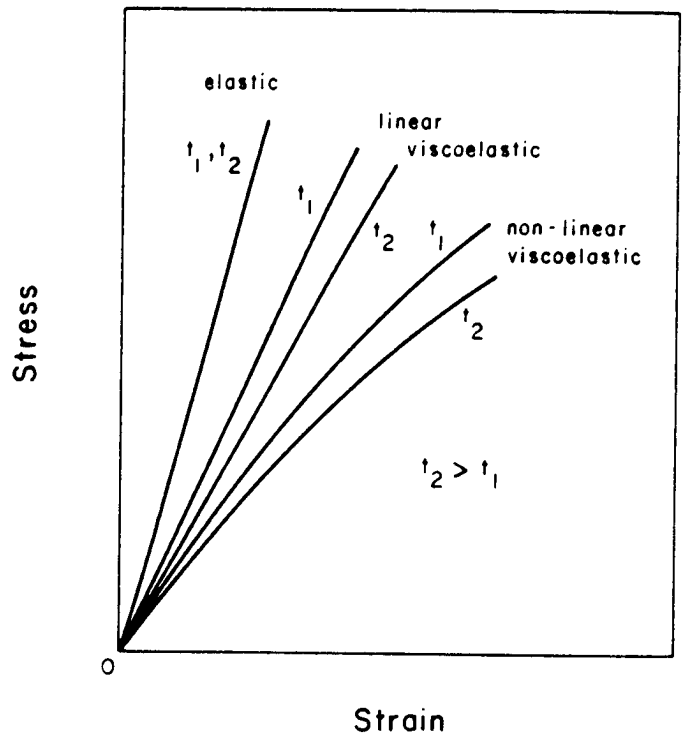

Fig. 2.1 Stress-Strain Behaviour of Elastic and Viscoelastic Materials after two Values of Elapsed Time, t.

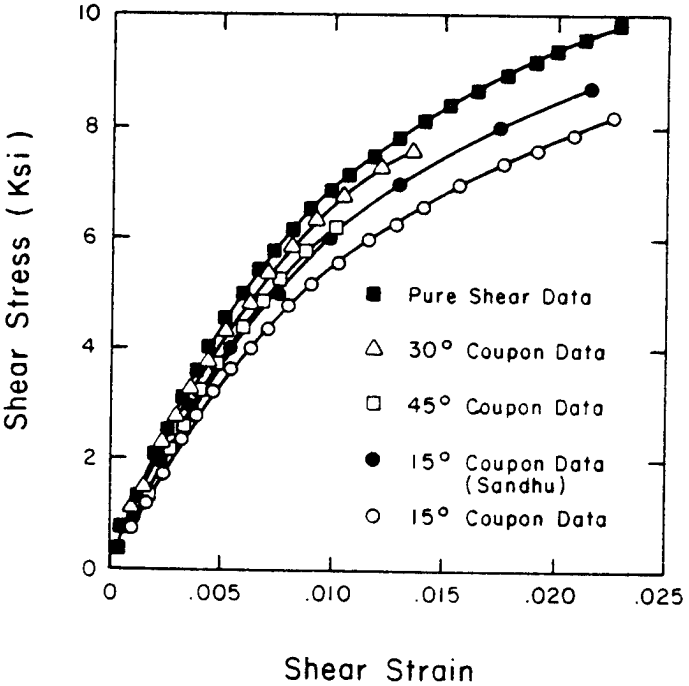

Fig. 2.2 Extent of Stress interaction in Off-axis Unidirectional Boron-epoxy Coupons - Cole and Pipes [14], 1974.

2.2 Representations of Constitutive Equations in Nonlinear Viscoelasticity

2.2.1 Multiple Integral Representations

The multiple integral representation is a very appealing theoretical concept, since it is not limited to a particular material or class of materials. The Volterra-Frechet expansion for a one-dimensional case is written as:

$$\epsilon = \int_{-\infty}^{t} D_1(t - \tau_1)d\sigma(\tau_1) + \int_{-\infty}^{t}\int_{-\infty}^{t} D_2(t - \tau_1, t - \tau_2)d\sigma(\tau_1)d\sigma(\tau_2) + \ldots \qquad (2.1)$$

The first integral of Eq. (2.1) describes the linear viscoelastic behavior, defined by the Boltzmann theory and the second and higher order integrals are representations of both magnitude nonlinearity and interaction nonlinearity, the latter implying an interaction effect between, e.g., the stress increments at times τ_1 and τ_2.

If a force is suddenly applied to a specimen, producing a constant stress σ, it follows from 2.1 that

$$\epsilon = D_1(t)\sigma + D_2(t,t)\sigma^2 + D_3(t,t,t)\sigma^3 + \ldots \qquad (2.2)$$

The functions $D_k(t,t,\ldots,t)$ can thus be determined from creep tests. The number of stress levels must be equal to the number of kernels J_k.

Gradowczyk [16] showed, however, that the system of linear equations which serves to determine the unknown functions is ill-conditioned and the procedure of finding the kernels D_k is unstable. Being unaware of Gradowczyk's work, this author attempted to use the

multiple integral representation for p.v.c. and had to give up the attempts due to the extreme instability of the results obtained [19].

The extension of the Volterra-Frechet expansion to the 3-dimensional case has been given by Green, Rivlin and co-workers [17]. Even if we limit their expression to triple integrals (small non-linearities) twelve kernels still must be determined by experiment.

An alternative of the Green-Rivlin approach has been formulated by Pipkin and Ropers [18] and is often referred to as nonlinear superposition theory (NLST) which can be written as

$$\epsilon(t) = \int_{-}^{t} D_1(t - \tau, \sigma(\tau))\dot{\sigma}(\tau)d\tau + \int_{-\infty}^{t}\int_{-\infty}^{t} D_2(t - \tau_1, \sigma(\tau_1), t - \tau_2, \sigma(\tau_2))\dot{\sigma}(\tau_1)\dot{\sigma}(\tau_2)d\tau_1\, d\tau_2 + \ldots \qquad (2.3)$$

It is clear that eq. 2.3 is nonlinear even on the first approximation. Thus, the additivity of incremental stress effects in the Boltzmann superposition sense is preserved.

Kinder and Sternstein [20] showed that difference in strains predicted by the two theories is in the transient portion if the material exhibits fading memory. Thus, in a single creep test, the equation 2.3 reduces to

$$\epsilon(t) = \int_{-\infty}^{t} D_1(t - \tau, \sigma(\tau))\dot{\sigma}(\tau)d\tau \qquad (2.4)$$

which is the most general representation of nonlinear creep provided the transient response from the step loadings has decayed. However, whether multiple loading and/or unloading programs require additional integrals to describe time interactions of the loading history remains

an open question.

2.2.2 Single Integral Representations

i) Modifications of the Boltzman Theory of Linear Heredity

Two schools of thought have been identified in the literature. The first one states that it is, in principle, possible to map a set of nonlinear isochronous stress-strain curves into a linear set, provided we nonlinearize the stress and strain measures as

$$\psi[\epsilon(t)] = \int_{-\infty}^{t} D(t - \tau) \frac{d}{d\tau} \nu[\sigma(\tau)]d\tau \tag{2.5}$$

Here the equation is linear but only in the nonlinear stress and strain measures ψ and ν. This form has been used by Koltunov [21]. A simplified form of Eq. 2.5 have been proposed by Leaderman [22]

$$\epsilon(t) = \int_{-\infty}^{t} D(t - \tau) \frac{d}{d\tau} \nu[\sigma(\tau)]d\tau \tag{2.6}$$

and by Rabotnov [23]

$$\nu[\epsilon(t)] = \int_{-\infty}^{t} D(t - \tau) \frac{d\sigma}{d\tau} d\tau \tag{2.7}$$

The second school allows for a stress or pressure-deformable time measure. Indeed, the pressure dependence of the mechanical response has been predicted theoretically on the basis of the free volume approach by Ferry and Stratton [24] who derived the pressure analog of the well-known WLF equation in the form:

$$\log a_p = \frac{(B/2.303\ f_o)(p - p_o)}{f_o/K_f - (p - p_o)} \tag{2.8}$$

where a_p is the ratio of the relaxation times at pressure p to the relaxation times at pressure p_o, B is a constant assumed to be of the order of unity, f_o is the fractional free volume at the reference pressure, and K_f is the isothermal compressibility of the free volume. Beuche [25] and O'Reilly [26] proposed the equation

$$\log a_p = C(p - p_o) \tag{2.9}$$

where C is a constant and other variables are as defined above.

Knauss and Emri [27] postulate a linear dependence of fractional free volume, on the instantaneous values of temperature, T; water concentration, C; and mechanical dilatation θ, i.e.

$$f = f_o + \alpha\Delta T + \gamma C + \delta\theta \tag{2.10}$$

where α is the coefficient of volume expansion, γ is the moisture coefficient of volume expansion and δ is the coefficient of mechanical volume expansion. By substitution of (2.10) in the Doolittle equation [28]

$$\log a = -\frac{B}{2.303}\left(\frac{1}{f} - \frac{1}{f_o}\right) \tag{2.11}$$

they obtain the following very general temperature, moisture and pressure dependent shift-factor

$$\log a = -\frac{B}{2.303\, f_o}\left[\frac{\alpha\Delta T + \gamma C + \delta\theta}{f_o + \alpha\Delta T + \gamma C + \delta\theta}\right] \tag{2.12}$$

Neither equation (2.8), (2.9) or (2.12) has so far been subject to extensive mechanical testing on solid polymers.

ii) Single Integral Representations Based on Thermodynamics

In order not to obscure the main issue of a literature review, we shall not attempt a full treatment of the thermodynamic foundations, but rather concentrate on the hierarchy of different continuum thermodynamic theories. This hierarchy, shown in Fig. 2.3, has been reviewed in a well-documented survey paper by K. Hutter [29]. Figure 2.3 shows that the main concepts which can be utilized to develop constitutive equations for inelastic materials are the rational thermodynamics approach and the state variable approach (also called irreversible thermodynamics). The latter will be discussed in detail in Chapter 3. Coleman and Noll [30] applied functional analysis to continuum mechanics in order to express current stress, free energy and entropy as functionals of the thermokinematic history. Their analysis continues to influence rational thermodynamics research up to this date.

The state variable approach includes certain internal variables in order to represent the internal state of the material. Constitutive equations which describe the evolution of the internal state are included as part of the theory. Onsager [31] published the concept of internal variables in thermodynamics. This formalism was used by Biot [32] in the derivation of constitutive equations of linear viscoelasticity. Ziegler [33] extended this work to include nonlinear viscoelastic materials and his approach has been used by Schapery [34] and Valanis [35] to develop specific theories. The extension to include viscoplastic materials was made by Perzyna [36].

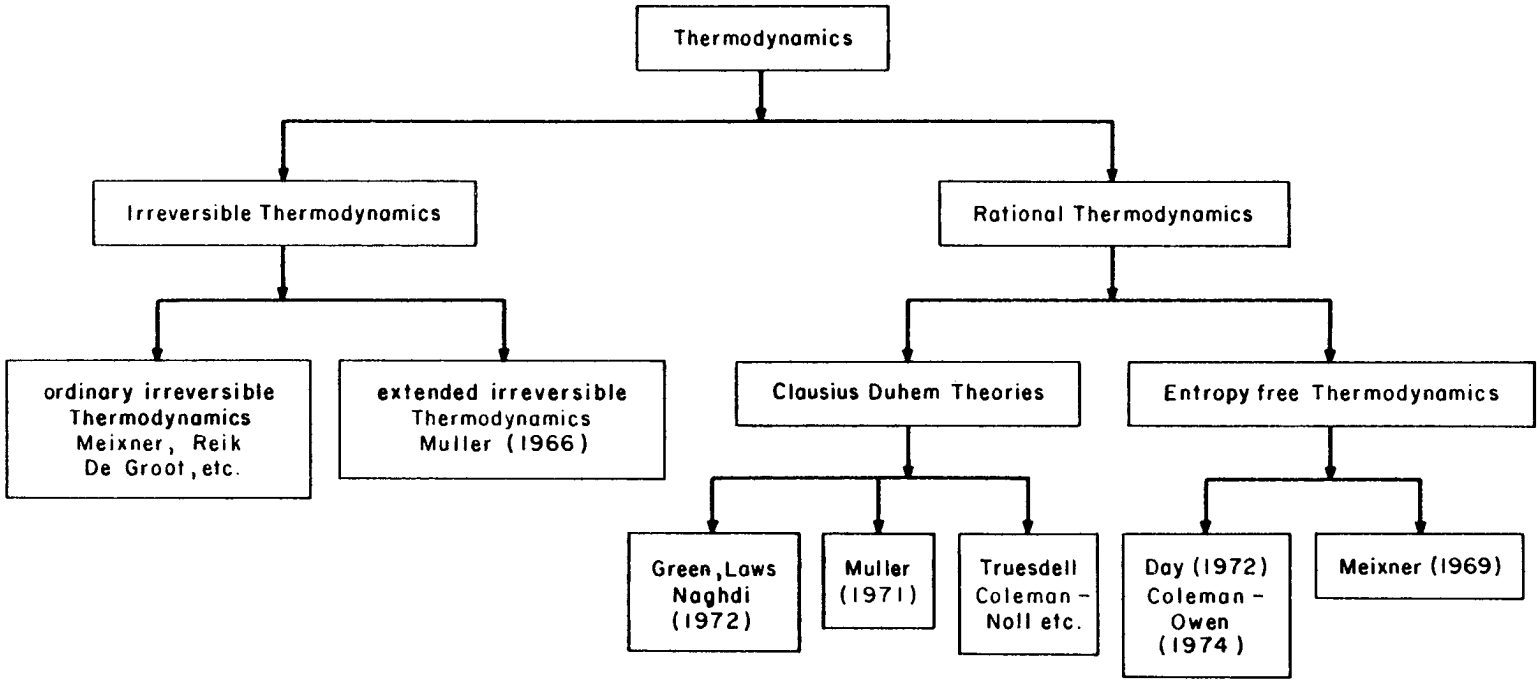

Fig. 2.3 Hierarchy of Different Theories of Continuum Thermodynamics - Hutter [29] 1977.

2.2.3 Mechanical (Rheological) Models

Elastic behavior is compared to that of a massless Hookean spring and the viscous behavior to that of a Newtonian dashpot. The successful description of the stress strain behavior depends on the proper choice and arrangement of the elements or hypothetical rheological units. The final hardware-system that describes the behavior of a material system in the linear range can, at least in principle, be extended into the nonlinear range by the introduction of nonlinear springs and dashpots. An example is the nonlinearized generalized Kelvin element whose mathematical equation for creep can be written as,

$$\varepsilon = \frac{\sigma}{E_o} f_1(\sigma) + \frac{f_2(\sigma)}{\eta} \cdot t + f_3(\sigma) \sum_{i=1}^{N} \frac{1}{E_i} (1 - \exp(-t/\tau_i)) \quad (2.13)$$

where $f_i(\sigma)$ is a nonlinearizing function of stress. Bach [37] used this form in his studies on wood. He separated the total creep strain into instantaneous, delayed-elastic and flow components. The instantaneous or glassy response was always independent of stress (thus $f_1(\sigma) = 1$), but the delayed elastic and flow compliances were independent of stress only within certain limits of stress, depending on moisture content and temperature.

We will show (Chapter 3) that Schapery's thermodynamic model, at least under certain circumstances, can be related to a spring-dashpot-hardware system.

2.2.4 Power Laws

It can be shown that the use of discrete spring-dashpot models will allow us to obtain an accurate representation of viscoelastic phenomena over a large time scale provided we use a sufficient number of elements—typically one per decade.

The idea behind the power law representation is to sacrifice accuracy at any one time in order to obtain a reasonable representation over the complete time scale between glassy (short term) behavior and rubbery (long time) behavior. This is often called broad-band approximation. Landel and Fedors [38] gave a form for spectral representation $H(\tau)$ guided by their understanding of polymer mechanics which may be written as,

$$H(\tau) = C \left(\frac{\tau_o}{\tau}\right)^n \exp\left(-\tau_o/\tau\right) \tag{2.14}$$

Clauser and Knauss [39] gave examples of this approximation of $H(\tau)$ which are shown in Fig. 2.4. These results lead to the following broad-band approximation for the relaxation modulus:

$$E_r(t) = E_e + \frac{E_g - E_e}{\left(1 + \frac{\tau_o}{t}\right)^n} \tag{2.15}$$

The representation is seen to possess four arbitrary constants, including the limiting moduli values. The exponent n gives the slope of the relaxation curve (Fig. 2.5) through the transition region between glassy and rubbery behavior and τ_o, for isothermal conditions, fixes the characteristic relaxation time.

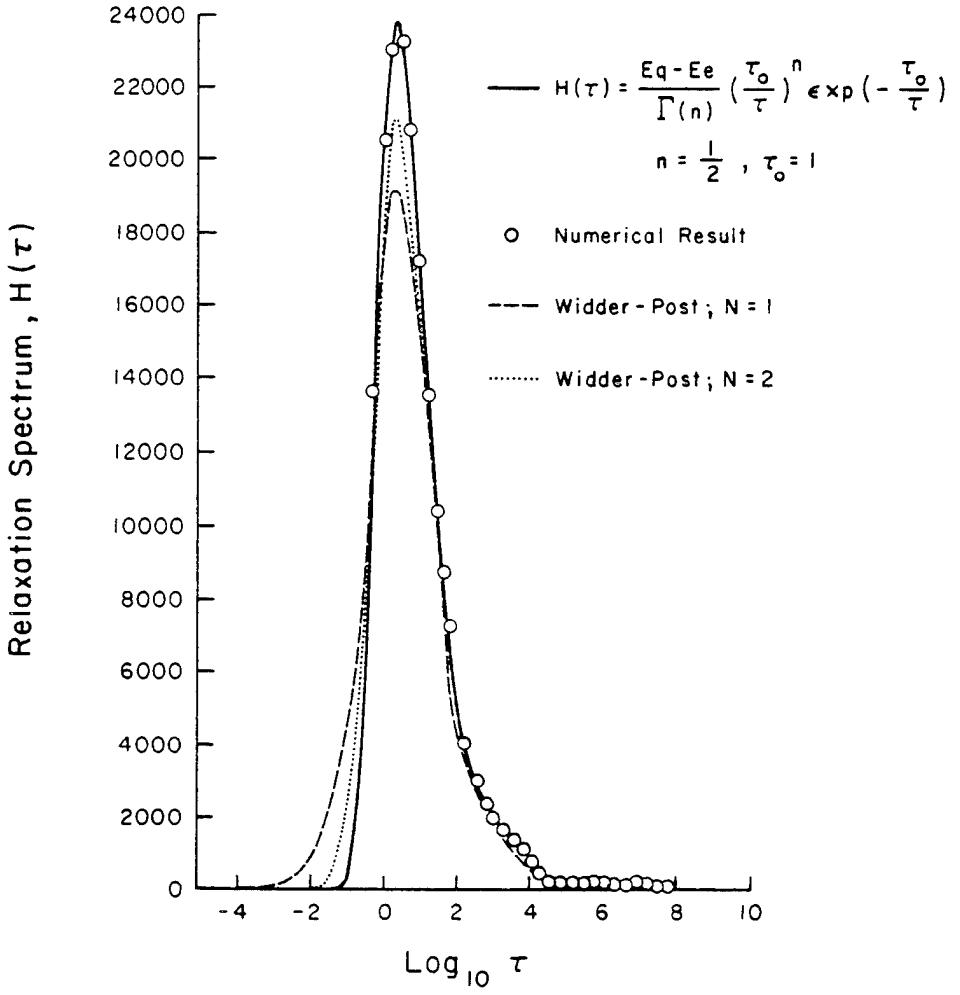

Fig. 2.4 Power Law Approximation for the Relaxation Spectrum H(t) - Clauser and Knauss [39], 1969.

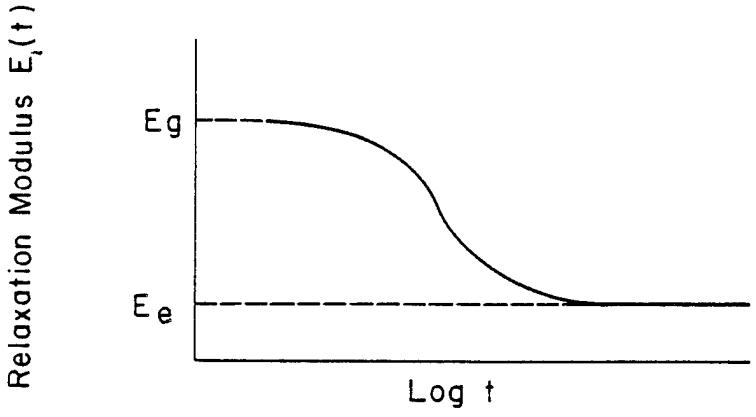

Fig. 2.5 Relaxation Modulus E(t) vs Log Time

Recognizing that relaxation and retardation are basically reciprocal, one could also postulate a modified power law for the compliance spectrum, $L(\tau)$, as

$$L(\tau) = C' \left(\frac{\tau}{\tau_o'}\right)^{n'} \exp(-\tau/\tau_o) \tag{2.16}$$

However, the integration for the creep compliance does not give a simple form and it is more direct to assume a reasonable expression as

$$D_C(t) = D_g + \frac{D_e - D_g}{\left(1 + \frac{\tau_o'}{t}\right)^n} \tag{2.17}$$

where n may be the same exponent as in the relaxation modulus and τ_o' is chosen for the best fit of the data. A special case results when $t \ll \tau_o'$ and $C = D_e - D_g$,

$$D_C(t) \simeq D_g + C \left(\frac{t}{\tau_o'}\right)^n \tag{2.18}$$

A slightly modified form can be written as

$$D_C(t) \simeq D_g + C^* \left(\frac{t}{1}\right)^n \tag{2.19}$$

where $\tau_o' = A\ U$, $C^* = C/A^n$, A is a dimensionless multiplication factor, and U = 1 is a time unit selected to accommodate data reduction (i.e. 1 sec, 1 min, 1 hr, etc.). The power law in this form (Eq. 2.19) is often called the "Findley power law" and has been found to give an accurate representation of creep behavior of an extremely broad range of amorphous, crystaline, crosslinked glass and carbon-fiber reinforced plastics and laminates. The equation has been verified mostly in

tensile tests, but in a few cases it has successfully described behavior in compression and under combined tensile and shear stresses as well.

Upon conducting a screening experiment on 934 neat resin (at room temperature), we identified the exponent, n, in Eq. 2.19 as the most sensitive indicator of experimental errors. In addition, n was shown to be dependent on the duration of the creep test as shown in Fig. 2.6. Thus any short time creep test will result in an underestimation of n or in other words a stable evaluation of n is impossible as long as the flow term (C^*t^n) is too small relative to the initial compliance D_o. The problem is easily handled, by performing a small additional experiment, which consists of recording the recovery strain after unloading. Creep recovery is mathematically given by

$$\epsilon_r = \Delta\epsilon[(1 + \lambda)^n - (\lambda)^n] \tag{2.20}$$

where $\lambda = \frac{t - t_1}{t_1}$, $\Delta\epsilon = \sigma \cdot C^* t_1^n$, and t_1 is the time at unloading. Eq. 2.20 can be very easily derived using the power law for creep together with the superposition principle. Fig. 2.7 shows that the n value obtained from recovery data is nearly insensitive to the duration of the recovery experiment.

The creep experiment was repeated on T300/934 carbon epoxy with the load perpendicular to the fiber direction. The result plotted in Fig. 2.6 is compared with the result obtained on the neat 934 resin (Fig. 2.8) and shows that the composite n-value comes within 5% of the resin value after 3000 min.

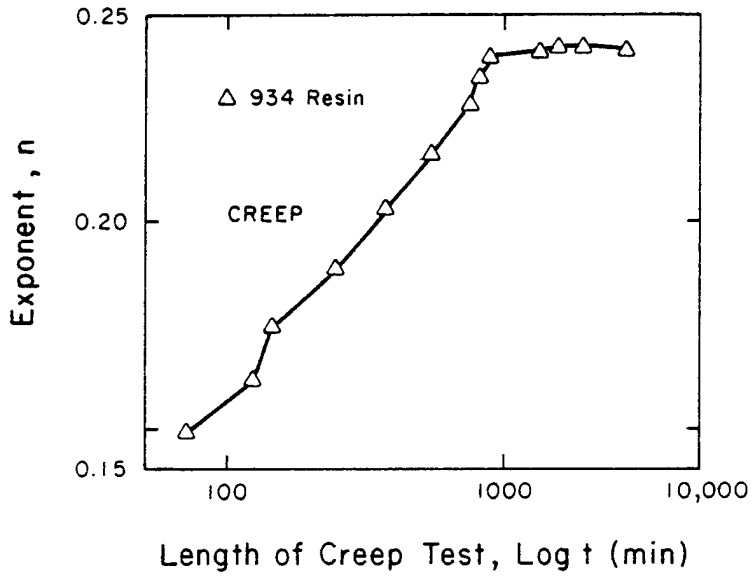

Fig. 2.6 The Variation of Power Law Exponent with Length of Creep Test.

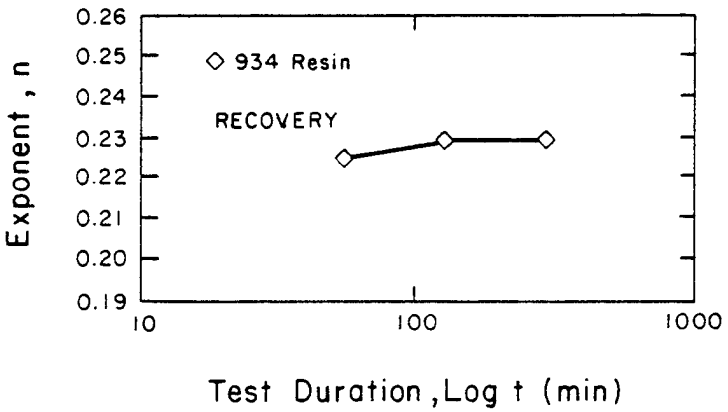

Fig. 2.7 The variation of Power Law Exponent with Length of Recovery Test.

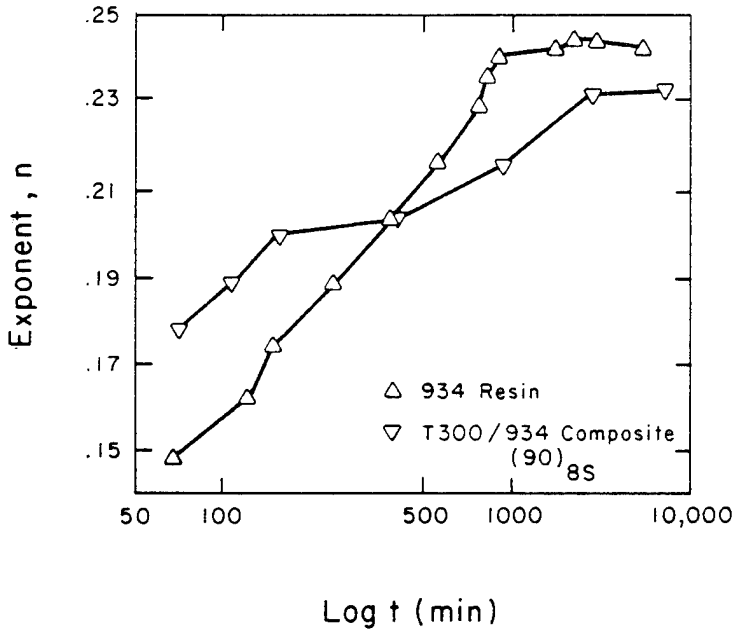

Fig. 2.8 Comparison of Power Law Exponent Variation with Length of Creep Test.

An alternative power-law type approach was developed by the Russian school, mainly under the influence of the ideas published by Yu. N. Rabotnov [23]. His formulation was based on the viscoelastic deformation of polymeric materials which can be described by an integral equation of the Boltzmann-Volterra type

$$\epsilon(t) = \frac{1}{E}\left[\sigma(t) + \int_0^t K(t - s)\sigma(s)ds\right] \tag{2.21}$$

where $\sigma(t)$ and $\epsilon(t)$ are the stresses and strains in a uniaxial stress field, E is the instantaneous Young's modulus, and K(t) is the transient compliance or kernel function. Young's modulus can be determined by the basic quasistatic measurements, while the kernel must include the smallest possible number of parameters that need to be determined experimentally. To satisfy the last condition, Rabotnov approximated the strain, $\epsilon(t)$, with a power law and proceeded to deduce the kernel function K(t) which can be written as,

$$K(t) = \lambda t^{\alpha} \sum_{n=0}^{\infty} \frac{\beta^n t^{n(1+\alpha)}}{\Gamma[(n+1)(1+\alpha)]} \tag{2.22}$$

In (2.22), λ, β and α are material parameters, $\Gamma[(n+1)(1+\alpha)]$ is the gamma function of the argument $(n+1)(1+\alpha)$, where $1 + \alpha > 0$. The kernel parameters can be determined graphically (when a full deformation curve is obtained) as well as numerically [19].

Functions of the type 2.22 are classified as exponential functions of fractional order. They behave as an Abel-type singularity for instantaneous loading and like an exponential for the succeeding period of time. A fairly detailed algebra for these operators has been

developed by Rabotnov and his collaborators.

Equation (2.21) can be modified for the case of creep where $\sigma(t)$ is constant and becomes,

$$\epsilon(t) = \frac{\sigma_o}{E} \left[1 + \int_o^t K(s)ds\right] \tag{2.23}$$

For small t, the first term in (2.22) dominates, i.e.,

$$K(t) = \frac{\lambda t^{\alpha}}{\Gamma(1+\alpha)} \tag{2.24}$$

By substituting (2.24) into (2.23), we obtain:

$$\epsilon(t) = \frac{\sigma_o}{E} \left[1 + \frac{\lambda}{\Gamma(2+\alpha)} t^{1+\alpha}\right] \tag{2.25}$$

This again reduces to the Findley equation (2.19)

$$D(t) = D_o + C^* t^n$$

where $C^* = \frac{\lambda}{\Gamma(1+n)}$ and $n = 1 + \alpha$. It is clear again that Eq. 2.19 is only able to describe a limited portion of the full deformation curve.

Chapter 3

SINGLE INTEGRAL REPRESENTATIONS BASED ON IRREVERSIBLE THERMODYNAMICS

3.1 Introduction

A single integral nonlinear viscoelastic constitutive equation has been developed by Schapery in a series of publications [34,40-44]. This chapter reviews his thermodynamic development with a special view to developing a better understanding of the nature of the four nonlinearizing parameters which appear as well as their physical origin.

The name irreversible thermodynamics is well established but confusing, since it suggests geometric irreversibility. This is not generally true because thermodynamic irreversibility relates to entropy production while a deformation accompanied by a change in entropy can be geometrically reversible as for example in rubber elasticity. Thus a name like "process thermodynamics" or non-equilibrium thermodynamics would be more related to the physics of a problem like viscoelastic deformation.

The consistency of constitutive equations with the fundamental theorems of thermodynamics has been discussed by Truesdell and Toupin [45]. No restriction on constitutive equations is given by the first and the third fundamental theorems. The second excludes processes with negative entropy production and thus limits the field of constitutive equations, but not to the extent desired. It was demonstrated by Biot [46] that the more precise statements about the nature of the second law, which were made by Onsager [47], are sufficient to treat

problems in linear viscoelasticity.

3.2 Gibbs Free Energy Formulation of the Schapery Equations

This formulation is particularly useful, since it allows the treatment of temperature and stress tensor components as independent variables. The Gibbs free energy g is defined as

$$g = u - Ts - \frac{1}{\rho} Q_m q_m \tag{3.1}$$

where u is the specific internal energy, T the absolute temperature, s the specific entropy, ρ the density, q_m (m = 1,2,...,k) a set of k state variables consisting of observed variables (strains), and Q_m (m = 1,2,...,k) is a set of k generalized forces defined by the virtual work condition $S_W = Q_i \delta q_i$. Eq. (3.1) shows that free energy can be accumulated by increasing internal energy by decreasing entropy or through a potential energy loss of the external loading.

A mathematical expression for the strength of the entropy source as a result of "irreversibility" has to be derived first. We assume that the classical concept of entropy is extendable into non-equilibrium situations. This leads to the following result which is called the fundamental equation of the system

$$s_I = s_I(u,q_i) \qquad (i = 1,2,...,n) \tag{3.2}$$

The index I, identifies the system under study. The state variables q_i (i = k+1,...,n) represent internal degrees of freedom.* These will allow us to describe micro-structural rearrangements related to

---

*The number n of independent thermodynamic variables depends on the nature of the system.

straightening and relative sliding of long chain molecules. These variables are thus eventually observable, but certainly not controllable. For this reason Q_i $(i = k+1,\ldots,n) = 0$ since any force associated with an internal degree of freedom would provide us with a means to control this internal coordinate. The entropy-increment ds_I created by a change in du and n variations of dq_i is measured by the total derivative of the fundamental equation, i.e.

$$ds_I = \left(\frac{\partial s_I}{\partial u}\right)_{q_i} du + \sum_{i=1}^{n} \left(\frac{\partial s_I}{\partial q_i}\right)_{u,q_i'} dq_i \tag{3.3}$$

where q_i' means all coordinates are held constant except q_i. The increment du is controlled by the first law of thermodynamics through

$$du = dh + \sum_{i=1}^{k} \rho^{-1} Q_i \, dq_i \tag{3.4}$$

Thus according to (3.4) any increment in internal energy is produced by an infinitesimal amount of heat (dh) crossing the boundary and/or an infinitesimal amount of mechanical work $\rho^{-1} Q_i \, dq_i$ done on the system.

The incremental process is reversible, when $dq_i = 0$. Then, $du = dh$ and according to the second law,

$$dh = T ds_I \tag{3.5}$$

By substituting (3.5) into (3.3), we obtain

$$\left(\frac{\partial s_I}{\partial u}\right)_{q_i} = \frac{1}{T} \tag{3.6}$$

In other words, the temperature measures the sensitivity of the internal energy for entropy changes. Thus (3.3), written now under

the restrictions of a reversible process becomes

$$Tds_I = du + T \sum_{i=1}^{n} \left(\frac{\partial s_I}{\partial q_i}\right)_{u,q_i'} dq_i \tag{3.7}$$

Since the partial derivative in the second term is an operation on a state function s_I, it defines a state function Q_i^R,

$$-\rho^{-1} Q_i^R = \frac{\partial s_I}{\partial q_i} \tag{3.8}$$

Thus

$$du = Tds_I + \sum_{i=1}^{n} \rho^{-1} Q_i^R dq_i \tag{3.9}$$

Eq. (3.9) is a result known in classical thermodynamics as Gibbs equation and describes the associated reversible process, that causes the same increment of internal energy du as the irreversible process described by Eq. (3.4).

By elimination of du between (3.9) and (3.4), we obtain

$$Tds_I = dh + \sum_{i=1}^{n} \rho^{-1} (Q_i - Q_i^R) dq_i \tag{3.10}$$

with $Q_i(k+1,\ldots,n) = 0$.

Thus the entropy of a mass element changes with time for two reasons. First, because entropy flows into the volume element occupied by this mass element, second because there is an entropy source due to irreversible phenomena inside the volume element. This entropy source is always a non-negative quantity.

Since the computational procedure needed for the derivation works only on isolated systems, we now create such a system by the artifice

of adjoining a large heat reservoir II to the physical system I. Eq. (3.11) states that the entropy is an extensive property, i.e. the entropy of the system is the sum of the entropies of the subsystems

$$ds_{I+II} = ds_I + ds_{II} \tag{3.11}$$

and

$$ds_{II} = -\frac{dh}{T} \tag{3.12}$$

Eq. (3.12) states that the reservoir plays the role of a reversible heat source, i.e. heat can be extracted from it without a change in its temperature T. A combination of (3.12), (3.11), and (3.10) leads to

$$\dot{s}_{I+II} = \frac{1}{\rho T} \sum_{i=1}^{n} X_i \dot{q}_i \tag{3.13}$$

with $X_i = Q_i - Q_i^R$. It turns out that the strength of the entropy source, $\dot{s}_{I+II}$ has a very simple appearance. It is a sum of n terms, each being a product of a flux characterizing an irreversible process and a quantity, called thermodynamic force.

In order to proceed from here we need to calculate the rate of approach to equilibrium. This is only possible by arguments outside the scope of continuum mechanics. The entropy source is explicitly related to the various irreversible processes that occur in the system through a linear phenomenological relation between forces X_i and fluxes $\dot{q}_i$ called Onsager's theorem,

$$X_i = \sum_{j=1}^{n} b_{ij}(Q_m,T)\dot{q}_j \tag{3.14}$$

This fundamental theorem states that when the flow $\dot{q}_j$, corresponding

to the irreversible process j, is influenced by the force X_i, corresponding to the irreversible process i, then flow $\dot{q}_i$ is then also influenced by the force X_j through the same influence coefficients, $b_{ij}(Q_m,T)$. Eq. (3.14) can be rewritten as

$$Q_i = Q_i^R + b_{ij}(Q_m,T)\dot{q}_j \tag{3.15}$$

It is shown in Appendix B that:

$$Q_i^R = \rho \frac{\partial g}{\partial q_i} \qquad i = k+1,\ldots,n$$

The generalized force Q_i^R associated with q_i through the Gibbs equation (3.9), is derivable from the Gibbs free energy g (Q_m, q_r, T)

$$q_m = - \rho \frac{\partial g}{\partial Q_m} \qquad m = 1,2,\ldots,k$$

The problem is thus reduced to the solution of two systems of equations,

$$q_m = - \rho \frac{\partial g}{\partial Q_m} \qquad m = 1,2,\ldots,k \tag{3.16a}$$

$$\rho \frac{\partial g}{\partial q_r} + b_{rs}(Q_m,T)\dot{q}_s = 0 \qquad r,s = k+1,\ldots,n \tag{3.16b}$$

A constitutive assumption on the dependence of the Gibbs free energy on Q_m, q_r and T has to be made. This is accomplished by a Taylor series expansion around the equilibrium state such that,

$$\rho g = c_R + c_m Q_m + c_r q_r + \frac{1}{2} d_{mn} Q_m Q_n + d_{rm} Q_m q_r + \frac{1}{2} d_{rs} q_r q_s \tag{3.17}$$

where c_R, c_i and d_{ij} may depend on temperature, but not on q_r and Q_m. Note that there exists a distinct relation between summation index

and physical dimension for these coefficients, i.e.

Coefficient	Represents	Summation Range
c_R	Energy	
c_m	Mechanical strain	$m = 1,2,\ldots,k$
c_r	Thermodynamic force	$r = k+1,\ldots,n$
d_{mn}	Mechanical compliance	$n,m = 1,2,\ldots,k$
d_{rm}	Transforms hidden variables g_r into mechanical strain units	$r = k+1,\ldots,n$; $m = 1,2,\ldots,k$
d_{rs}	Thermodynamic modulus	$r,s = k+1,\ldots,n$

A further approximation of the free energy is found by an expansion with respect to the uncontrollable variables q_i only, i.e. we can be far away from equilibrium with respect to Q_m.

$$\rho g = \rho g_R + c'_r\, q_r + \frac{1}{2}\, d'_{rs}\, q_r\, q_s \tag{3.18}$$

g_R, c'_r and d'_{rs} can be functions of the independent variables Q_m and T. Eq. (3.18) must reduce to (3.17) under sufficiently small forces, which leads to the relations

$$\rho g_R = c_R + c_m\, Q_m + \frac{1}{2}\, d_{mn}\, Q_m\, Q_n \tag{3.19}$$

$$c'_r = c_r + d_{rm}\, Q_m \tag{3.20}$$

$$d'_{rs} = d_{rs} \tag{3.21}$$

The various terms in equation (3.18) have the following physical significance;

- ρg_r An energy term that acts as a potential for the time independent response. The dependence of c_m and d_{mn} on stress and temperature can be lumped together with c_R into a single nonlinearizing parameter.
- $c'_r q_r = (c_r + d_{rm} Q_m)q_r = \beta_r \theta q_r + d_{rm} Q_m q_r$ This term is defined by the energy associated with a simultaneous action on the internal coordinates q_r and the controllable variables Q_m and θ.
- $\frac{1}{2} d'_{rs} q_r q_s$ This term is defined by the interaction energy associated with the simultaneous action on internal coordinates q_r and q_s.

The above items which make up equation (3.18) are of particular interest as they define the basic interaction mechanisms involved in three different nonlinearizing functions which appear in Schapery's final single integral equation as developed subsequently.

Substitution of (3.18) into (3.16b) gives

$$c'_r + d'_{rs}(Q_m,T)q_s + b_{rs}(Q_m,T) \frac{dq_s}{dt} = 0 \tag{3.22}$$

In order to reduce (3.22) to a system of n-k differential equations with constant coefficients, the further assumption is made that,

$$b_{rs}(Q_m,T) = a_D(Q_m,T)b_{rs} \tag{3.23}$$

in which b_{rs} are now defined as viscosities. This equation implies that the flow is Newtonian but with stress and temperature dependent viscosity. The implicit stress and temperature dependence can be made explicit through a shift function $a_D(Q_m,T)$. A lot of experimental

evidence exists for the special case where all viscosities have a common shift factor independent of stress. In such cases a_D becomes the familiar $a_T(T)$ shift factor found in polymer literature [28].

The following form for d'_{rs} is guided by (3.23),

$$d'_{rs}(Q_m,T) = a_G(Q_m,T)d^R_{rs} \qquad r,s = k+1,\ldots,n \tag{3.24}$$

where the constant symmetric "thermodynamic" modulus, d^R_{rs}, is now defined at the reference temperature T_R and $Q_m = 0$ as indicated schematically in Fig. 3.1 and $a_G(Q_m,T)$ is a shift function as defined below.

$$d'^R_{rs} = d'_{rs}(0,T_R) = d_{rs}(T_R) \tag{3.25}$$

It follows from Eq. (3.13), (3.14) and (3.23) that a_D nonlinearizes the entropy production,

$$\dot{s}_{I+II} = \frac{1}{\rho T} a_D(Q_m,T)\ b_{ij}\ \dot{q}_i\ \dot{q}_j \tag{3.26}$$

On the other hand a_G nonlinearizes the third term in the Gibbs free energy expansion (3.18) and therefore ρg is proportional to the above quantities as indicated by,

$$\rho g \sim \frac{1}{2} a_G(Q_m,T)\ d^R_{rs}\ q_r\ q_s \tag{3.27}$$

We cannot make an a-priori statement on the dependence of a_G with stress, but the dependence of $d'_{rs}(Q_m)$ at a certain temperature T can increase, decrease, or be independent of the force Q_m (Fig. 3.2).

A constitutive assumption on a_G has been developed by Schapery [48] for the case where microcracking and flaw growth (in the opening mode) are the dominant softening (damage) mechanisms. The reciprocal, $1/a_G$, is an increasing function of the q-th order Lebesque norm of tensile stress, ϕ', as specified by,

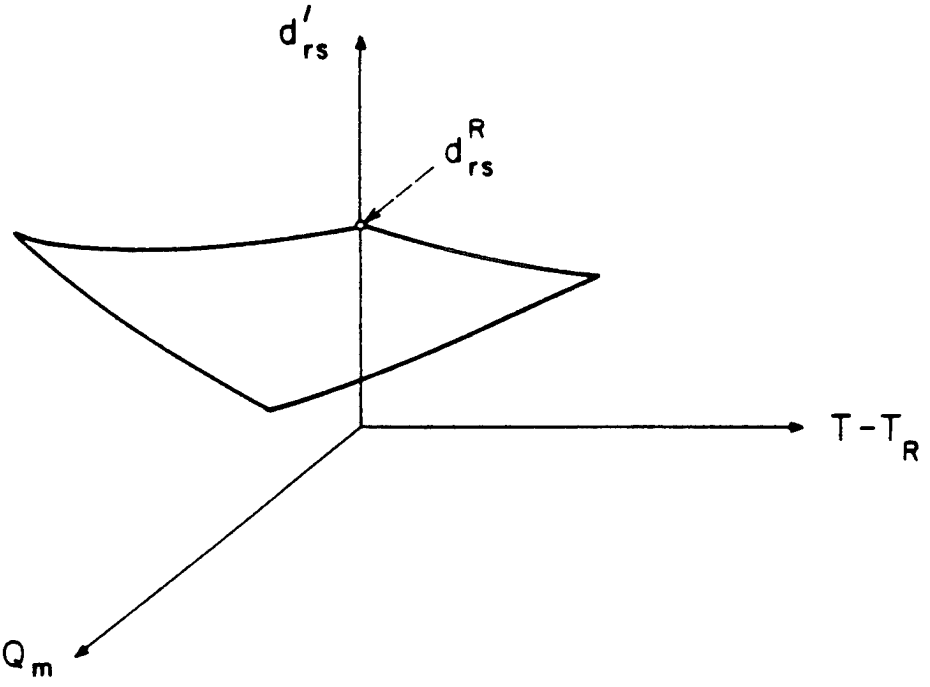

Fig. 3.1 Schematic Definition of "Thermodynamic Modulus".

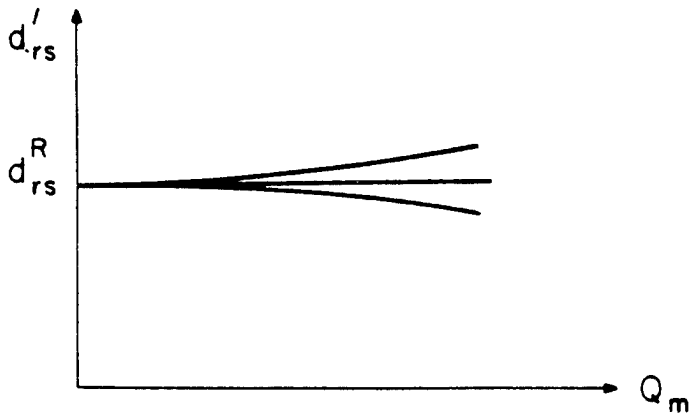

Fig. 3.2 Dependence of Thermodynamic Modulus, d'_{rs}, with the Generalized Force, Qm.

$$\frac{1}{a_G} = 1 + \int_{\phi'}^{\infty} G(\phi)\, d\phi \tag{3.28}$$

where,

$$\phi' = \left(\int_0^{\xi} \sigma^q \, d\xi \right)^{\frac{1}{q}} \tag{3.29}$$

$G(\phi)$ is positive and reflects the statistical distribution of damage. The quantity, $\int_{\phi'}^{\infty} G(\phi)d\phi$, can be found from mechanical property tests wherein q is a positive constant.

Extensions of Eq. (3.29) have been made for multiaxial stress conditions through incorporation of the first and second invariants of the stress tensor (θ and J_2), while aging and/or rehealing is introduced through a function M(t) such that,

$$\phi' = \left\{ \int_0^{\xi} M^{\frac{1}{n}} \left[A_1 \theta + A_2 \sqrt{J_2} \right]^q d\xi \right\}^{\frac{1}{q}} \tag{3.30}$$

Here, A_1 and A_2 are constants which satisfy the relation $A_2 = \sqrt{\frac{3}{2}}\,(1 - A_1)$ and when they are both positive there is a suppression of crack growth by ($\theta < 0$).

Due to the simplifications introduced in (3.23) and (3.24), a system of n-k differential equations with constant coefficients solvable for $q_{k+1},\ldots,q_n$ now remains. These together with the k algebraic equations obtained by substituting the free energy expression (Eq. 3.18) into the k equations of (3.16a) are,

$$a_G\, d^R_{rs}\, q_s + a_D\, b_{rs} \frac{dq_s}{dt} = - c'_r \qquad \text{(n-k equations)} \tag{3.31}$$

$$q_m = - \rho \frac{\partial g_R}{\partial Q_m} - \frac{\partial c'_r}{Q_m} q_r \qquad \text{(k-equations)} \tag{3.32}$$

The former equations (3.32) can be rewritten with the reduced time ψ as,

$$d^R_{rs}\, q_s + b_{rs} \frac{dq_s}{d\psi} = \frac{-\, c'_r}{a_G} \tag{3.33}$$

where,

$$d\psi = dt/a_\sigma \qquad \text{and} \qquad a_\sigma = a_D \mid a_G$$

The final system of equations can be explicitly written as,

$$\left[\begin{array}{cccc|cccc}
-\frac{\partial c'_{k+1}}{\partial Q_1} & -\frac{\partial c'_{k+2}}{\partial Q_1} & \cdots & -\frac{\partial c'_n}{\partial Q_1} & 0 & 0 & \cdots & 0 \\
-\frac{\partial c'_{k+1}}{\partial Q_2} & -\frac{\partial c'_{k+2}}{\partial Q_2} & \cdots & -\frac{\partial c'_n}{\partial Q_2} & 0 & 0 & \cdots & 0 \\
\cdots & \cdots & \cdots & \cdots & \cdots & \cdots & \cdots & \cdots \\
\frac{\partial c'_{k+1}}{\partial Q_k} & -\frac{\partial c'_{k+2}}{\partial Q_k} & \cdots & -\frac{\partial c'_n}{\partial Q_k} & 0 & 0 & \cdots & 0 \\
\hline
d^R_{k+1,k+1} & d^R_{k+1,k+2} & \cdots & d^R_{k+1,n} & b_{k+1,k+1} & b_{k+1,k+2} & \cdots & b_{k+1,n} \\
d^R_{k+2,k+1} & d^R_{k+2,k+2} & \cdots & d^R_{k+2,n} & b_{k+2,k+1} & b_{k+2,k+2} & \cdots & b_{k+2,n} \\
\cdots & \cdots & \cdots & \cdots & \cdots & \cdots & \cdots & \cdots \\
d^R_{n,k+1} & d^R_{n,k+2} & \cdots & d^R_{n,n} & b_{n,k+1} & b_{n,k+2} & & b_{n,n}
\end{array}\right]
\left[\begin{array}{c} q_{k+1} \\ q_{k+2} \\ \vdots \\ q_n \\ \hline \frac{dq_{k+1}}{d\psi} \\ \frac{dq_{k+2}}{d\psi} \\ \vdots \\ \frac{dq_n}{d\psi} \end{array}\right]
=
\left[\begin{array}{c} q_1 \\ q_2 \\ \vdots \\ q_k \\ \hline -\, c'_{k+1} \\ -\, c'_{k+2} \\ \vdots \\ -\, c'_n \end{array}\right]
+
\left[\begin{array}{c} \rho \frac{\partial g_R}{\partial Q_1} \\ \rho \frac{\partial g_R}{\partial Q_2} \\ \vdots \\ \rho \frac{\partial g_R}{\partial Q_k} \\ \hline 0 \\ 0 \\ \vdots \\ 0 \end{array}\right] \tag{3.34}$$

Remark that the matrix partition on the upper left hand corner side has a maximum dimension of 6 x (n-6) while the two lower partitions are square matrices with dimensions (n-6) x (n-6) where n can be very large, since this is the number of internal coordinates, needed for an adequate description of the inelastic material phenomena.

It can be proven that a simultaneous diagonalization of d^R_{rs} and b_{rs} is always possible, which means physically that a transformed space exists where the n-k internal deformation modes do not interact. Thus,

$$b_{rs} = \begin{Bmatrix} b_r \\ 0 \end{Bmatrix} \quad \text{and} \quad d_{rs} = \begin{Bmatrix} d_r \\ 0 \end{Bmatrix} \quad \text{for} \quad \begin{Bmatrix} r = s \\ r \neq s \end{Bmatrix} \tag{3.35}$$

and

$$d_r\, q_r + b_r \frac{dq_r}{d\psi} = - \frac{c'_r}{a_G} \tag{3.36}$$

The solution of (3.36) is

$$q_r = (1 - e^{-\psi/\tau_r}) \left(\frac{1}{d_r}\right) \left(- \frac{c'_r}{a_G}\right) \tag{3.37}$$

with $\tau_r = b_r/d_r$. Eq. (3.37) has a fading-memory Kelvin-type kernel and can thus be seen as the evolution equation for a Kelvin unit associated with the physical process represented by q_r. A point of interest here is that there is no force Q_r associated with the (n-k) functions q_r which describe the evolution of the internal system. It appears however that these internal mechanisms are driven by forces $- c'_r/a_G$ spiked into the Kelvin unit through a force transfer mechanism, which was mathematically given as and includes a thermodynamic force c_r due to temperature differences ($\phi = T - T_R$).

$$c'_r = c_r + d_{rm}(Q_m, T)Q_m \tag{3.20}$$

The transfer function (Eq. 3.20) describes how forces Q_m associated with the observed coordinates $(q_1, q_2, \ldots, q_k)$ diffuse down into the internal material structure where they drive the hidden coordinates

This force transfer process is not necessarily linear and introduces a third nonlinear function $\hat{Q}_m$ through the equation

$$c'_r = \beta_r \phi + d^R_{rm} \hat{Q}_m(Q_n, T) \tag{3.38}$$

where ϕ is $T - T_R$ and β_r is the thermal modulus.

Note that functions d'_{rs} (which show up in the third term of the free energy expansion (3.18)) and d_{rm} (which show up in the second term) represent two completely different nonlinear-physical phenomena. This reasoning leads to the two distinct functions a_G and $\hat{Q}_m$ respectively.

Substitution of (3.37) into (3.31) gives

$$q_m = - \rho \frac{\partial g_R}{\partial Q_m} + \sum_r \frac{\partial c'_r}{\partial Q_m} (1 - e^{-\psi/\tau r}) \frac{1}{d_r} \frac{c'_r}{a_G} \tag{3.39}$$

and for time varying forces,

$$q_m = - \rho \frac{\partial g_R}{\partial Q_m} + \sum_r \frac{\partial c'_r}{\partial Q_m} \frac{1}{d_r} \int_{-\infty}^{\psi} (1 - e^{-(\psi-\psi')/\tau r}) \frac{d(c'_r/a_G)}{d\psi'} d\psi' \tag{3.40}$$

By substituting (3.38) in (3.40),

$$q_m = - \rho \frac{\partial g_R}{\partial Q_m} + \frac{\partial Q_n}{\partial Q_m} \left\{ \int_{-\infty} \Delta S_{np}(\psi-\psi') \frac{d(\hat{Q}_p/a_G)}{d\tau} d\tau \right.$$

$$\left. + \int_o^t \Delta\alpha_n(\psi-\psi') \frac{d(\phi/a_G)}{d\tau} d\tau \right. \tag{3.41}$$

where

$$\Delta S_{np} = \sum_r A^{(r)}_{np} (1 - e^{-\psi/\tau r}) \tag{3.42a}$$

$$\Delta\alpha_n = \sum_r \alpha^{(r)}_n (1 - e^{-\psi/\tau r}) \tag{3.42b}$$

$$A_{np}^{(r)} = \frac{d_{rn}^{R} \; d_{rp}^{R}}{d_r} \tag{3.42c}$$

$$\alpha_n^{(r)} = \frac{d_{rn}^{R} \; \beta_r}{d_r} \tag{3.42d}$$

For uniaxial loading where q_1 is the tensile strain, ϵ, and Q_1 is the tensile stress, σ, Eq. (3.41) can be written as

$$\epsilon = - \rho \frac{\partial g_R}{\partial \sigma} + \frac{\partial \hat{Q}_1}{\partial Q_1} \left\{ \int_0^t \Delta D(\psi - \psi') \frac{d(\hat{Q}_1 / a_G)}{d\tau} \, d\tau \right\} \tag{3.43}$$

or

$$\epsilon = g_0 \, D_0 \, \sigma + g_1 \left[\int_0^t \Delta D(\psi - \psi') \frac{d(g_2 \sigma)}{d\tau} \, d\tau \right] \tag{3.44}$$

with

$$g_0 = - \rho \frac{\partial g_R}{\partial \sigma} \frac{1}{D_0 \, \sigma} \tag{3.45a}$$

$$g_1 = \frac{\partial \hat{Q}_1}{\partial Q_1} \tag{3.45b}$$

$$g_2 = \frac{\hat{Q}_1}{a_G} \frac{1}{\sigma} \tag{3.45c}$$

$$a_\sigma = a_D \mid a_G \tag{3.45d}$$

By way of summary, the nonlinear parameters g_0, g_1, g_2 and a_σ have the following physical significance.

- g_0 Nonlinearizes the elastic response and can in principle increase or decrease with stress. The former is described as a softening phenomenon while the latter is considered to be a hardening phenomenon.

- g_1 Experimental results indicate that g_1 is an increasing function of stress which requires $\hat{Q}_1$ to be a monotonically increasing function of Q_1 as seen in Fig. 3.3. This means that the stresses that are transferred to the microstructure may have a higher intensity than the external force. Note also that when the material is linear viscoelastic, $g_1 = 1$ and $\hat{Q}_1$ is a linear function of Q_1.

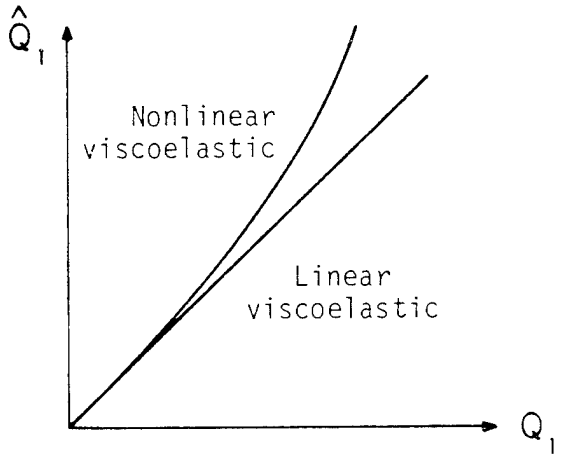

Fig. 3.3 Dependence of Generalized Force $\hat{Q}_1$ or Q_1

- g_2 This factor contains two nonlinearizing functions, $\hat{Q}_1$ and a_G. It can be seen as the ratio of the force that could be spiked into Kelvin-type microunits taking into account that the moduli of the springs in these units change by a factor a_G. This change can be stiffening ($a_G > 1$) or softening ($a_G < 1$).

- $a_\sigma = \frac{a_D}{a_G}$ Represents a stress and temperature dependent shift along the time axis. Here $a_D(Q_m,T)$ decreases with

temperature and with increases in stress-induced free volume. Also, $a_G(Q_m,T)$ decreases with temperature but an increase in stress would produce more shift.

The Kelvin type kernel ΔD in Eq. (3.44) can be approximated by a power law which was proved to be valid under restricted conditions in Chapter 2,

$$\Delta D(\psi-\psi') = \sum_r D_r(1 - e^{-(\psi-\psi')/\tau r}) \tag{3.46}$$

or

$$\Delta D(\psi-\psi') \approx c(\psi-\psi')^n \tag{3.47}$$

With this approximation Eq. (3.44) becomes,

$$\epsilon = g_o D_o \sigma + g_1 \int_o^t C(\psi-\psi')^n \frac{d(g_2\sigma)}{d\tau} d\tau \tag{3.48}$$

For a creep test $\sigma = \sigma_o H(t)$, eq. (3.48) reduces to,

$$\epsilon = g_o D_o \sigma_o + g_1 g_2 C \left(\frac{t}{a_\sigma}\right)^n \sigma_o \tag{3.49}$$

The experimental procedure that should be followed to obtain the three linear parameters (D_o,C,n) and the four nonlinearizing parameters (g_o,g_1,g_2,a_σ) has been described in detail by Lou and Schapery [49] on the basis of a graphical shifting procedure based on creep and creep-recovery data. A computerized procedure that avoids tedious graphical shifting was developed during the current research effort by Bertolotti et al. [50].

The general equation (3.44) can be simplified to model specific thermorheological complex materials. For sufficiently low stresses, $-\hat{Q}_m = Q_m = \sigma$ which means that $g_1 = 1$ and $g_2 = 1/a_G$. Also, a_G and a_D

are only functions of temperature ($a_D/a_G = a_T$). Eq. (3.44) now reduces to

$$\epsilon = g_o D_o \sigma + \int_o^t \Delta D(\psi-\psi') \frac{d}{d\tau}\left(\frac{\sigma}{a_G}\right) d\tau \tag{3.50}$$

where $\log \psi = \log t - \log a_T$. For $\sigma = \sigma_o H(t)$ this becomes

$$D_T = D_I(T) + \Delta D(\psi)/a_G(T) \tag{3.51}$$

with $D_T = \epsilon \mid \sigma_o$ and $D_I(T) = g_o(T) D_o$. Thus,

$$\log (D_T - D_I) = \log \Delta D - \log a_G \tag{3.52}$$

Eq. (3.52) shows that master curves can be obtained by rigid horizontal $|\log a_T|$ and vertical $|\log a_G|$ shifts.

Eq. (3.52) suggest that the machinery needed for accelerated characterization can only be effective when the vertical shift $a_G(T)$ can be separated from the horizontal shift $a_T(T)$. This is only possible with additional transient temperature tests as suggested from Eq. (3.41). Some actual data were obtained by Schapery and Martin [51] and very recently by Weitsman [52]. In the former, a theoretical form for $a_G(T)$ which applies below and in the neighborhood of the glass transition temperature Tg was given as,

$$a_G = \frac{\gamma \ell n (1 + z)}{\exp [\gamma^2/(1 + z)] - 1} \tag{3.53}$$

where $\gamma = \Delta H/RT_R$ and $z = (T - T_R)/T_R$. Eq. (3.53) is based on kinetic theory wherein ΔH is the constant activation enthalpy for hole formation. Simple forms for a_G on the basis of rubber elasticity are well established at and above the Tg.

The results discussed herein have been applied to composite materials by Schapery and his co-workers [49,53].

Chapter 4

DELAYED FAILURE

4.1 Introduction

Failure is most often treated as a separate issue from the determination of modulus properties of materials. In fact, most failure laws are derived empirically from observations related to a catastrophic event such as yielding or rupture. As a result, a great deal of testing and data analysis is necessary to establish an appropriate failure law for a material. On the other hand, modulus or constitutive laws are derived by more rational means of relating deformations to the forces which produce them. For this reason, often much less testing is necessary to define a constitutive law for a material especially if deformations do not depart from the elastic or reversable deformation range for a material.

Failure, however it is defined, should be a part of a complete constitutive description of a material. In other words, the key to dealing effectively with failure lies in treating its behavior as a termination of a nonlinear viscoelastic process. Perhaps, for this reason, a number of investigators have suggested that modulus and strength laws should be related to each other for viscoelastic materials [4,38,54].

The concept of distortional energy as a measure for the criticality of a given state of stress in an elastic material (von Mises criterion) cannot be carried over directly as a governing criterion for failure in viscoelastic materials, mainly because viscoelastic deformation

involves dissipative mechanisms. Thus at any time the energy balance can be written as:

Total deformation energy = Free (stored) energy + Dissipated energy

In case of a perfectly elastic/viscoplastic material, inelastic deformations occur only after a limiting value of stress has been exceeded. Owing to this assumption, such a yield criterion does not differ from the known criteria of the inviscid plasticity theory. The most appropriate form on the latter is often based on the energy approach (Huber-Henkey-von Mises) in which a critical value of the conserved (accumulated) distortion energy defines the transition from the elastic to the inelastic state.

In case of an elastic-viscoplastic material, the rheological response occurs from the beginning of the loading process. Under such conditions it seems appropriate to take into account the accumulated energy W_E, as well as the dissipated power $\dot{W}_D$ where both quantities are regarded to be responsible for the behavior of the viscoelastic material. The yield condition is then given by a function with two arguments such that

$$f(W_E, \dot{W}_D) = 0$$

where the specific form is based on experimental evidence. The simplest possible form is the linear combination

$$\xi_E \, W_E + \xi_D \, C\dot{W}_D = k^2$$

with

$$0 \leq \{\xi_E, \xi_D\} \leq 1$$

With $\xi_D = 0$ we assume that the dissipated energy has no effect on the yield criterion. This corresponds to Reiner and Weissenberg's point of view. Reiner and Weissenberg [55] suggest that the energy storage capacity is responsible for the transition from viscoelastic response to yield in ductile materials or fracture in brittle ones. They assume that a threshold value of the distortional free energy, called the resilience of the material, is the governing quantity. It is clear that the Reiner-Weissenberg criterion applied to a material with zero dissipation (elastic material) becomes identical to the von Mises criterion. When applied to a viscoelastic material, however, we have to keep track of the free energy which is history dependent. If the mechanisms through which total deformation energy is transformed into dissipated energy are so activated that no free energy can be accumulated, there is practically no limit to the amount of deformation energy which can be applied without impairing the strength. That is, forces up to a certain magnitude can be applied for any length of time without leading to rupture. If it turns out that the material cannot accommodate this energy redistribution fast enough then the material will store energy initially but after a period of time failure will occur. The failure process is therefore delayed which limits the life of a given structure to a finite value. The instant of yielding is thus clearly dependent on the final outcome of a conjection between deviatoric free energy and dissipated energy. Thus the effect of the strain history on the delayed yielding phenomenon follows from this model in a natural way. In this respect, it should be noted that both Naghdi and Murch [56] and Crochet [57] have used a modified von Mises

criteria for viscoelastic materials by assuming, ab initio, that the radius of the yield surface Y does depend upon the strain history, through a Euclidian metric, χ, in strain space. Their formulation can be expressed as,

$$f = \frac{1}{2} s_{ij} s_{ij} - Y^2 = 0 \quad , \quad Y = Y(\chi) \tag{4.1}$$

$$\chi = [(\epsilon^{V}_{ij} - \epsilon^{E}_{ij})(\epsilon^{V}_{ij} - \epsilon^{E}_{ij})]^{1/2} \tag{4.2}$$

where χ represents the distance between the purely elastic strain response ϵ^{E}_{ij} and the strain state corresponding to yield ϵ^{V}_{ij} as is geometrically shown in Fig. 4.1. The functional relationship between

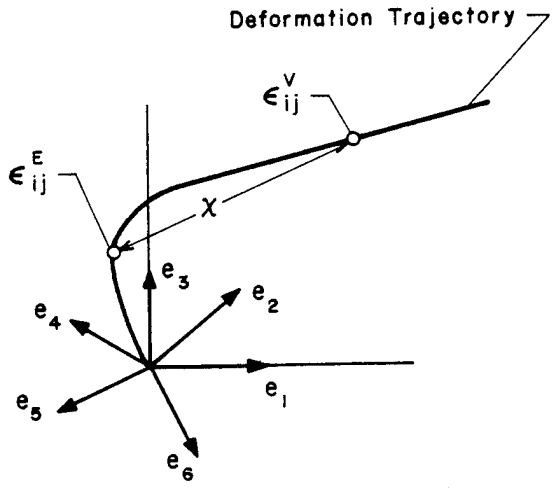

Fig. 4.1 Geometric interpretation of the Euclidian metric χ (as defined by Crochet).

Y and χ for one-dimensional behavior was given by Crochet [57] to be,

$$Y(t) = A + Be^{-C\chi} \tag{4.3}$$

where A, B and C are material parameters. The radius of the yield surface is thus a continuously decreasing function of the "distance" between

two states of strain (e^{E}_{ij} and e^{v}_{ij}).

An extension of the Naghdi and Murch-Crochet approach to fiber reinforced material systems is possible when we can relate the stress in the matrix phase $\{\sigma\}_m$ to the applied external stress $\{\sigma\}$. The introduction of stress concentration factors, which relate both these stress-fields is suggested by Hill [58]

$$\{\sigma\}_m = B_m \{\sigma\} \tag{4.4}$$

and equation (4.1) becomes

$$f = \{\sigma\}^T [B_m] \{\sigma\} - Y^2 = 0 \tag{4.5}$$

in which Y is the tension yield stress in the matrix, as defined by eq. (4.3). It should be noted, however, that eq. (4.5) only describes initial yielding. The incorporation of a hardening rule, together with a flow rule should be considered in order to model accurately the phenomena after initial yielding up to final fracture.

The extension of the Reiner-Weissenberg approach to a general anisotropic material system can be done quite easily when we use the general definition of distortional energy, as defined by von Mises [59]

$$\begin{aligned} W_{dist} = {} & \frac{1}{2}\left(s_{11}\,\sigma_x^2 + s_{22}\,\sigma_y^2 + \ldots + s_{66}\,\tau_z^2\right) + s_{12}\,\sigma_x\sigma_y + \ldots \\ & + s_{14}\,\sigma_x\tau_x + \ldots + s_{66}\,\tau_y\tau_z \\ & - \frac{1}{2}\,\frac{\left[\sigma_x(s_{11}+s_{12}+s_{13}) + \ldots\, \tau_z(s_{61}+s_{62}+s_{63})\right]^2}{s_{11}+s_{22}+s_{33}+2(s_{12}+s_{23}+s_{31})} \end{aligned} \tag{4.6}$$

The advantage of this approach is that the onset of yielding or failure is controlled by only one material constant W_{dist}, while the former

approach (Naghdi et al.) introduces at least three parameters. It has been argued by Pagano [60], on the other hand, that the distortional energy, as defined by von Mises, has only physical significance in the special case of an isotropic material. The full implications of Pagano's comments are unknown at the present time. A possible alternative way to extend the Reiner-Weissenberg criterion, would be to evaluate the free energy in the matrix phase. This could also be done through Hill's concentration factors.

The following is a brief review of the Reiner-Weissenberg criterion which follows Brüller's [61-68] extensive investigation along these lines.

4.1.1 Free Energy Accumulation for a Linear Kelvin Chain in Creep

For a single Kelvin unit in series with a spring as shown in Fig. 4.2,

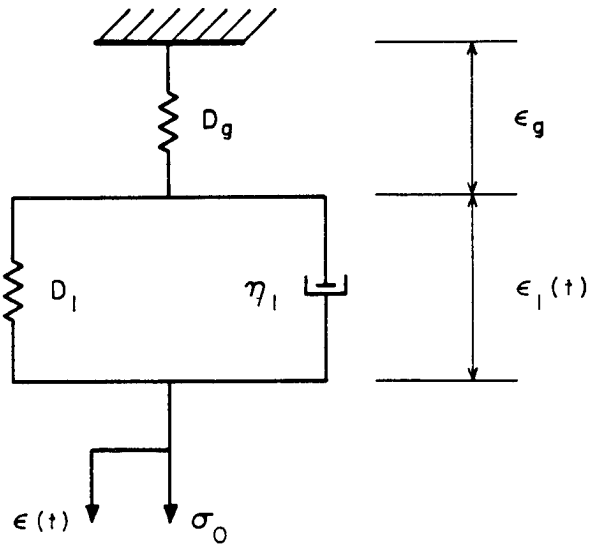

Fig. 4.2 Linear Kelvin model

$$\epsilon = \epsilon_g + \epsilon_1 \tag{4.7}$$

where

$$\epsilon_g = D_g \sigma_o$$
$$\epsilon_1 = D_1 \sigma_o[1 - \exp(-t/\tau_1)] \tag{4.8}$$

or

$$\epsilon(t) = [D_g + D_1(1 - \exp(-t/\tau_1)]\sigma_o \tag{4.9}$$

The stress, σ_s, in the spring with compliance D_1 is,

$$\sigma_s = \frac{\epsilon_s}{D_1} = \sigma_o [1 - \exp(-t/\tau_1)] \tag{4.10}$$

The stress, σ_d, in the dashpot is then,

$$\sigma_d = \sigma_o \exp(-t/\tau_1) \tag{4.11}$$

A physical interpretation of free energy would be the energy stored in the springs D_g and D_1,

$$W_{springs} = \sigma_o^2 \frac{D_g}{2} + \int_o^t \sigma_s \dot{\epsilon}_s \, dt$$
$$= \sigma_o^2 \frac{D_g}{2} + \sigma_o^2 \frac{D_1}{2} [1 - \exp(-t/\tau_1)]^2 \tag{4.12}$$

In the same way we can calculate the energy dissipation in the dashpot,

$$W_{dashpot} = \int_o^t \sigma_d \dot{\epsilon}_d \, dt$$
$$= \sigma_o^2 \frac{D_1}{2} [1 - \exp(-2t/\tau_1)] \tag{4.13}$$

The total energy in the three parameter system is given by,

$$W_{total} = W_{springs} + W_{dashpot}$$

$$= \sigma_o^2 \left[\frac{D_g}{2} + D_1 \left(1 - \exp\left(-t/\tau_1\right)\right)\right] \tag{4.14}$$

The extension of Eq. (4.12), (4.13) and (4.14) to a n-element Kelvin unit with a free spring is straightforward.

$$W_{springs} = \sigma_o^2 \left[\frac{D_g}{2} + \sum_{i=1}^{N} \frac{D_i}{2} \left(1 - \exp\left(-t/\tau_i\right)\right)^2\right] \tag{4.15}$$

$$W_{dashpots} = \sigma_o^2 \sum_{i=1}^{N} \frac{D_i}{2} \left(1 - \exp\left(-2t/\tau_i\right)\right) \tag{4.16}$$

$$W_{total} = \sigma_o^2 \left[\frac{D_g}{2} + \sum_{i=1}^{N} D_i \left(1 - \exp\left(-t/\tau_i\right)\right)\right] \tag{4.17}$$

By taking the limits for $t \to \infty$ of these equations, we obtain

$$\lim_{t\to\infty} W_{springs} = \sigma_o^2 \left[\frac{D_g}{2} + \sum_{i=1}^{N} \frac{D_i}{2}\right] \tag{4.18}$$

$$\lim_{t\to\infty} W_{dashpots} = \sigma_o^2 \sum_{i=1}^{N} \frac{D_i}{2} \tag{4.19}$$

$$\lim_{t\to\infty} W_{total} = \sigma_o^2 \left[\frac{D_g}{2} + \sum_{i=1}^{N} D_i\right] \tag{4.20}$$

Thus half the work done by the external forces goes to increase the free energy while the other half is dissipated.

4.1.2 Power Law Approximations for Free Energy

The free energy expression in the form of Eq. (4.15) forces us to identify the 2N material constants D_i and τ_i. This can be avoided

using a power law approximation as follows,

$$\frac{W_{total}}{\sigma_o^2} - \frac{D_g}{2} = \sum_{i=1}^{N} D_i \left(1 - \exp\left(-t/\tau_i\right)\right) \simeq Dt^n \tag{4.21}$$

and

$$\frac{W_{dashpots}}{\sigma_o^2} = \frac{1}{2} \sum_{i=1}^{N} D_i \left(1 - \exp\left(-2t/\tau_i\right)\right) \simeq \frac{1}{2} D(2t)^n \tag{4.22}$$

This allows us to obtain the following simple expression for the free energy

$$W_{springs} = \sigma_o^2 \left[\frac{D_g}{2} + D\left(t^n - \frac{1}{2}(2t)^n\right)\right] \tag{4.23}$$

$$\sigma_{failure} = \frac{\sqrt{W}}{\frac{D_g}{2} + D\left(t^n - \frac{1}{2}(2t)^n\right)} \tag{4.24}$$

The nonlinearizing parameters introduced in Eq. (4.24) lead to

$$\sigma_{failure} = \frac{\sqrt{W}}{g_o \frac{D_g}{2} + g_1 g_2 C \left[\left(\frac{t}{a_\sigma}\right)^n - \frac{1}{2}\left(\frac{2t}{a_\sigma}\right)^n\right]} \tag{4.25}$$

The ability of Eqs. (4.15) and (4.25) to model experimental data is checked in Chapter 7.

Note on the Zhurkov Criterion

The existence of a strength limit as a real physical characteristic of a material was seriously doubted by Zhurkov [69] due to experimental evidence that solids may also fracture at stresses below the strength limit. He set up systematic and careful measurements of the lifetime of solids under a constant tensile stress. Both tensile stress and temperature were widely varied among experiments. More than

a hundred substances of all principal types of solids were investigated--metals, alloys, glasses, polymers, crystals. It turned out that the time to fracture possessed a surprisingly uniform dependence when suitably expressed in terms of the stress (σ) and temperature (T). Analytical treatment of this vast amount of data led him to the universal formula for the temperature and stress dependence of lifetime, τ, (except for very small stresses),

$$\tau = \tau_o \exp [(U_o - \gamma\sigma)/kT] \tag{4.26}$$

where k is the Boltzmann constant, τ_o is a constant on the order of the molecular oscillation period of 10^{-13} sec., U_o is a constant for each substance regardless of its structure and treatment, and γ depends on the previous treatment of the substance and varies over a wide range for different materials.

Equation (4.26) can be formally incorporated into a continuum mechanics analysis in a modified form to account for time varying stresses and/or temperatures,

$$\int_o^\tau \frac{dt}{\tau_o \exp [(U_o - \gamma\sigma(t))/kT(t)]} = 1 \tag{4.27}$$

Roylance and Wang [70] used Eq. (4.27) in a finite element code where the current value of the above integral was computed at each node. The time and location of fracture was determined when the integral value reached unity at any node.

Williams and his collaborators [71,72] disagree with Eq. (4.26). They argue that the rupture process is much more detailed than reflected by this equation. Their experiments on stress history induced

rupture led them to the conclusion that "Zhurkov's impressive findings appear to be the somewhat fortuitous result of a particular test method."

When Eq. (4.27) is applied to such highly heterogeneous material systems as composites, the question of whether or not fracture can be regarded as a thermally activated process of damage accumulation is far from settled. It is also obvious that τ_o, U_o and γ lose their physical meaning. Regel et al. [73] suggest a life of mixture type predictions for these variables.

Chapter 5

RESIN CHARACTERIZATION: EXPERIMENTAL RESULTS AND DISCUSSION

5.1 Introduction

In order to understand experimentally observed discolorations of the Fiberite 934 neat resin due to postcuring and some anomalities of the creep response in the temperature region, 200-250°F (93.3-121°C), it was decided to study details of the relationship between resin chemistry, various postcuring procedures, and mechanical properties. General resin information is summarized in 5.2 while experiments and analysis related to the mechanical characterization of the resin are reported in 5.3.

5.2 General Resin Information

5.2.1 Resin Chemistry and Curing Procedure

Many composites, especially carbon-fiber based composites, utilize an epoxy resin matrix. From the hundreds of different epoxies that are available, only a small number (≈ 10) are used for composites. The epoxy of interest in this study is a polyfunctional epoxide based on the tetraglycidyl derivative of methylenedianiline (TGDDM), available from Ciba-Geigy under the tradename MY 720. This epoxide, which is now the basis of virtually all aerospace matrices for carbon fibre both here and abroad, is shown in Fig. 5.1a. The Ciba-Geigy Eporal hardener used in conjunction with MY 720 is 4,4' diaminodiphenyl sulfane (DDS) Ciba-Geigy Eporal and is shown in Fig. 5.1b.

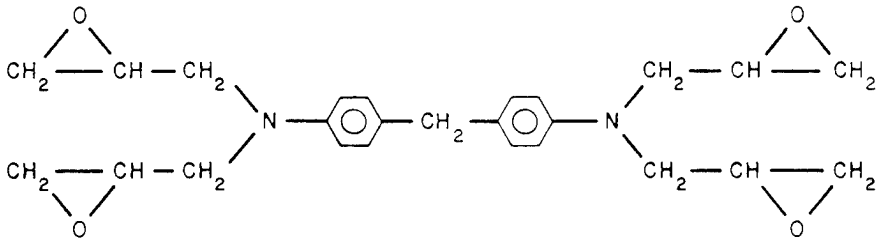

a) Tetraglycidyl 4,4' diaminodiphenyl methane epoxy TGDDM

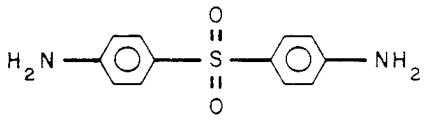

b) 4,4' diaminodiphenyl sulfane (DDS)

Fig. 5.1 Chemical Structure for Epoxy Resins

Because the DDS cure is sluggish, even at moderately high temperatures, a boron trifluoride catalyst is used (BF_3) in order to produce a more manageable cure cycle. Despite the fact that these ionic curing agents often have poor humidity resistance, they are used as a compromise between mechanical properties and manufacturing convenience. The final epoxy network structure depends not only on the chemistry of the system, but also on the initial epoxy versus curing agent ratio and cure conditions. At the beginning of this research program, we obtained three different panels manufactured with three different curing procedures. Cure details are given in Appendix A.

It is usually assumed that the properties of the cured resin in a composite are the same as those of the bulk material. However, McGullough [74], Hancox [75] and Yang, Carlsson and Sternstein [76] suggest otherwise. The reasons mentioned by these authors are:

- The structure in a small volume of resin may be more ordered than in the bulk material, because the exotherm in the composite will be limited to the overall curing temperature by the presence of good conducting fibers.
- The small distance between the fibers may provide steric hindrance and inhibit epoxy-amine cross-link reactions during the latter stages of cure and limit the overall achievable cross-link density.
- Due to the large amount of surface area of the fibers, adsorption of epoxy segments at the fiber surface would cause a tighter network.
- A state of negative hydrostatic stress could be imposed on the epoxy due to the fibers, restricting the volume expansion of epoxy during heating.

No convincing evidence has been produced yet (to this author's knowledge) that one or a combination of these mechanisms leads to the resin in the composite that is thermorheologically different from the neat resin.

As a polymer is cooled at a finite rate through the glass transition into the glassy state, a sudden increase in modulus parallels a rapid decrease in molecular mobility. The process of molecular rearrangements operates on its own internal time scale. Equilibrium can only be achieved if the cooling rate is so slow that the molecular rearrangements are given sufficient time to operate. If the cooling rate is too fast, these rearrangements are essentially quenched into a non-equilibrium state, i.e., a state characterized by excess entropy, enthalpy and volume. This gives rise to a driving force towards

equilibrium, i.e., the system densifies till the free volume, excess entropy and excess enthalpy all reach zero. This process can operate on a scale of days, months or years and is known as aging.

Experimental equilibrium has been unexpectedly difficult to achieve. Spontaneous changes in the properties of glassy polymers have been observed long after vitrification.

Excess entropy cannot be measured directly but excess enthalpy is easily measured by calorimetric methods (DSC). The latter show a decrease in enthalpy with time in a similar fashion as the time dependent mechanical properties as reported by Petrie [77,78]. As indicated in Fig. 5.2, she did not find a one to one correspondence to specific volume behavior.

In our experiments, we tried to achieve this equilibrium state by a postcuring of 350°F ± 10°F (176°C ± 5°C) for 4 hr ± 15 min. followed by a slow, controlled cooldown at a rate of 5°F/hr (2.5°C/hr)(see Fig. 5.3).

5.2.2 Thermal Transitions in the Epoxy System

Two distinct transition temperatures at 140°F (60°C) and 356°F (180°C) respectively have been identified by Yeow and Brinson [4] during their experiments on T300/934 graphite epoxy. The latter was the primary glass-transition temperature, T_g, while the former was a secondary transition. Their measurements were based on detecting discontinuities in the coefficient of thermal expansion which were measured using electrical strain gages.

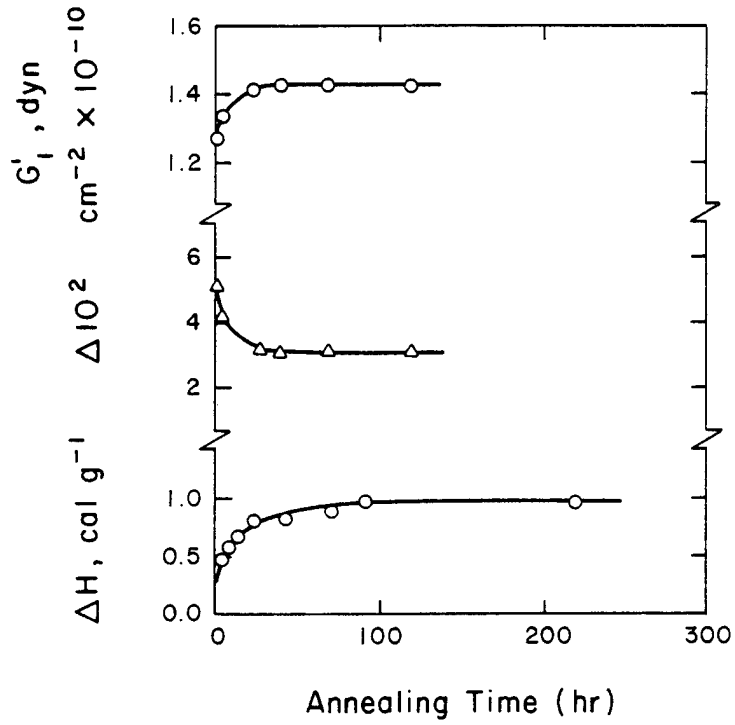

Fig. 5.2 Shear Storage Modulus, G_1', Logarithmic Decrement, Δ, and Enthalpy Relaxation, ΔH, of Quenched Atactic PS vs. Annealing Time at 92°C. G_1' and Δ Were Measured at 0.6 Hz. Petrie [77,78].

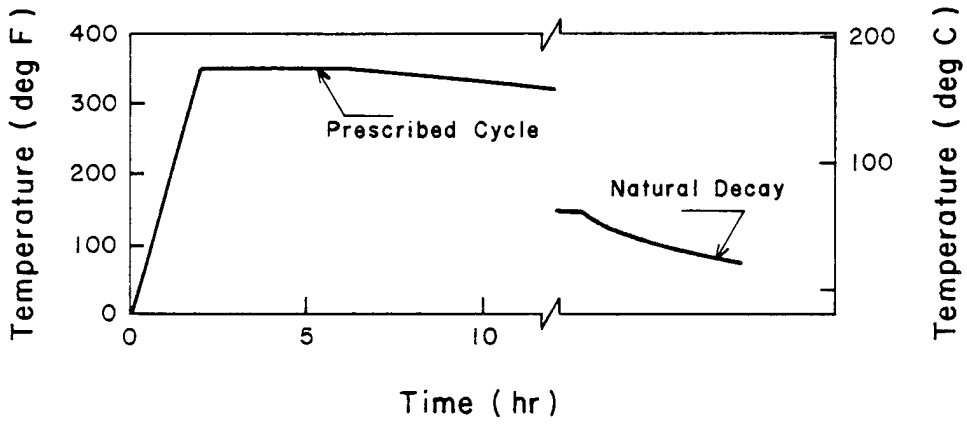

Fig. 5.3 Postcure Cycle Used for 934-Resin and for T300/934 Composite.

Keenan, Seferis and Quilivan [79] used oscillating mechanical fields to characterize the dynamic mechanical behavior of an epoxy system. Their results are shown in Fig. 5.4 with an ω-transition centered around 212°F (100°C) and an α-transition at 464°F (240°C). However, these definitions of T_g suffer from the fact that they are based on dynamic mechanical quantities which are quite sensitive to the frequency of experimentation as well as the sample heating rate.* Consequently, the T_g values defined from dynamic mechanical experiments are invariably higher than those obtained by a more conventional method, i.e., dilatomeric experiments.

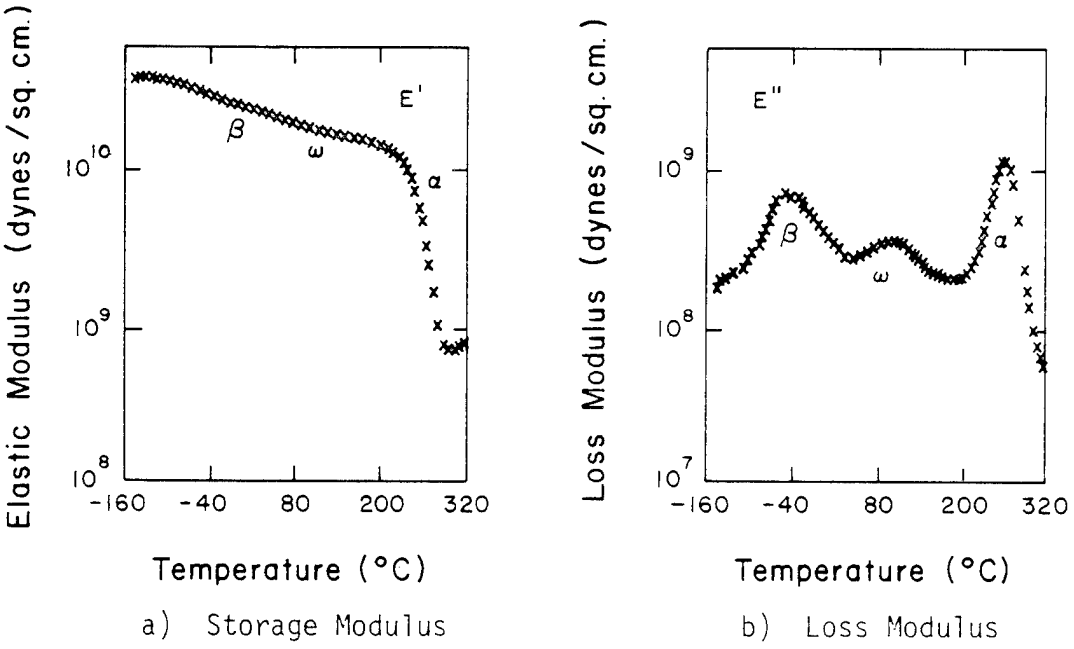

Fig. 5.4 Storage Modulus and Loss Modulus after Keenan et al. [79].

*The conclusions obtained by Keenan et al. can be carried over to the 934 resin, since this particular member of the TGDDM-DDS epoxy family has the same basic network. Any difference should be one of degree, not in kind.

5.2.3 Environmental Stability

1) Thermal Stability

Different IR analysis of an epoxy postcured above 350°F (180°C) reveals an additional broad sorption band in the 5.5 - 14.3 μ region according to Morgan [80]. The intensity of this sorption increased with exposure time and increasing temperature. A strong IR sorption at 5.85 μ appears during the initial stages of the degradation process, which indicates the formation of carbonyl groups. Such groups should result from oxidation of unreacted epoxide rings to form α-hydroxy alolehyde and carboxylic acid [81].

Degradation causes a discoloration of the 934 epoxy as indicated in Fig. 5.5 and may indicate a significant change of behavior in the glassy region due to postcuring. We observed that heating above 356°F (180°C) for 36 hr seemed to cause embrittlement, i.e. decreased tensile strength and ultimate elongation accompanied by a slightly increased modulus (Fig. 5.6). In addition, an increased moisture absorption rate (Fig. 5.7) was found. This is most likely due to a thermal oxidation phenomenon. Figure 5.8 shows the storage modulus E' and the damping ratio δ for the same resin.

2) Moisture Absorption

One consequence of diffused water is that it lowers the mechanical rigidity of the resin. In extreme cases the effect is to lower the glass transition temperature by as much as 212°F (100°C). The effect of moisture on the glass transition temperature and the rates of absorption and desorption for different resins (including the Fiberite

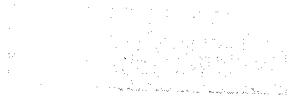

As delivered

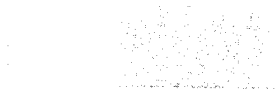

4 hours at 350° F (177°C), slow cooled, 5° F (2.5° C) per hour.

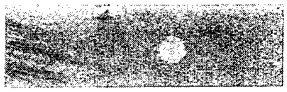

15 minutes at approximately 10-15° F (5-8° C) above T_g, then quenched down to room temperature.

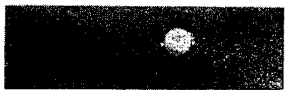

Short overheating at 500° F (260° C), then quenched down to room temperature.

36 hours at 380° F (193° C), slow cooled, 5° F (2.5° C) per hour.

Fig 5.5 Effect of Cure Cycle on Resin Color

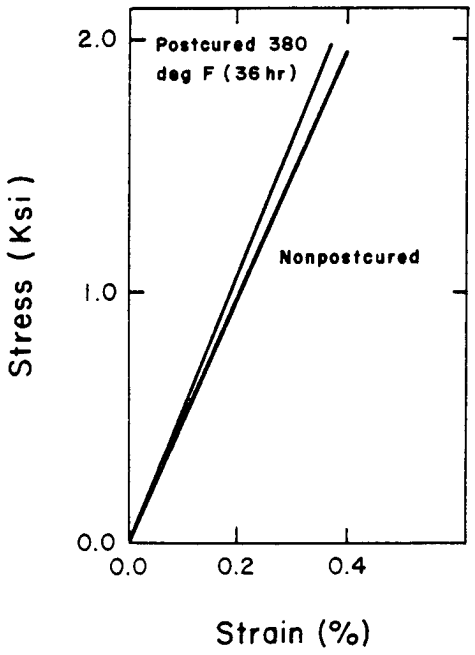

Fig. 5.6 Effect of Postcuring on the Modulus.

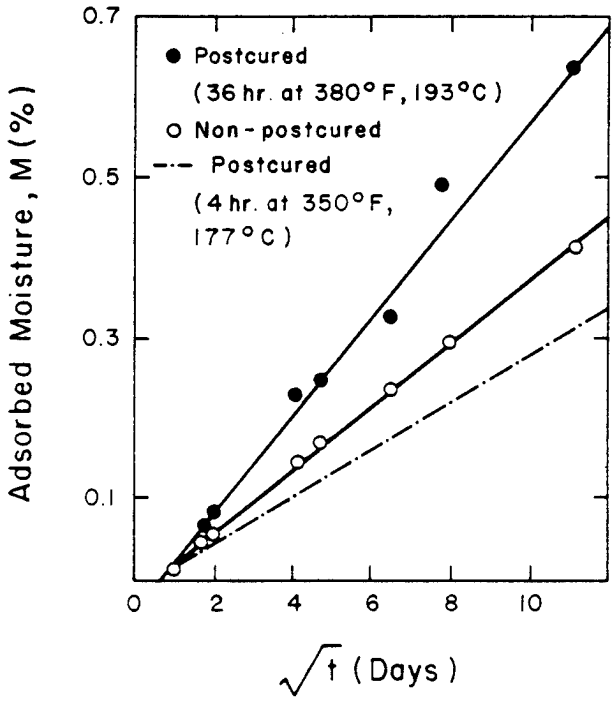

Fig. 5.7 Effect of Postcuring on Moisture Absorption Rate of 934 Resin at Room Temperature.

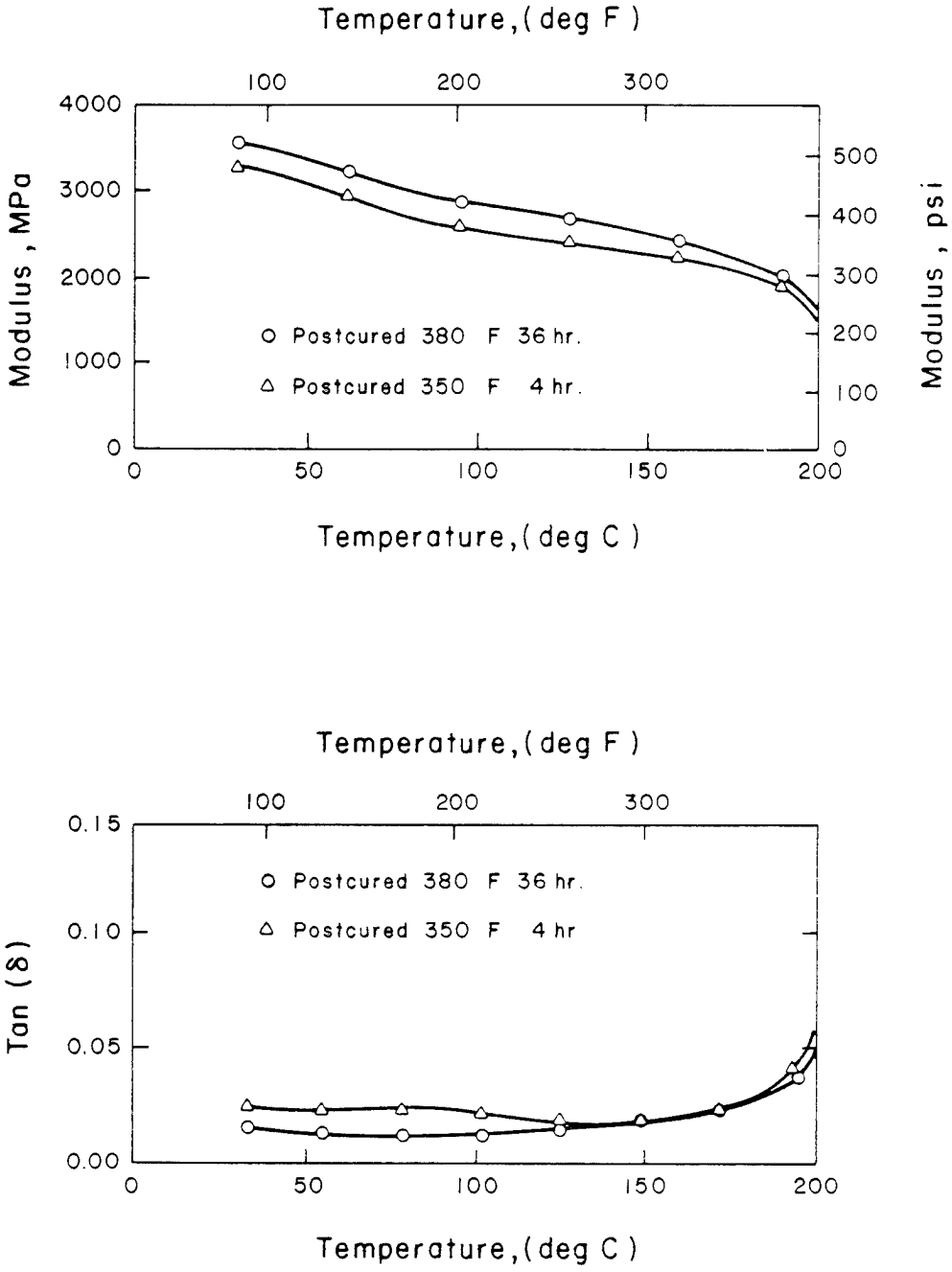

Fig. 5.8 Storage Modulus and Phase Angle (Tangent Delta) as a Function of Temperature for 934 Resin.

934) has been studied by Deisai and Whiteside [82]. Figure 5.9 shows the relationship between equilibrium moisture concentration and primary glass transition temperature for several epoxy resins. Figure 5.10 shows the effect of the humidity in the test environment on the equilibrium moisture content in the same resins. Figure 5.10 shows that a prolonged postcure period could adversely affect the moisture absorption rates, indicating a damaged matrix. The specimens were allowed to pick up moisture in the lab [75-80°F (24-27°C) and ≈ 45% RH]. Figure 5.11 shows the influence of moisture on the ω-transition. It is seen that moisture has a strong effect especially on the width of the ω-transition.

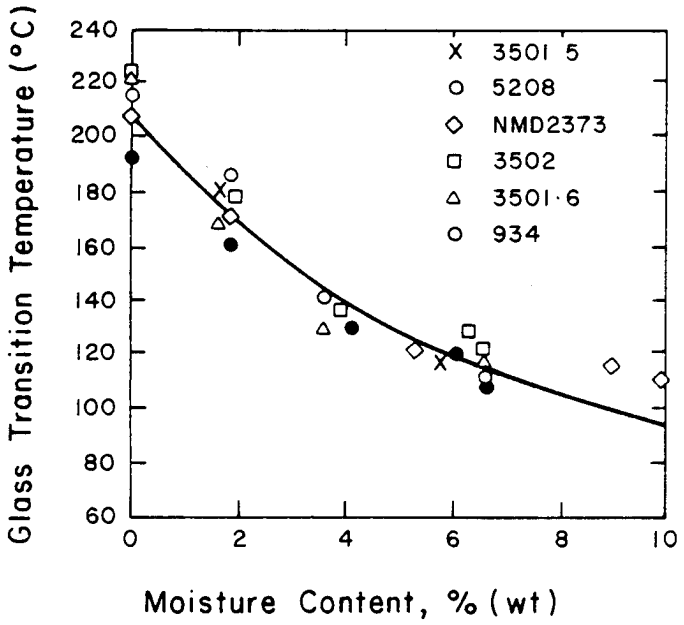

Fig. 5.9 Effect of Moisture Content on T_g [82].

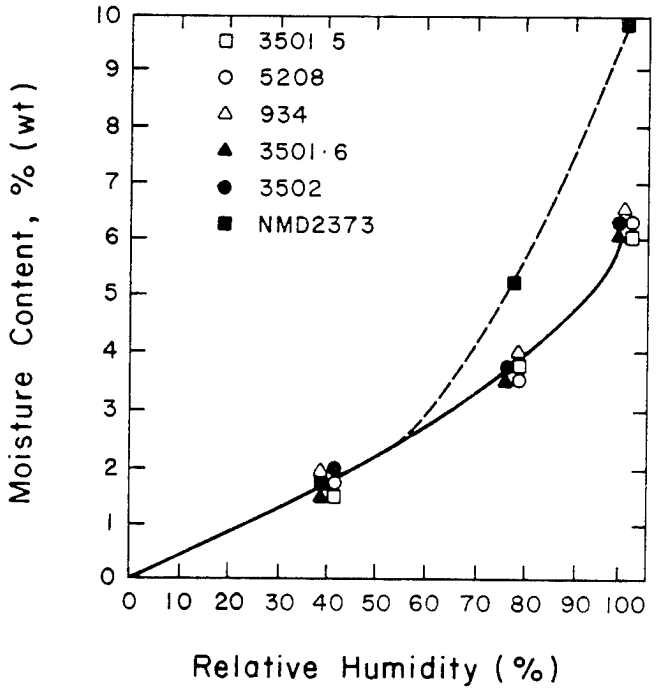

Fig. 5.10 Effect of Relative Humidity on Equilibrium Moisture Concentration in Epoxy Resin [82].

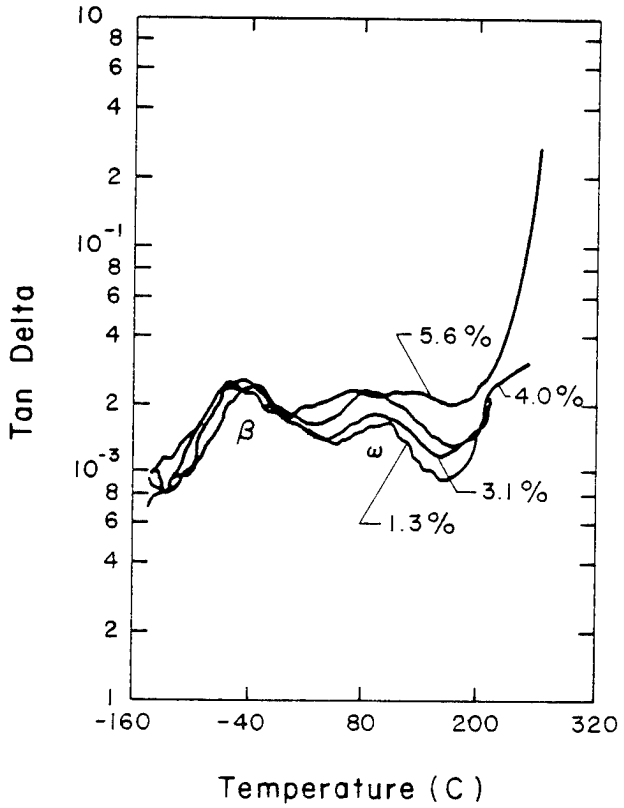

Fig. 5.11 Influence of Moisture on the ω-Transition [79].

The specimens we used for creep and creep-recovery lost approximately 1.5% of their total weight during postcuring. For this reason, the following precautions were taken to control moisture absorption:

- The specimens were dessicated immediately after postcuring. (The relative humidity in the dessicator was monitored and kept below 20%.)
- All specimens were tested within a month after postcuring when possible.
- The specimens tested at room temperature were surrounded with dessicant that was kept in the oven space.

In conclusion, our own moisture absorption experiments, together with a careful study of the literature available, let us believe that the precautions taken were sufficient to keep the moisture level well below .3% WT, a level that is believed to be negligible.

5.3 Results and Discussion on 934 Resin

Two 934-resin panels were fabricated by Graftech as detailed in Appendix A. These panels, labeled I and II, were rectangular plates of approximately 25" x 20" x .12", while one thick plate of 10" x 10" x .39" was made by Fiberite. The panels were cut into 8" x 1" rectangular specimens and labeled according to batch and position. In order to have as homogeneous a set of specimens as possible, each was subjected to a postcure cycle of 350°F (176°C) for 4 h as discussed in 5.1. A screening experiment did not reveal substantial differences between the creep rates of specimens cut from different panels.

The sequence of elevated temperature creep and creep-recovery tests, indicated in Fig. 5.12, was applied at a moderate stress level of σ_0 = 1600 psi (11 KPa). The inverse compliance at t = 1 min, i.e.

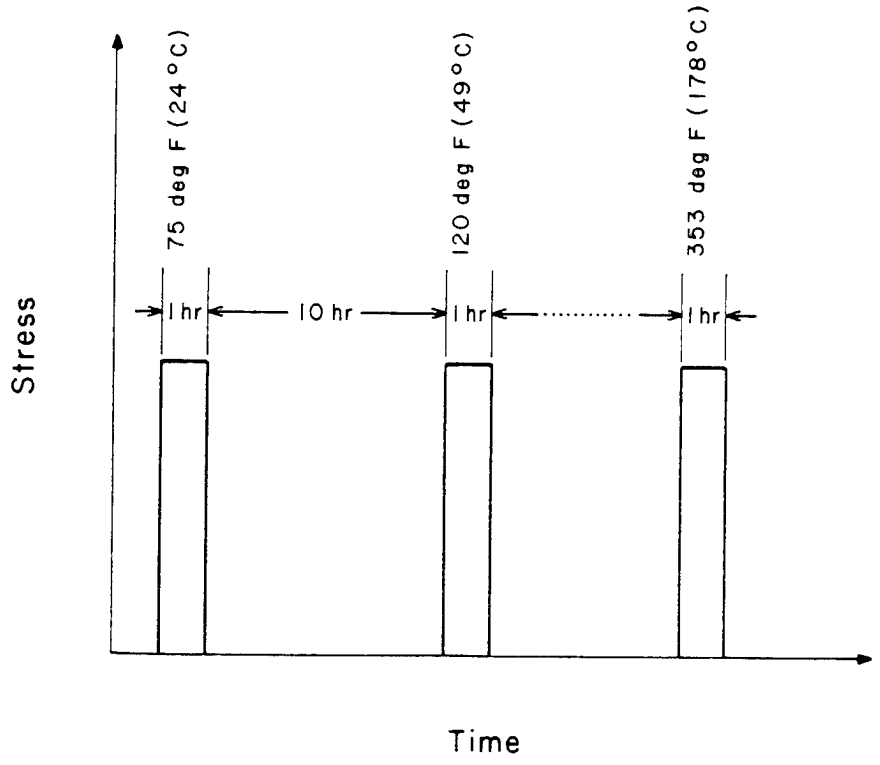

Fig. 5.12 Creep (1 hr) and Creep-Recovery (10 hr) Test Sequence at Different Temperatures.

σ_0/ϵ (1 min) is plotted in Fig. 5.13. Moduli obtained from Instron tests are plotted on the same graph.*

The creep and creep-recovery curves obtained during the test sequence given in Fig. 5.12 are very accurately modelled by the power law equation,

$$D(T) = D_0(T) + D_1 t^n \qquad (2.19)$$

and the result is shown in Fig. 5.14.

---

*The Instron test results were obtained using a 2-in extensometer, whereas the creep and creep-recovery results were obtained using Micro-Measurements WK-06-125AD-350 strain gages.

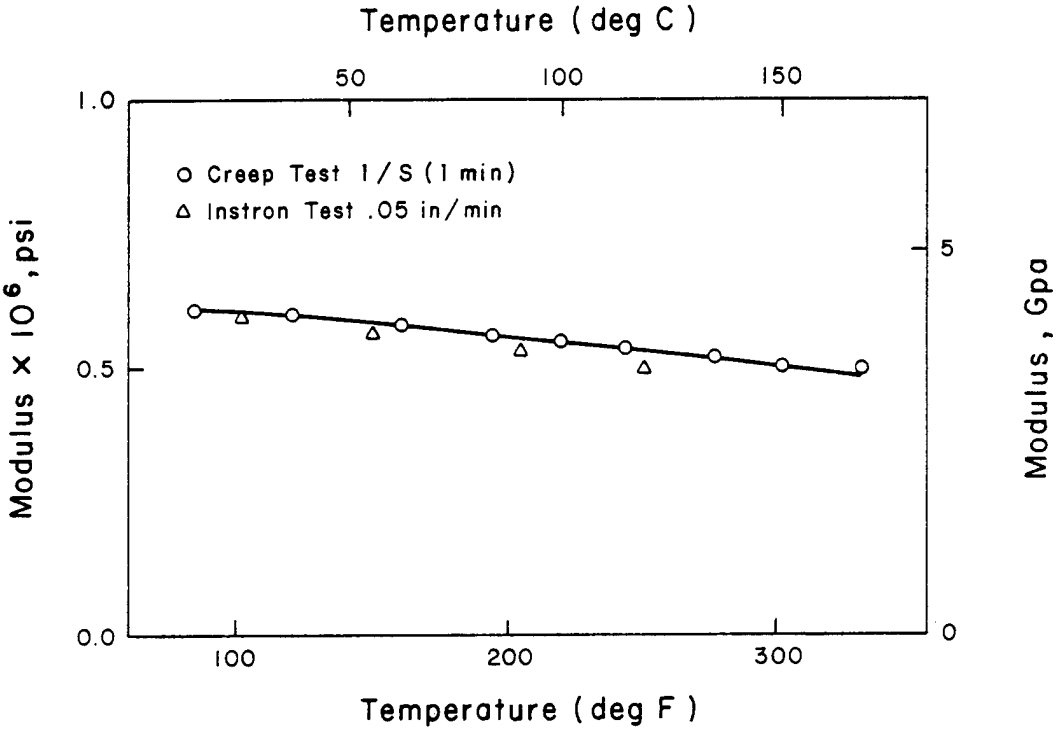

Fig. 5.13 Neat Resin Modulus Versus Temperature.

The temperature dependence of $D_0(T)$, (Fig. 5.15), indicates a thermorheologically-complex material. Figure 5.15 also shows that the simple power law [Eq. (5.21)] breaks down above 300°F (149°C). The temperature dependence of $D_1(T)$ versus temperature is shown in Fig. 5.16. The irregularity in this curve identifies the ω-transition. The transition is centered around 200°F (93.3°C), which is in agreement with the results obtained by Keenan et al. [79], i.e. 212°F (100°C), on this type of epoxy as well as those reported by Griffith [7] for the ω-transition of the T300/934 composite system, 220°F (104°C). The value obtained by Yeow [5], 140°F (60°C), could be simply due to the combined effects of moisture absorption and uncertainties in the identification of a small discontinuity in the thermal expansion versus

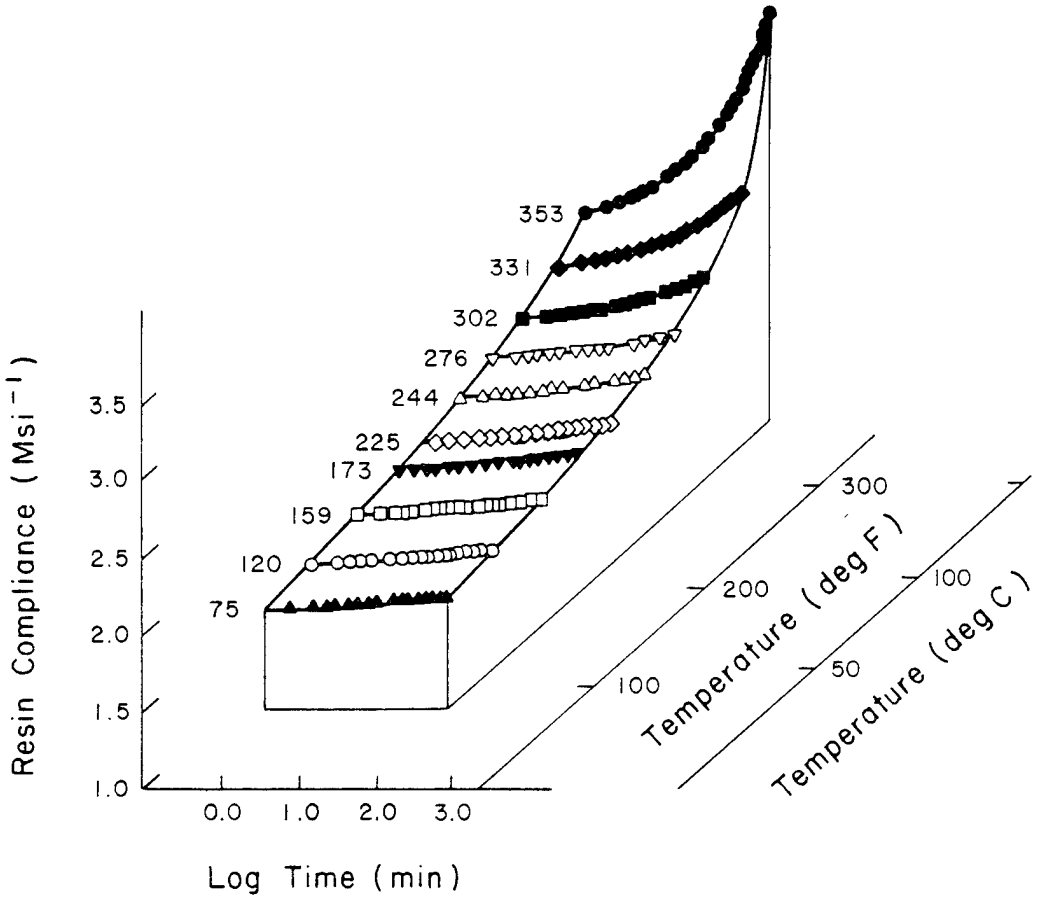

Fig. 5.14 Temperature Dependence of Compliance.

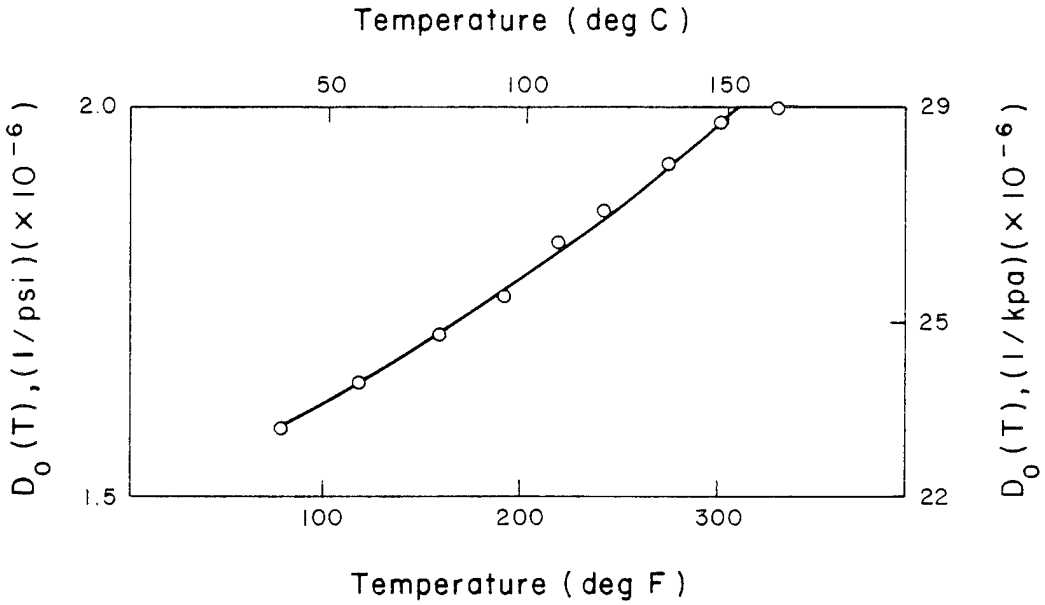

Fig. 5.15 Temperature Dependence of Initial Compliance $D_0(T)$.

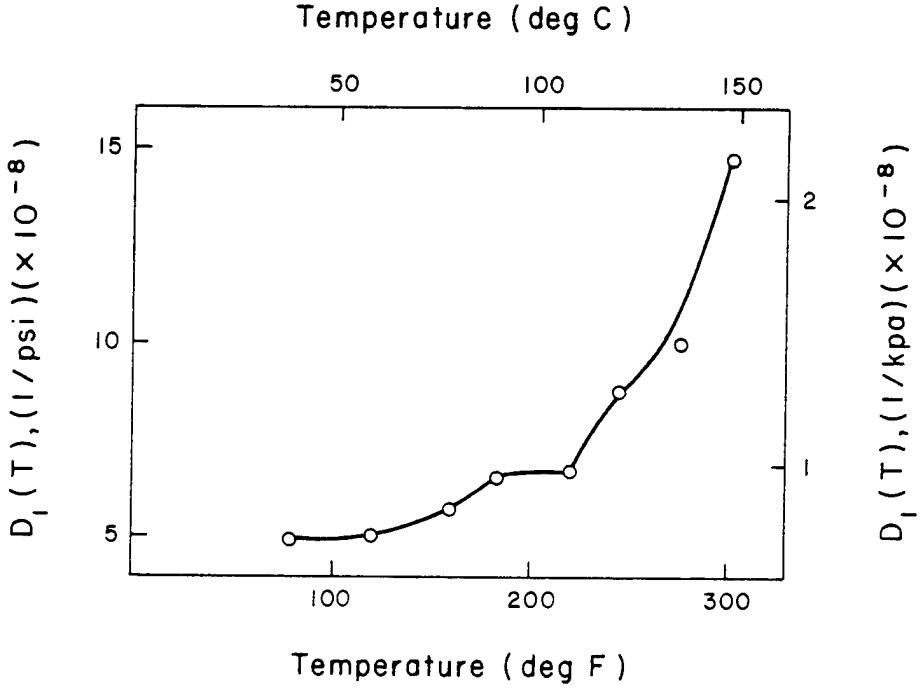

Fig. 5.16 Temperature Dependence of $D_1(T)$.

temperature curve.

The master curve, obtained by horizontal and vertical shifting of the data in Fig. 5.14 is shown in Fig. 5.17 while the amount of vertical versus horizontal shift is shown in Fig. 5.18. This latter figure can be approximated by two straight lines with slopes α and β respectively. The discontinuity in the slope is an indication of the change from one activation mechanism to another. It is well known that the horizontal shift in the glassy region can be represented by an Arhenius type of temperature dependence

$$\log a_T = \frac{\Delta F}{2.303\ R}\left[\frac{1}{T} - \frac{1}{T_R}\right]$$

where ΔF is the activation energy (per mole), R is the universal gas constant, and T_R is an arbitrary reference temperature. Figure 5.19

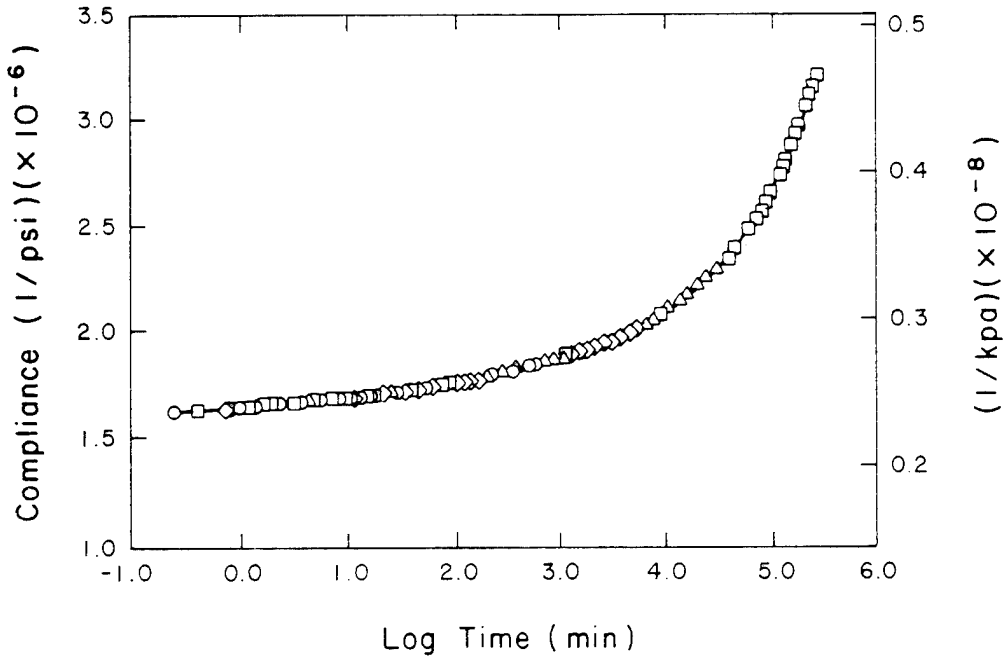

Fig. 5.17 Room Temperature Master Curve for 934 Resin.

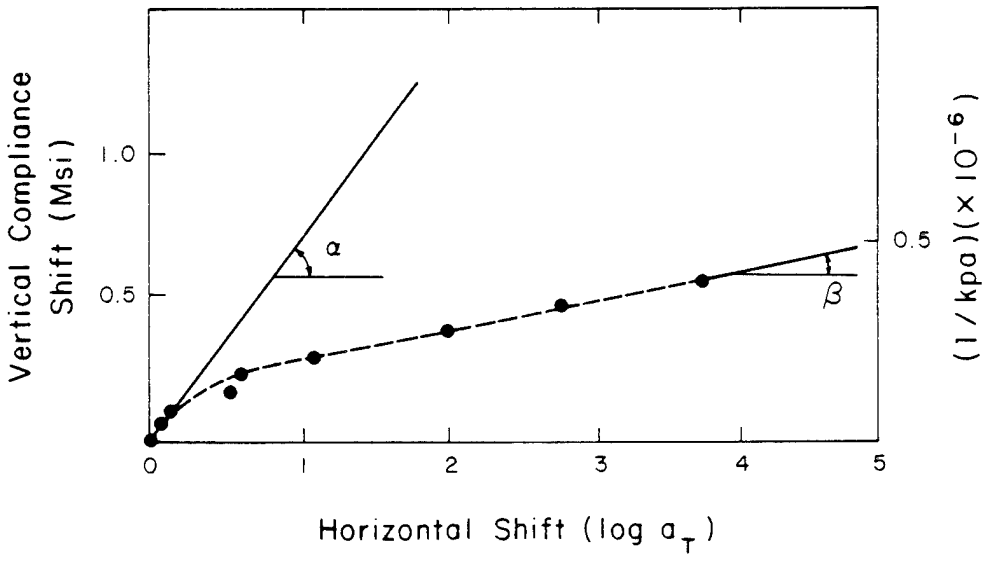

Fig. 5.18 Vertical (Downward) Compliance Shift Versus Horizontal Shift.

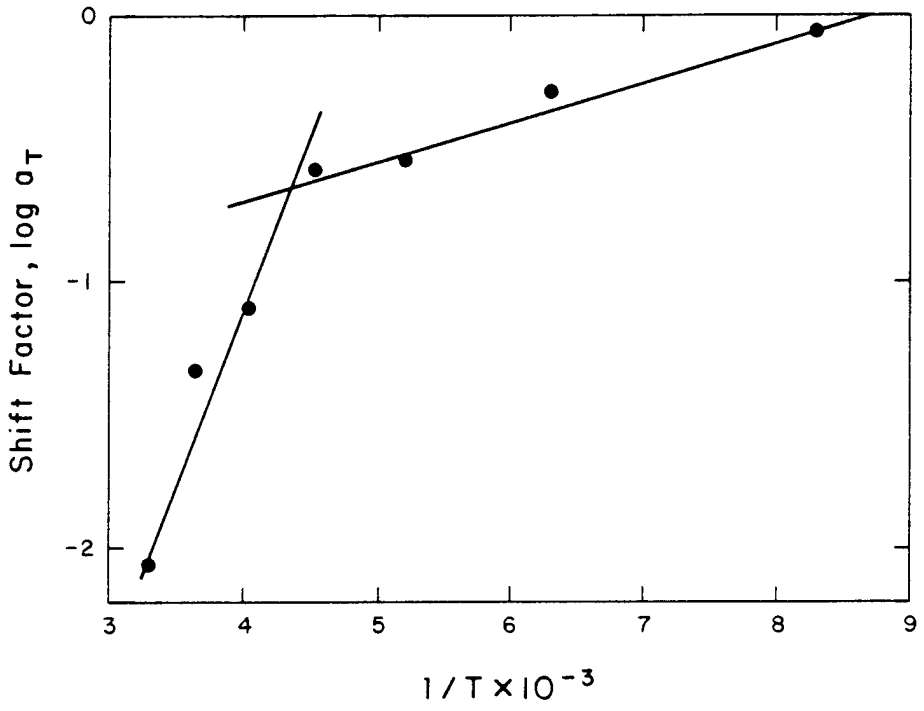

Fig. 5.19 Horizontal Shift Versus the Reciprocal of Temperature.

reveals a discontinuity in the log a_T versus T^{-1} curve. This again is an indication of a changing mechanism. The activation energy below 220°C was found to be 4.76 kcal/gm-mole while above 220°F (104°C) a value of 23.50 kcal/gm-mole was found.

Instron stress-strain curves (Fig. 5.20) revealed a brittle-ductile transition in the temperature range 200-300°F* (93-149°C). All curves have an initially linear stress-strain behavior. The values of stress and strain at the "linear-nonlinear transition point" are plotted versus temperature in Fig. 5.21. Based on these results, a test program was developed. At a given temperature, the same specimen was forced through a series of creep and creep recovery tests

*Probably after the ω-transition has decayed.

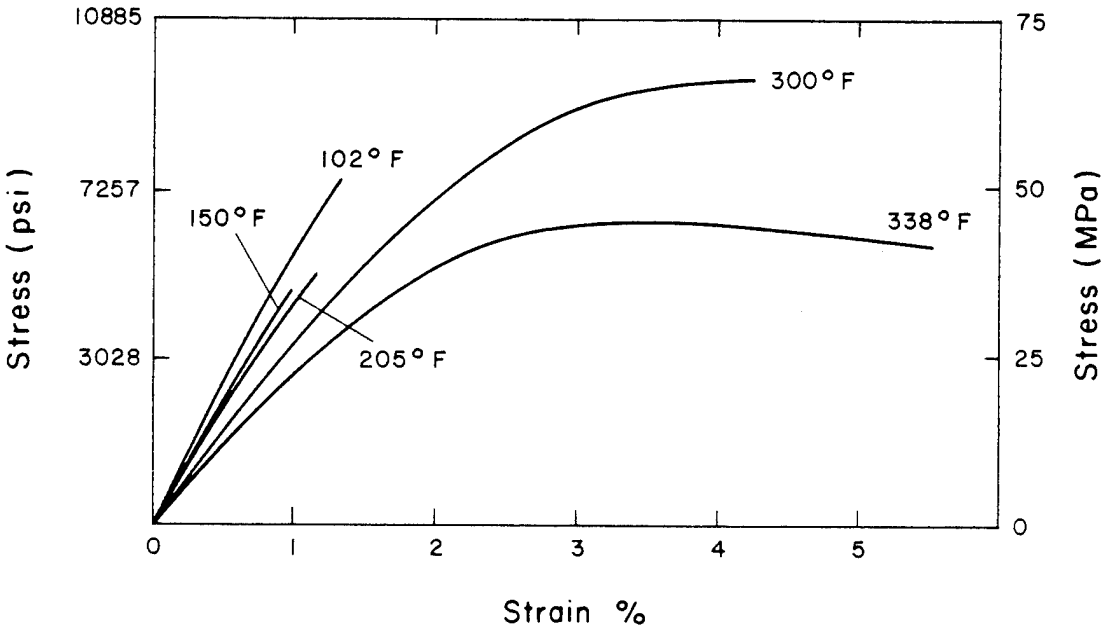

Fig 5.20 Stress-Strain Curves for 934 Resin Postcured at 350 F (177 C)

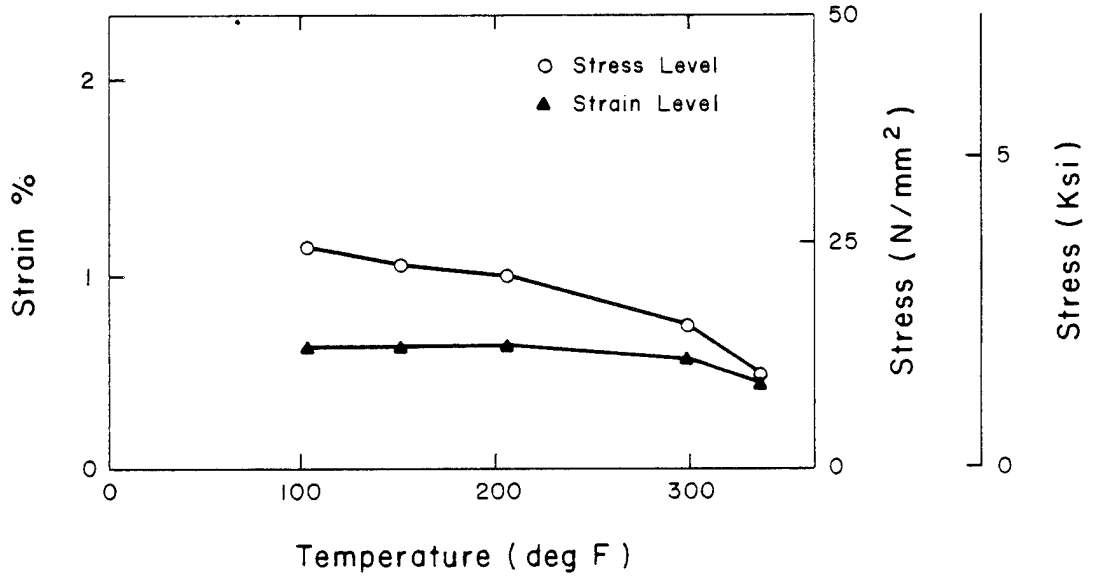

Fig. 5.21 Values of Stress (o) and Strain (▲) at the Linear-Nonlinear Transition Point.

as indicated in Fig. 5.22. A fresh specimen was used for each new temperature. Test results obtained at five different temperatures, with at least eight subsequent creep and creep-recovery tests at each temperature, up till 320°F (160°C) did not show evidence of nonlinear viscoelastic behavior. As an example, Fig. 5.23 shows that the compliance versus time evolution at the highest temperature, 320°F (160°C), is stress independent. Similar results were obtained for the lower temperature tests.

When we proceeded through the loading-unloading cycles (Fig. 5.22) we observed an accumulation of nonrecoverable strain (Fig. 5.24). The importance of this permanent strain accumulation process with respect to the viscoelastic deformation process can be judged when we replot

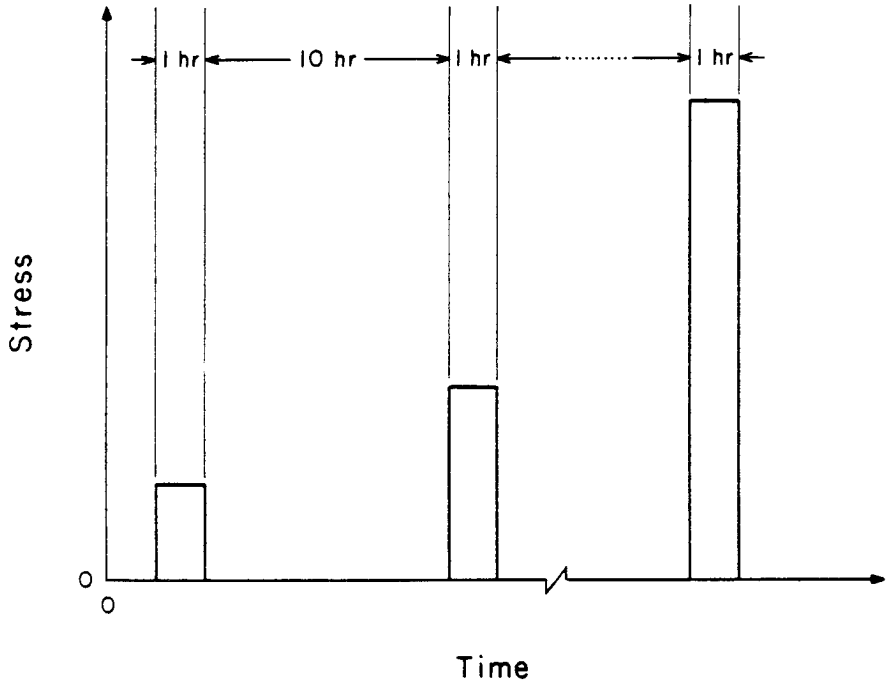

Fig. 5.22 Test Sequence of Creep and Creep Recovery Tests at a Single Temperature and Different Stress Levels.

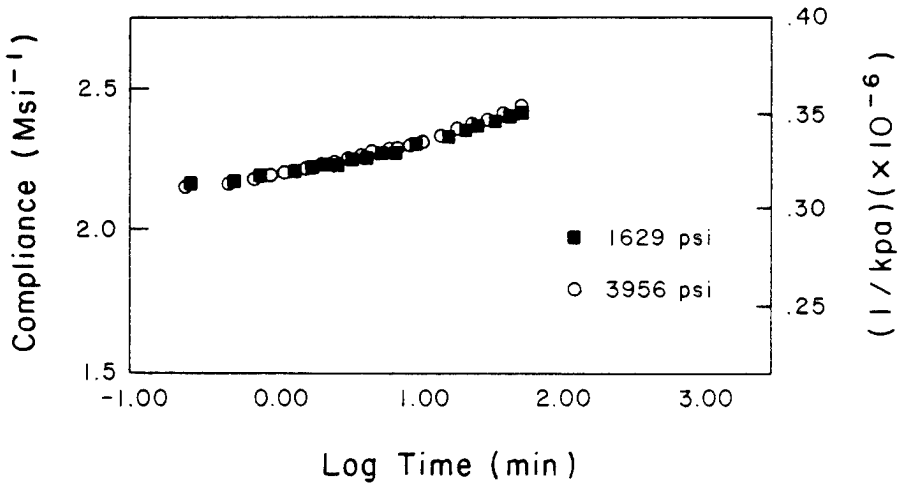

Fig. 5.23 Comparison of Resin Compliance for Low (1.63 ksi (11.2 MPa)) and High (3.95 ksi (27.3 MPa)).

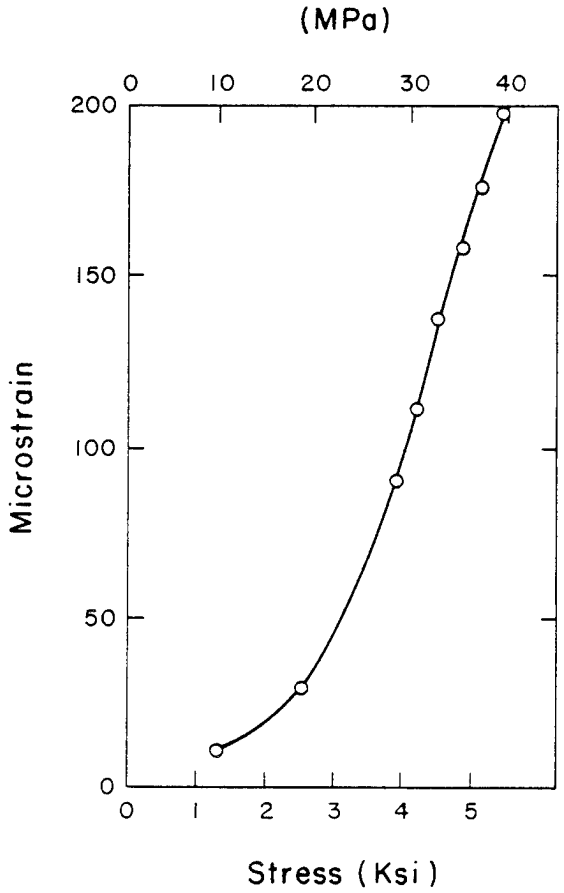

Fig. 5.24 Permanent Strain Accumulation Versus Stress (for 934 Resin at 246°F (119°C)).

Fig. 5.24 with a vertical scale R, being defined as:

$$R = \frac{\text{total permanent set accumulated after k creep and creep-recovery cycles}}{\text{the time dependent deformation at stress level } \sigma_k} \times 100\%$$

This figure (5.25) shows that the permanent set accumulation tends to 30% of the transient deformation at the highest stress levels. The nonlinearizing parameters g_2 and a_σ became stress independent when we subtracted the accumulated strain (Figs. 5.26 and 5.27). This leads to the conclusion that the matrix material behaves linear viscoelastic at lower stress levels and linear viscoelastic-plastic at higher stress levels.

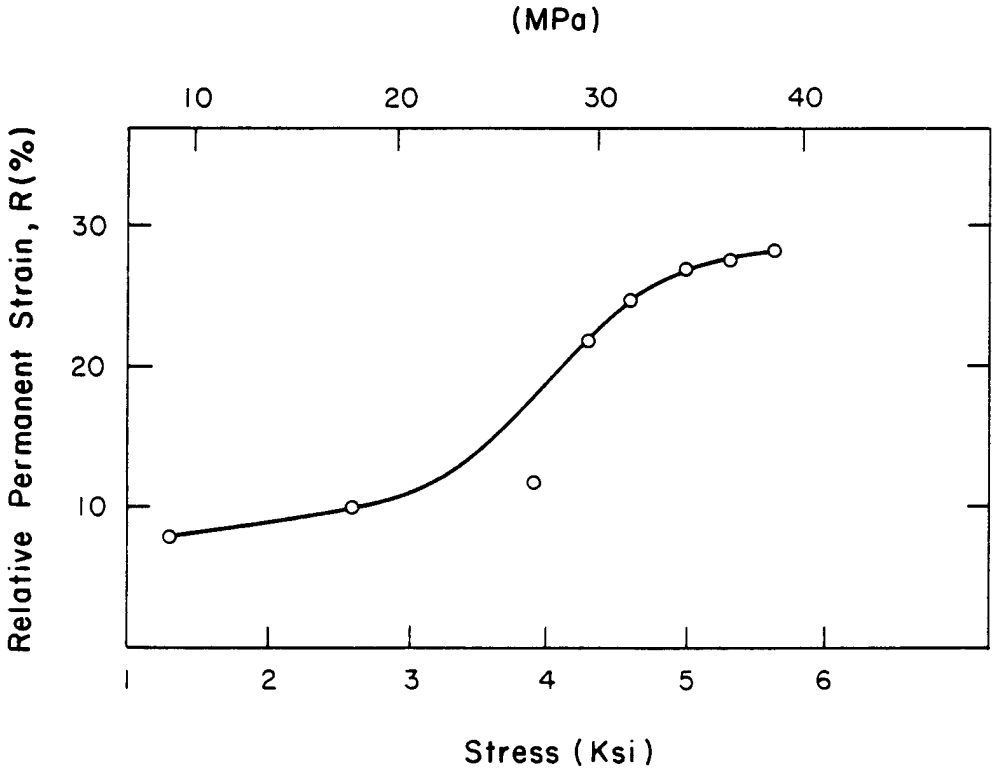

Fig. 5.25 Relative Importance of Permanent Deformation Compared to the Viscoelastic Deformation for Different Stress Levels.

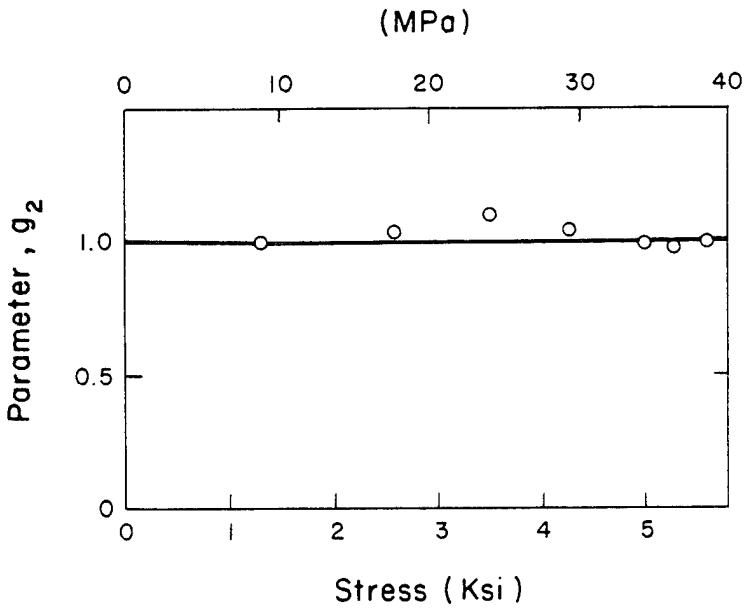

Fig. 5.26 (a) Nonlinear Parameter g_2 for 934 Resin with Subtraction of Accumulated Permanent Strain.

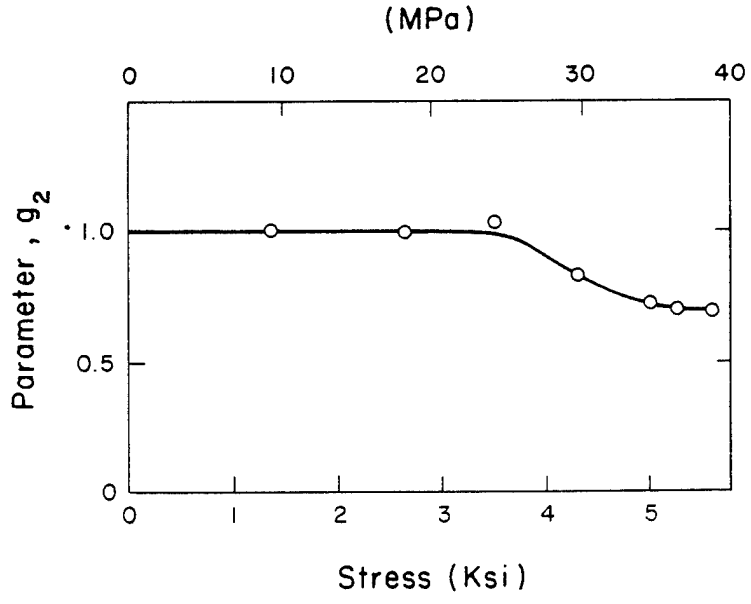

Fig. 5.26 (b) Nonlinear Parameter g_2 for 934 Resin Without Subtraction of Accumulated Permanent Strain.

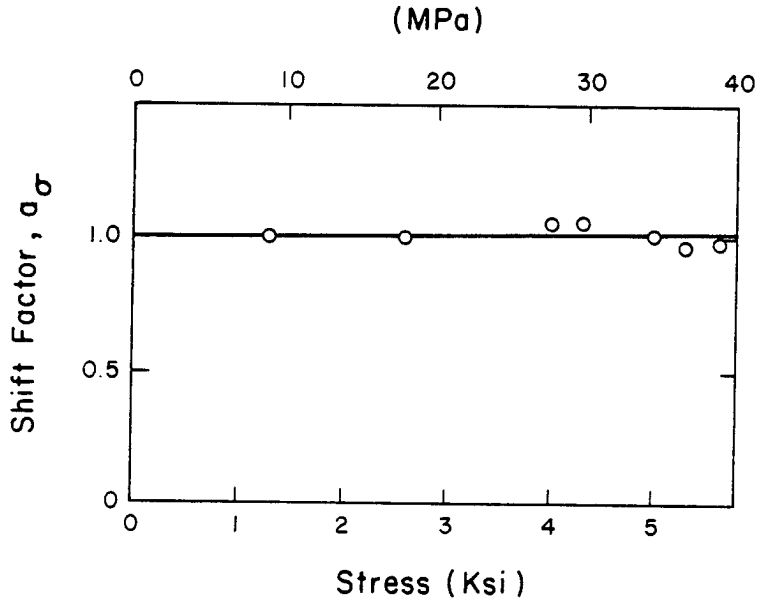

Fig. 5.27 (a) Shift Factor for 934 Resin with Subtraction of Accumulated Permanent Strain.

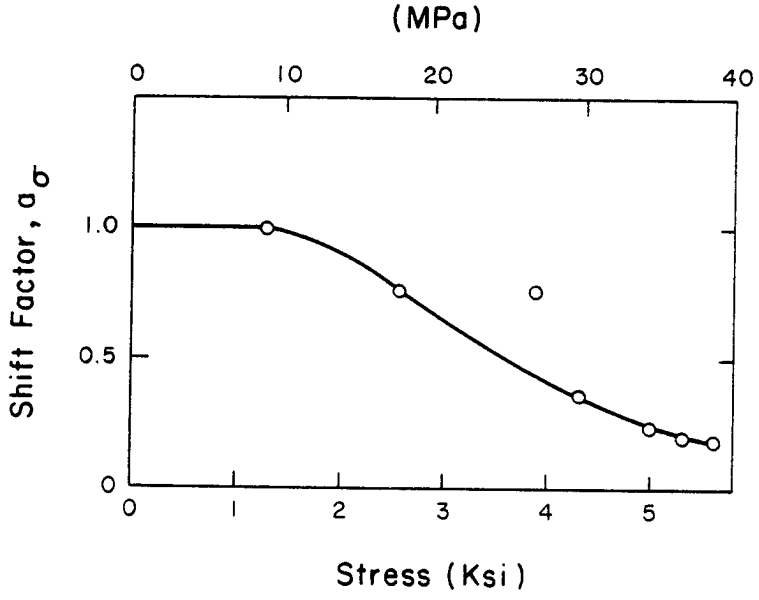

Fig. 5.27 (b) Shift Factor for 934 Resin Without Subtraction of Accumulated Permanent Strain.

Chapter 6

EXPERIMENTAL RESULTS AND DISCUSSION FOR T300/934 COMPOSITE

6.1 Introduction

Only creep measurements were made in our previous studies [4-13]. The Schapery nonlinear viscoelastic method described earlier could not be used as it requires both creep and creep recovery data. The present investigation was undertaken to obtain the proper information on T300/934 laminates such that the Schapery analysis could be developed. We also wished to compare the results of our measurements with new batches of T300/934 from a new source, Fiberite (see Appendix A for curing details), and earlier batches supplied by Lockheed-Sunnyvale. A further objective was to compare the nonlinear viscoelastic properties of the T300/934 composite with those of the 934 resin given in Chapter 5.

The plane stress constitutive properties of a linear orthotropic material is completely characterized by four independent properties. These may be the compliances, D_{11}, $D_{12} = D_{21}$, D_{22} and D_{66}. The first two, D_{11} and D_{12}, can be determined from a tensile test of a unidirectional laminate tensile coupon with the fibers in the load direction (see Fig. 6.1). D_{22} and D_{66} can be determined from tensile tests of a unidirectional laminate with the fibers transverse to the load axis and the fibers at 10° to the load axis respectively. Performing creep tests to express these parameters as a function of time permits the calculation of orthotropic linear viscoelastic response for an arbitrary direction of the fibers.

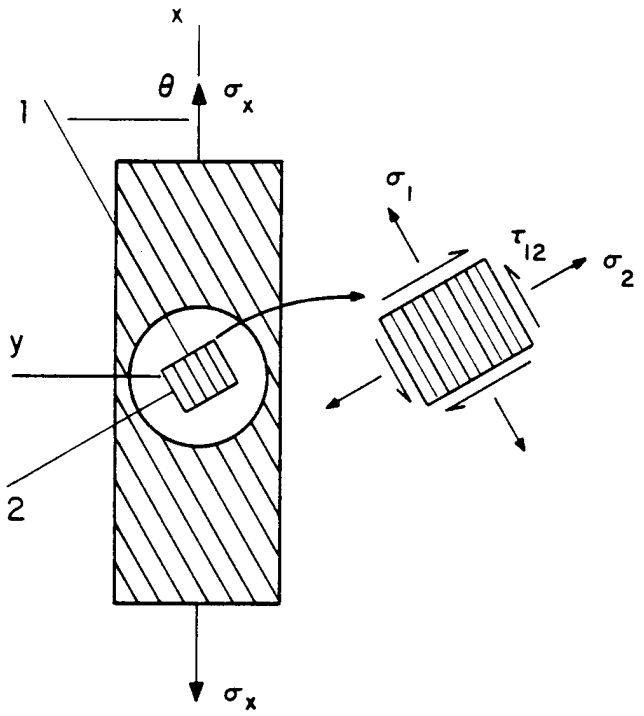

Fig. 6.1 Off-Axis Test Geometry and Internal Stress State.

Normally, because the graphite fibers of a G/E laminate are very stiff and nearly time independent, creep tests to determine time dependent responses are only performed for the 90° and 10° cases respectively.

If an orthotropic material is nonlinear, D_{22} is not only a function of σ_2 but may be a function of σ_1 and τ_{12} as well [15]. This gives rise to an interaction among stress components not present for a linearly viscoelastic orthotropic material. In order to account for this interaction effect, various methods have been employed usually based on the introduction of a flow rule. Such an approach is not always straightforward due to the possibility of various stress interactions at the microlevel. A simple method to account for interaction

effects is to replace the one-dimensional stress by the octahedral shear stress. This stems from the intuitive hypothesis that creep is caused by the shearing of the polymer molecules past one another.

A somewhat more intricate approach was proposed for fiber reinforced materials by Lou and Schapery [49] and was in turn used by Dillard [9]. Their procedure utilized the octahedral shear stress only in the matrix phase as a nonlinearizing parameter. The relationship between the octahedral stress is the matrix $\left\{\tau^m_{oct}\right\}$ and the plane stress components $(\sigma_1,\sigma_2,\tau_{12})$ shown in Fig. 6.1 was given through a micromechanics model. The compliance model proposed by Dillard [9] was given as,

$$\begin{Bmatrix}\varepsilon_1\\ \varepsilon_2\\ \gamma_{12}\end{Bmatrix} = \begin{bmatrix}D_{11} & D_{12} & 0\\ D_{12} & D_{22}\left\{t,\tau^m_{oct}\right\} & 0\\ 0 & 0 & D_{66}\left\{t,\tau^m_{oct}\right\}\end{bmatrix}\begin{Bmatrix}\sigma_1\\ \sigma_2\\ \tau_{12}\end{Bmatrix} \tag{6.1}$$

An alternate approach would be the use of the free energy expansion of Eq. (3.18) which could accommodate higher orders of the strain or stress components or their invariants. Hahn and Tsai [83] used a fourth order strain expansion of the complementary energy density to handle shear nonlinearities. In other words, temperature was excluded from the Gibbs free energy of the system. We feel this approach should be extended and explored further.

Nonlinear viscoelastic effect was not observed in the transverse direction for our T300/934 material. During the final compilation of the results it was realized that this result should be reexamined, since there is some indication that the nonlinear mechanism could

operate on such a long time scale that it becomes impossible to discriminate between materials response and experimental error on the basis of short time accelerated characterization results.

6.2 Results and Discussion on $[90]_{8s}$

The laminate used in this investigation consisted of sixteen unidirectional plies, with about sixty percent volume of T300 graphite fibers in a matrix of Fiberite-934 epoxy resin.

Tensile specimens were cut from a unidirectional plate by means of a diamond cutting wheel, postcured at 350°F (177°C) for 4 hours and dessicated as discussed earlier. A series of elevated temperature creep and creep-recovery tests were performed in the same manner as those for the resin shown in Fig. 5.12. The strain response was measured using back to back strain gauges to avoid the effects of bending. Parenthetically, it is easily shown that an eccentricity (e) of 1% of the depth (d) of the rectangular cross section as shown in Fig. 6.2 causes a bending stress at the gauge location which is 6% of the average stress σ_2. (This is discussed in more detail in Appendix C.)

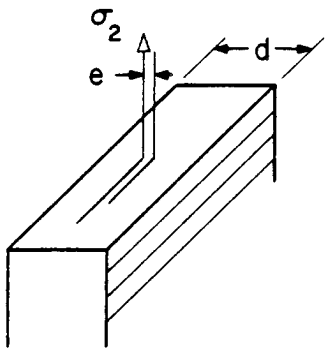

Fig. 6.2 Possible Bending of Tensile Specimen

The eccentricity in creep tension tests has been estimated by Isaksson [84] to be of the order of 5% of the depth (d) causing a 30% deviation of the average stress σ_2.

The change of the gauge factor with temperature was neglected because it was typical only 1.5% for a temperature change from room temperature up to 320°F (177°C).

Another experimental necessity was to avoid heat leakage through the lower oven load train entrance as illustrated in Fig. 6.3. Efforts to insulate this entrance in the same way as the top load train entrance caused interference with the recovery data. The rod that was used to connect and disconnect the specimen with the lower and movable end of the load train needed to be completely free. A satisfactory solution for this problem was to place a heavy mass of metal at the lower entrance as shown in Fig. 6.3b. This "heat sink" contained an

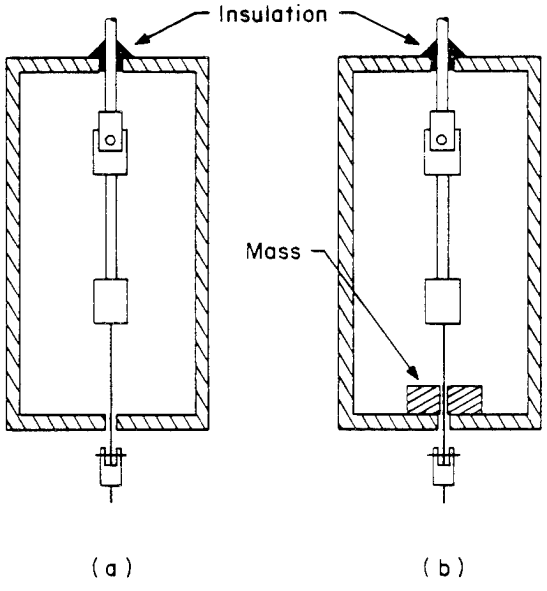

Fig. 6.3 Loading and Oven Insulation Details

opening trough which the connecting rod could move freely, but at the same time allowed a uniform oven temperature to be maintained.

The transverse compliance as a function of time for different temperatures in the range 200-320°F (93-160°C) is shown in Fig. 6.4. An expanded vertical scale was used as compared with the similar resin-compliance plot of Fig. 5.3, because the continuous interruptions of the matrix by time independent filaments prohibited a large transverse creep strain buildup.

Additional tests at different stress levels were performed for the transverse compliance as a function of temperature as shown in Fig. 6.4. However, these are not shown as the compliance appeared to be independent of stress level, i.e., was linear, for the time scale of our tests as will be discussed subsequently.

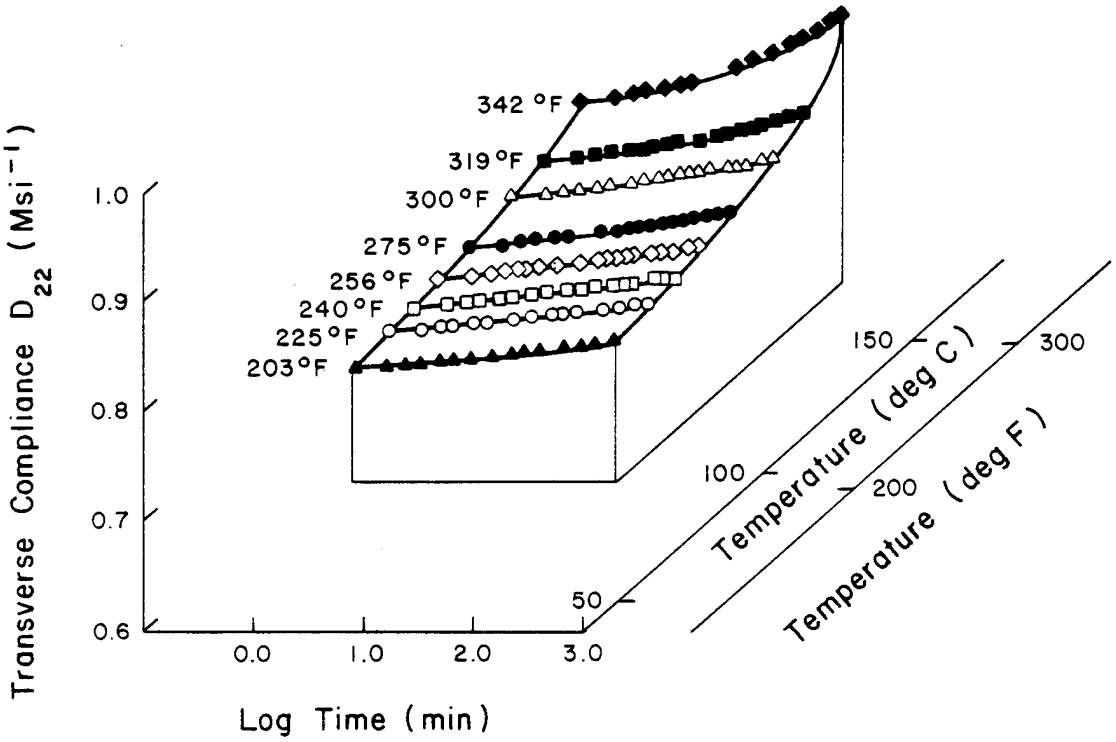

Fig. 6.4 Transverse or D_{22} Compliance of T300/934 as a Function of Time and Temperature

The inverse compliance at t = 1 min is plotted versus temperature in Fig. 6.5. Similar results obtained by Yeow [5] and Griffith [7] are plotted on the same graph, together with a micromechanics prediction, based on the previously measured resin modulus as a function of temperature.

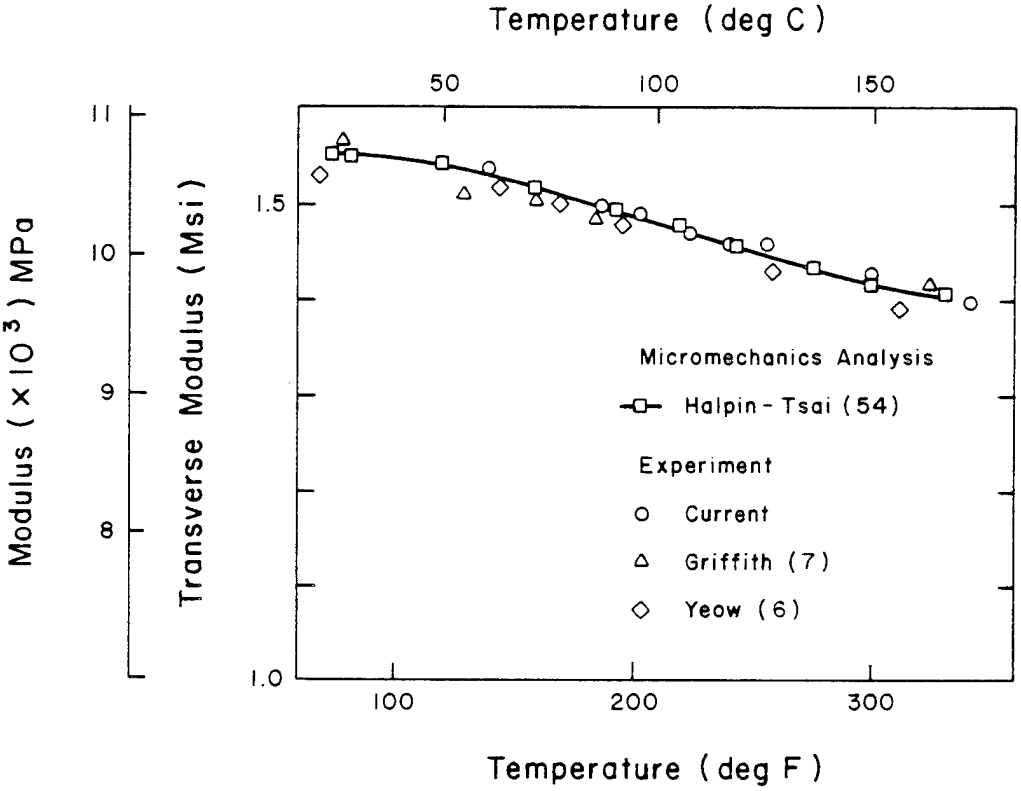

Fig. 6.5 T300/934 $1/D_{22}$ (1 min) Versus Temperature

The micromechanics equation used to produce Fig. 6.5 was the Halpin-Tsai equation [54]

$$E_2(t,T) = E_m(t,T)\left[\frac{1 + \xi \cdot \eta \cdot v_f}{1 - \eta \cdot v_f}\right] \tag{6.2}$$

where

$$\eta = \frac{E_f/E_m - 1}{E_f/E_m + \xi}$$

in which ξ is a measure of reinforcement and depends on the fiber geometry, packing geometry and loading conditions as discussed in [54].

Equation 6.2 is valid only for an elastic material but can be extended to the viscoelastic problem using the so-called "quasi-elastic" approach. It means that if the solutions to the elastic field equations are found, an approximate viscoelastic solution can be obtained by replacing elastic constants by time dependent moduli. Sims [85] showed that for a creep time of several hours, this quasi-elastic approach deviates little from the more theoretically justified Laplace transform inversion approach. In Fig. 6.5 it was also tacitly assumed that $E(t) = 1/D(t)$, which, according to Aklonis and Tobolsky [86], does not introduce an error larger than our experimental uncertainty in determining the compliance.

As may be observed, good agreement was obtained between the Halpin-Tsai micromechanics equation and current and previous experimental work. Such is the case even though the model is based on isotropic properties on both fibers and matrix even though the graphite fibers are known to be very anisotropic. This confirms a statement by Whitney [87] which indicates that a straightforward substitution of appropriate isotropic constants appears to be adequate to account for transversely isotropic fiber properties.

Micromechanics solutions based upon an exact or approximate solution to the field equations have been developed, however, which include complete anisotropy of the fibers. These include the upper and lower bound method of Bulavs et al. [90] and Hashin [91]. Experimental studies have been conducted by Ishikawa et al. [88] and Thompson [89] which show the Thornel 300 high strength fibers to be greatly anisotropic. These results are shown in Table 6.1.

Table 6.1

	Ishikawa et al. [88] (T-300A)	Thompson [89] (T-300, wyp 15)
E_{11}	32.5 (MSI)	32 ± 3 (MSI)
E_{22}	2.93 (MSI)	/
ν_{12}	.2	/
ν_{23}	.42	/
G_{12}	6.82 (MSI)	/

A comparison of Halpin-Tsai equations (6.2), Hashin's upper and lower bound method with anisotropic properties, Hashin's equations with equivalent longitudinal (E_{fl}) and transverse (E_{ft}) fiber properties, Bulav's square array method and our current experiments are given in Fig. 6.6. As may be observed, Whitney's conclusion is once again confirmed.

Hashin's upper and lower bound results are shown in Fig. 6.7 as a function of the ratio of longitudinal to transverse fiber moduli.

Equation 6.1 was modified to include the micromechanics approach given by Eq. 6.2. Using the quasi-elastic approach mentioned previously predictions of the time dependent transverse modulus were made and these are given together with experimental results in Fig. 6.8. Good agreement was obtained which would indicate a simple time dependent micromechanics analysis to be a reasonable approach to represent our data over the time range involved.

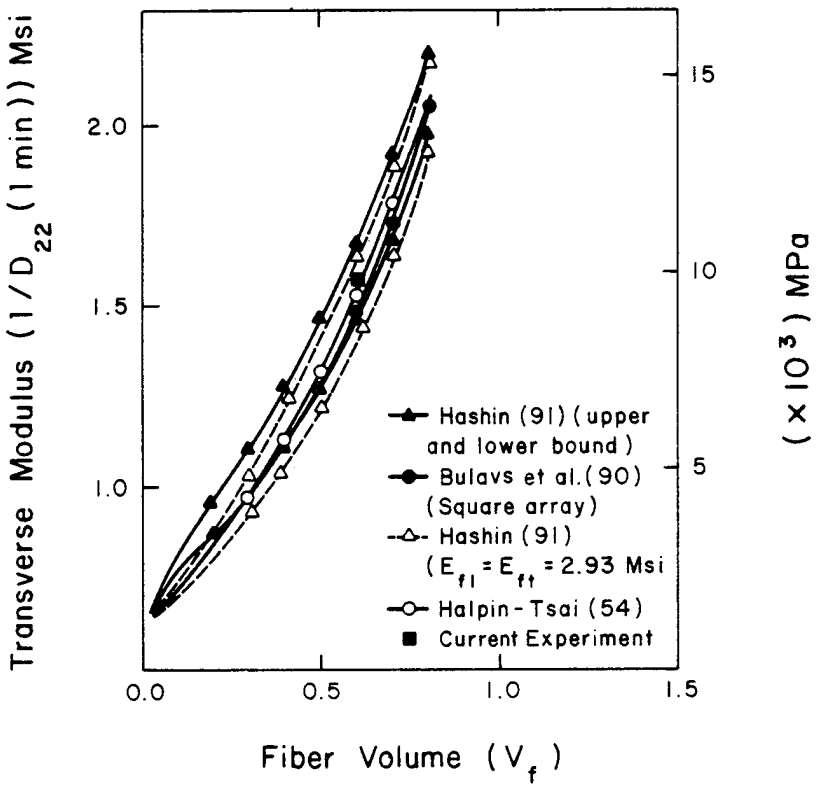

Fig. 6.6 Modulus Prediction Based on Different Micromechanical Models

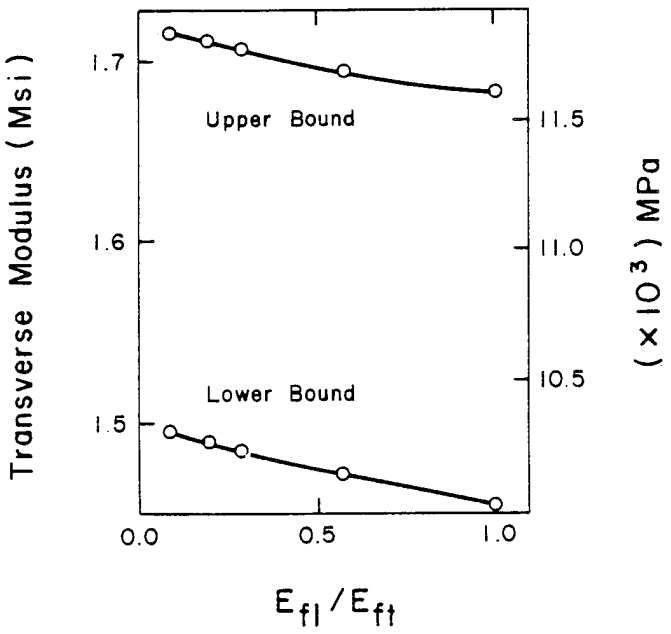

Fig. 6.7 Evolution of Upper and Lower Hashin Bound as a Function of the Ratio of Longitudinal and Transverse Moduli

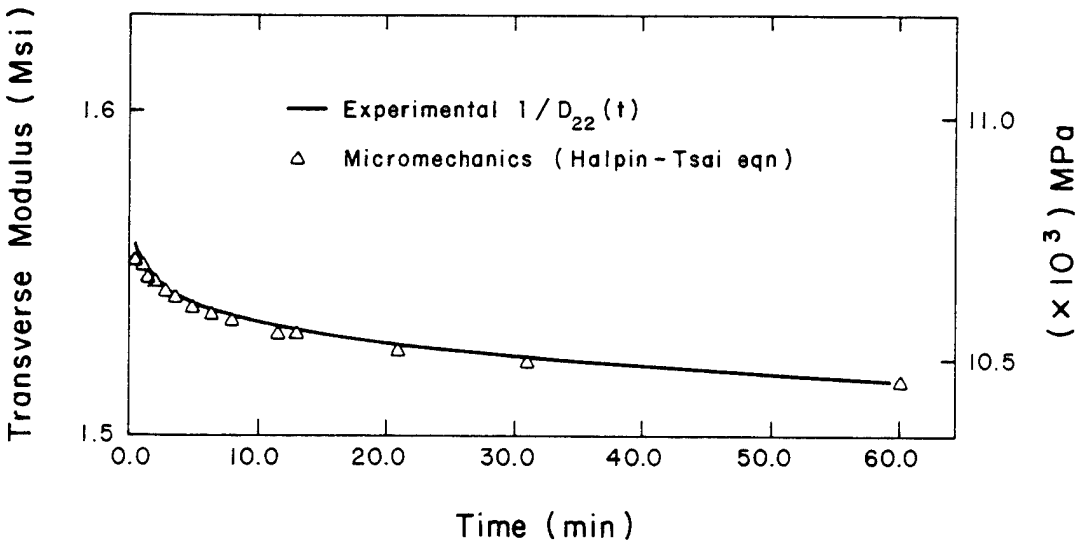

Fig. 6.8 Comparison Between Experimental (-) and Micromechanics (Δ) Prediction of E_{22} Versus Time (T300/934

An attempt was made to model the creep response with a Schapery type power law equation

$$D(t) = g_0^{(T)} D_0 + \frac{g_1^{(T)} \cdot g_2^{(T)}}{a_\sigma^n} D_1 \cdot t^n \qquad (6.3)$$

where all quantities are as defined previously in Equation 3.49. The upper index T indicates that the nonlinearizing functions are evaluated in the transverse fiber direction.

A series of 40 (one hour) creep and (ten hour) creep recovery tests at eight different stress levels and five different temperatures, using a fresh specimen at each new temperature, did not show any dependence of the transverse compliance on the stress level. In other words,

$$g_0^{(T)} = g_1^{(T)} = g_2^{(T)} = a_\sigma = 1$$

which means that the transverse response was linear within our time frame and within experimental error.

The stress-strain diagram (Fig. 6.9) obtained from an Instron test at 100°F (37°C) also shows little dissipation and a fracture strain of about 5000 microstrain.

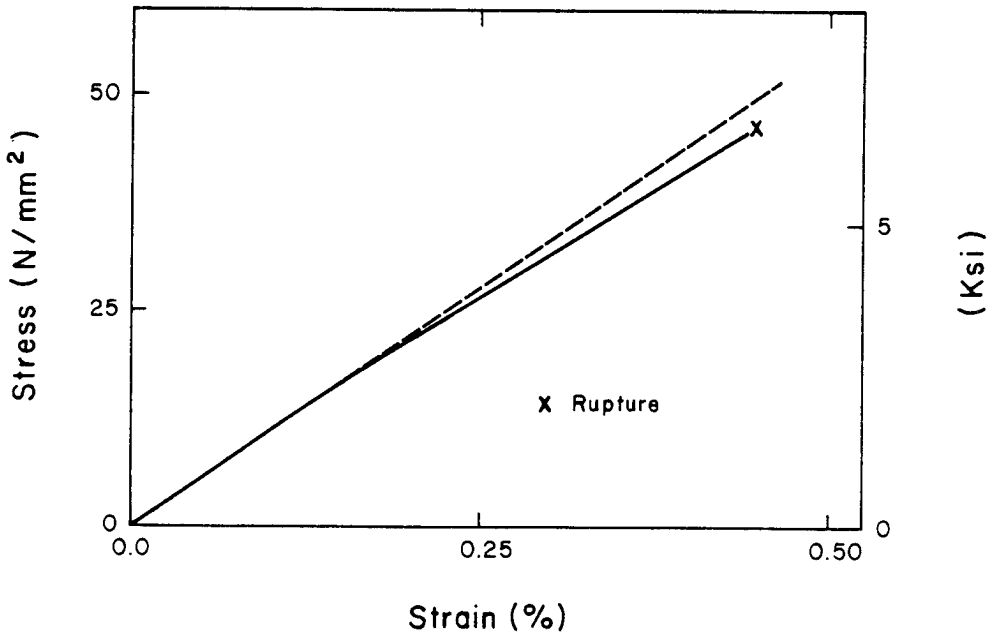

Fig. 6.9 Stress-Strain Curve (Solid Line) for $[90]_{8S}$ T300/934 Laminate at Room Temperature (0.05 in/min) Compared with Linear Response (Dashed Line).

Equation (6.3) reduces to

$$D(t) = D_0 + D_1 t^n \tag{6.4}$$

Figure 6.10 shows the temperature dependence of the first term (D_0) in Eq. (6.4). It is clear that the dependence is almost perfectly linear in the temperature interval which we studied. The temperature dependence of the coefficient D_1 has a pronounced nonlinear variation as can be seen in Fig. 6.11. Notice that the ω-mechanism which was identified in the neat resin (Fig. 5.2) is also clearly visible in Fig. 6.11. However the minimum in the curve is now approximately 20°F ($\approx$ 10°C) higher.

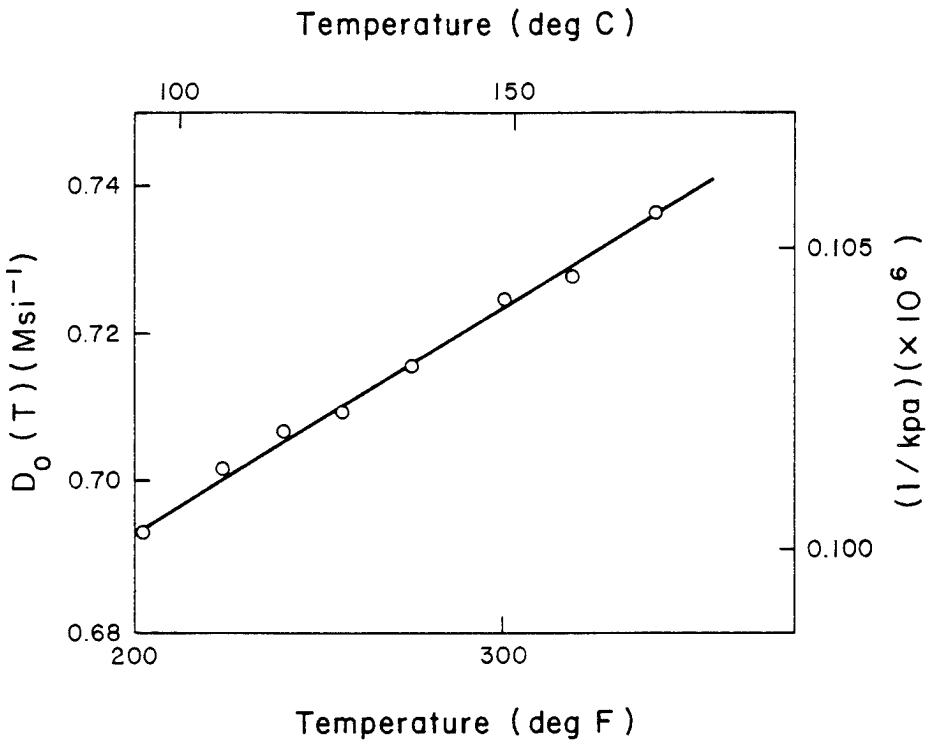

Fig. 6.10 Instantaneous Transverse Compliance as a Function of Temperature

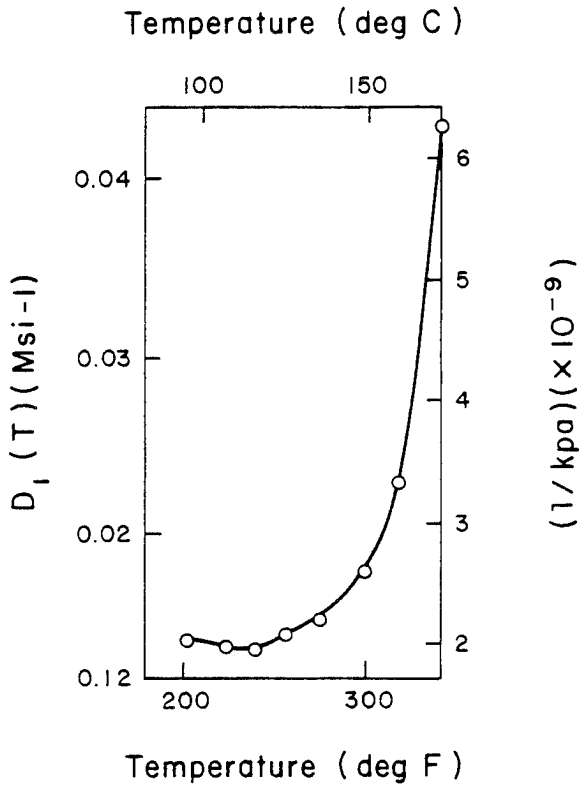

Fig. 6.11 $D_1(T)$ as a Function of Temperature

Such differences have been reported for the primary transition by a number of investigators [76,79,92], but the cause is unclear.

The long time creep data plotted in Fig. 6.12 reveals that our experimental time scale for short time creep (1 hour) was probably too short to be able to discriminate between stress dependence of the compliance curve and small experimental irregularities such as misalignment in the load train, fluctuation in temperature, etc. Or, in other words, the shorter the test period, the more precise the test conditions need be in order to allow stress dependent discrimination of the compliance curve. Thus our earlier conclusion about the linear viscoelastic or stress independence of our transverse compliance data for T300/934 needs to be reexamined over a longer time scale. However

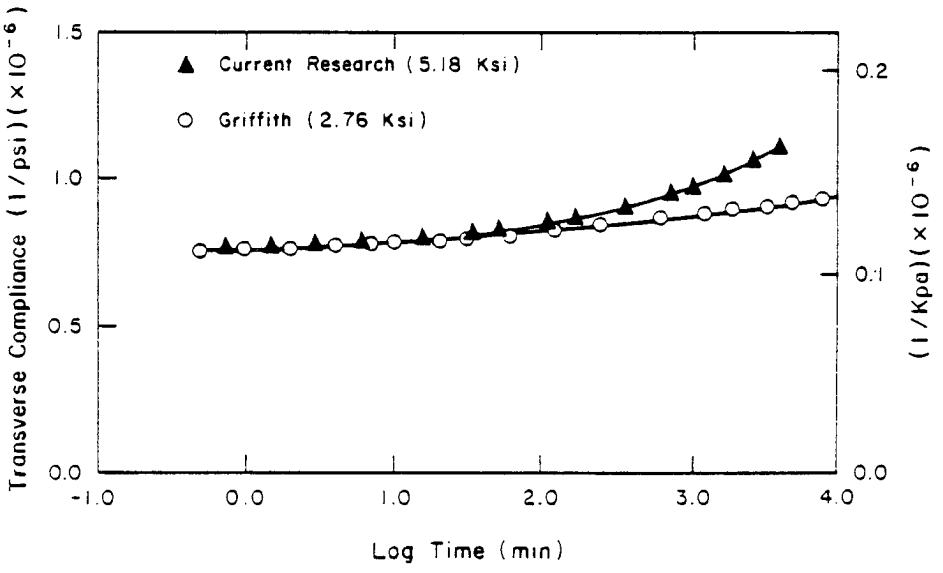

Fig. 6.12 Comparison of Transverse Compliance Versus Time for Moderate (2.76 Ksi) 19 Mpa) and High (5.18 Ksi = 35.7 Mpa) Stresses

for a first approximation, linear would be a reasonable assumption.

6.3 Results and Discussion on $[10]_{8S}$

6.3.1 Experimental Background

An efficient intralaminar (in plane) shear characterization technique known as the 10-deg off-axis test has been proposed and analyzed by C. C. Chamis and J. H. Sinclair [93]. Their analysis shows that the major contribution to fracture comes from intralaminar shear, i.e. the configuration activates a long continuous shear path, along which load diffusion into the reinforcing fibers occurs. One difficulty with the off-axis test is that shear coupling effects are a function of the load to fiber angle or the aspect ratio. The Pagano-Halpin [94] shear coupling analysis was used to generate Fig. 6.13. Their analysis suggest that for an aspect ratio or off-axis angle of 10°, the shear modulus, $G_{12})_{approx.}$, is approximately 10% higher than the true shear modulus G_{12}. This is confirmed by the inverse shear compliance versus temperature plot of Fig. 6.14 which indicates a measured value somewhat above .8 MSI at room temperature, while a widely published value is closer to .7 MSI.

Two back-to-back 45 deg rosette strain gages [WK-06-062R-350] were used to eliminate out of plane bending from test results. The orientation of the gages with respect to the fiber axis was checked under the microscope. Misalignments were taken into account during subsequent data reduction. Figure 6.15 shows the orientation of the strain gage rosette as well as the manner in which aluminum tabs were adhesively bonded to each specimen.

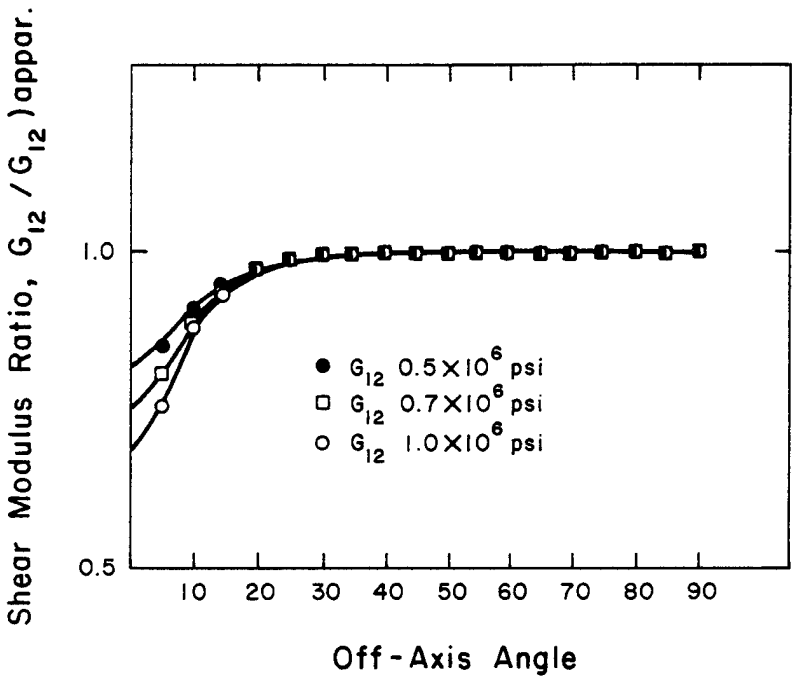

Fig. 6.13 Ratio of Actual to Apparent Shear Modulus in Off-Axis Test.

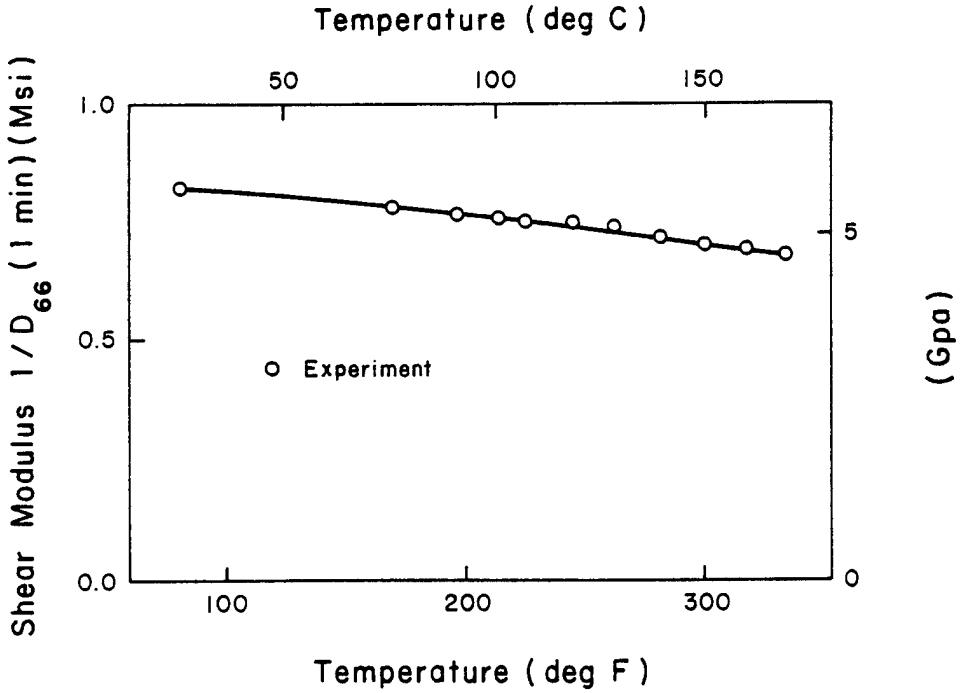

Fig. 6.14 Shear Modulus as a Function of Temperature.

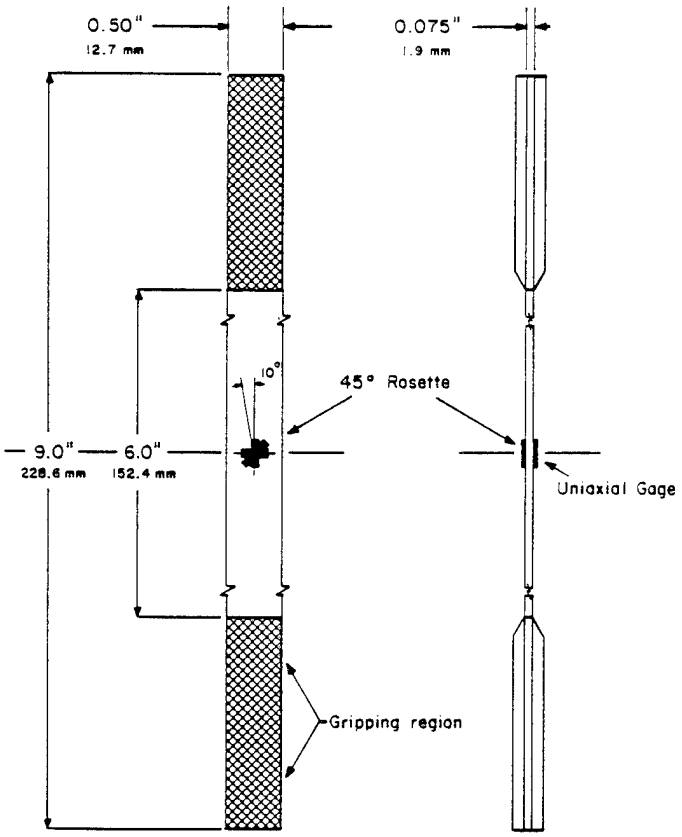

Fig. 6.15 Specimen, Strain Gage and Tab Configuration.

Each specimen was postcured with the same temperature cycle as were the transverse and neat resin coupons.

The shear compliance $D_{66}(t)$ for a 10° specimen loaded in tension as illustrated schematically in Fig. 6.1 is given by the following expression

$$D_{66}(t) = \frac{w \cdot h \cdot (-.598\ \epsilon_x(t) + 1.879\ \epsilon_{45}(t) - 1.282\ \epsilon_y(t))}{.171\ \sigma_x}$$

where $\epsilon_x(t)$, $\epsilon_{45}(t)$ and $\epsilon_y(t)$ are the strains measured along the longitudinal, 45° and transverse directions of the specimen, respectively. The angle between the measured strain directions and the fiber-direction of the material are 10°, 45° and 100° respectively. W and h represent

the width and thickness of the tensile coupon. The strains measured along the x and 45° direction were positive, while the strain measured along the y-direction was negative. It should be noted, of course, that if the rectangular rosette is mounted with the 90° and 45° arms different than shown in Fig. 6.15, different signs will be obtained and the preceding equation for D_{66} must be altered appropriately. The shear compliance D_{66} is thus easily obtained through simultaneous measurement of $\epsilon_x(t)$, $\epsilon_{45}(t)$ and $\epsilon_y(t)$ but caution should be taken with respect to the gage orientation.

6.3.2 Experimental Results

The shear compliance versus log t curves obtained at four different temperatures are shown in Figs. 6.16a, b, c and d. They clearly indicate the behavior to be dependent upon stress. In the context of nonlinear viscoelasticity, as discussed earlier in Chapter 3, this means that a set of molecular processes which are sensitive to stress must also contribute to the observed deformation in addition to those normally associated with linear viscoelasticity.

A definite accumulation of nonrecoverable permanent strain was observed during the creep and creep-recovery test sequences. The amount obtained at 246°F (119°C) is shown as an example in Fig. 6.17. Thus the molecular structure moves out of the positions which it occupied on release of the stress but does not reach its former spatial arrangement under the action of the restoring forces. One possibility is that this former spatial arrangement is unattainable due to a "plasticity" type structural change in the matrix phase. Thus, for our material it seems

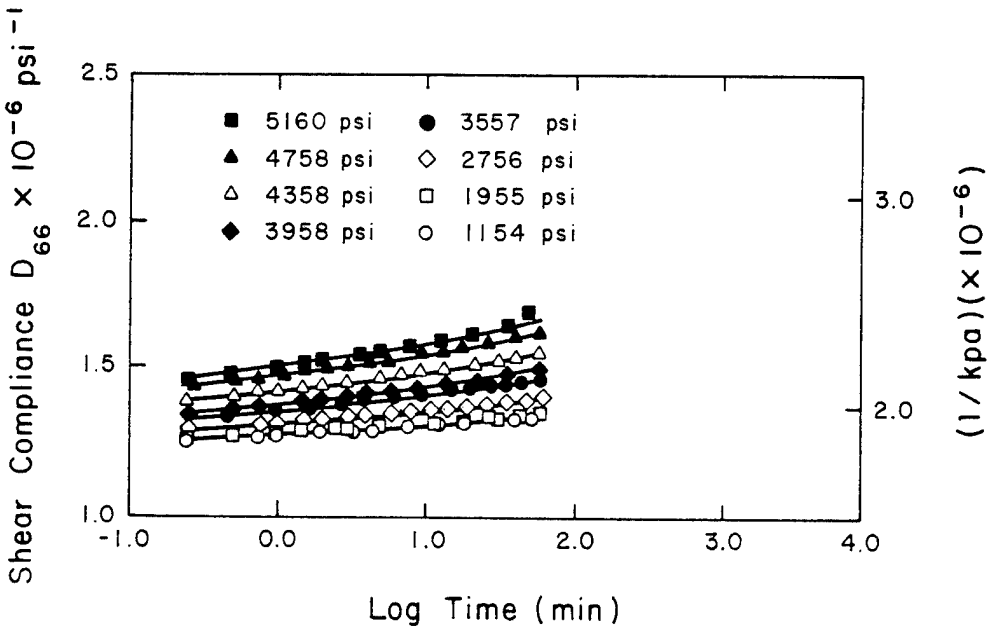

Fig. 6.16a Shear Compliance Versus Time at 246°F (119°C).

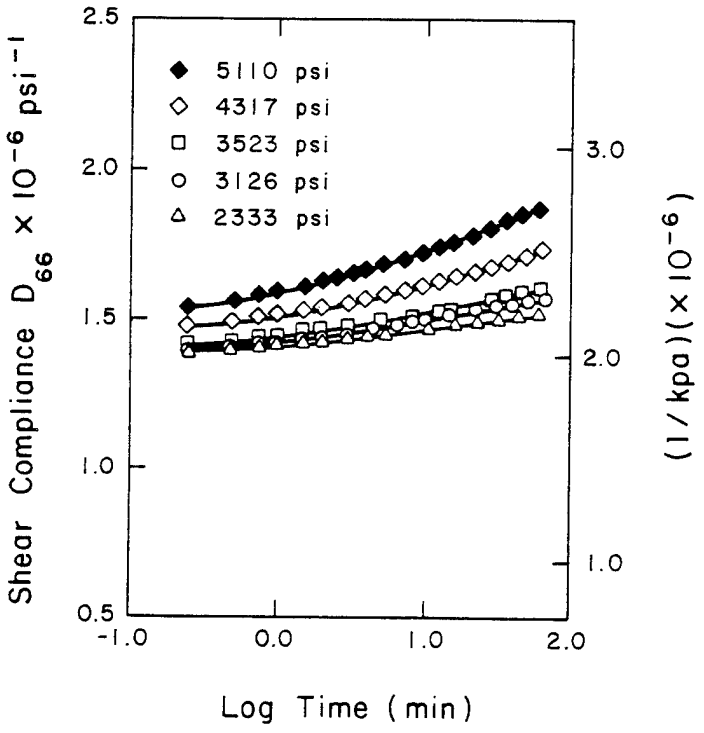

Fig. 6.16b Shear Compliance Versus Time at 300°F (149° C).

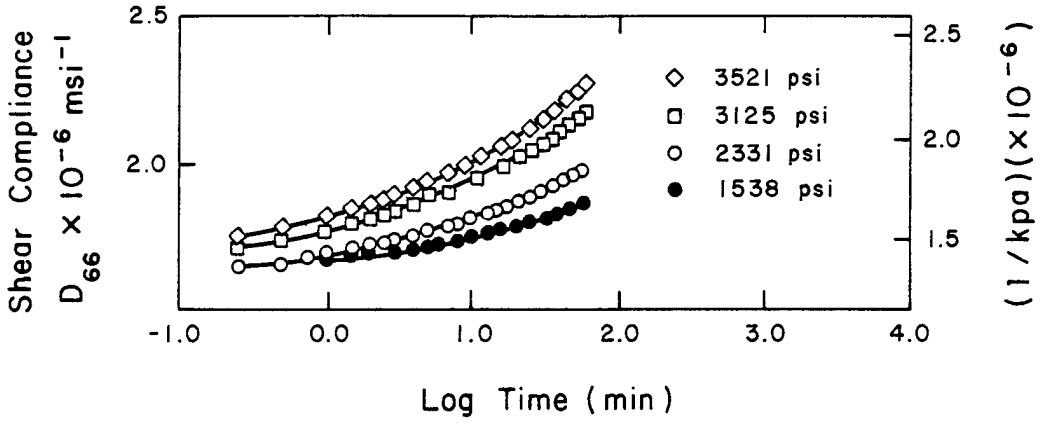

Fig. 6.16c Shear Compliance at 320°F (160°C).

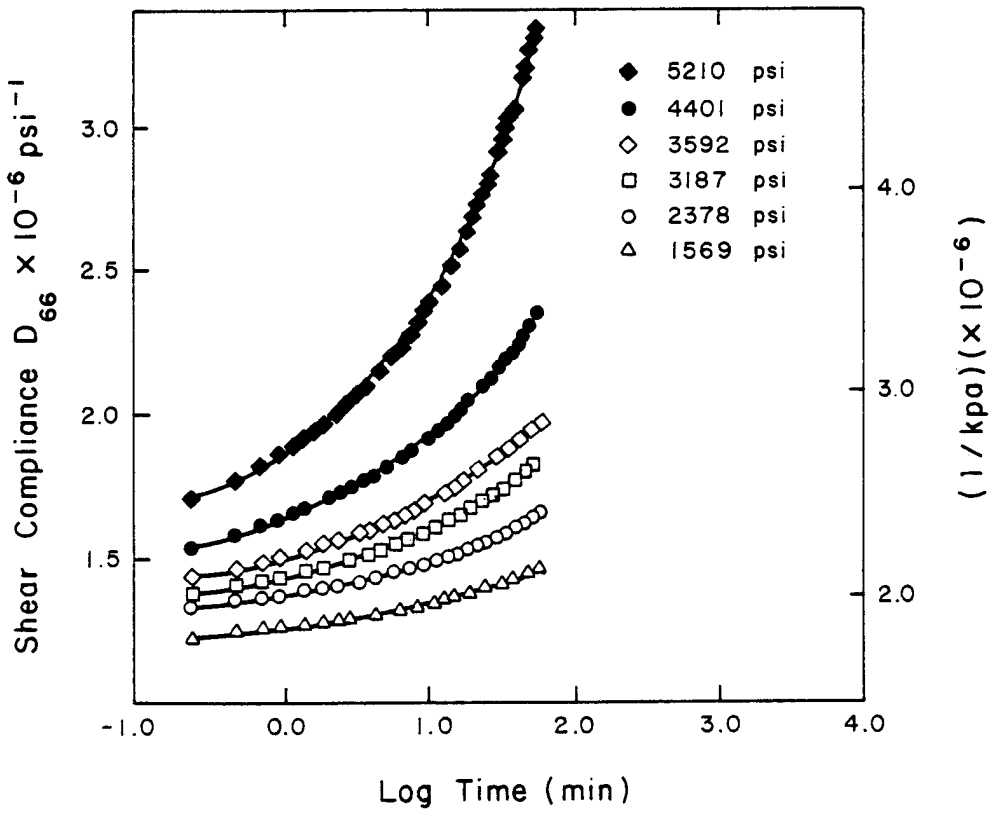

Fig. 6.16d Shear Compliance Versus Time at 335°F (168°C).

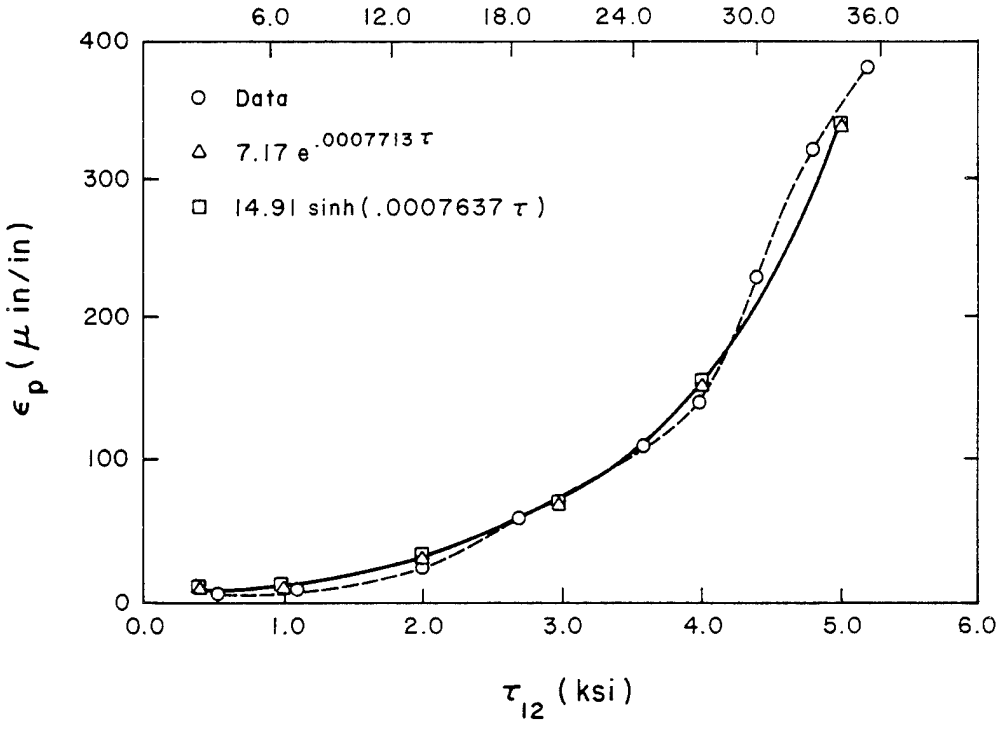

Fig. 6.17 Permanent Strain Accumulation During 10 Deg. Off Axis Test at 246°F (119°C).

not possible for nonlinear viscoelasticity to occur without involving other irreversible deformation mechanisms. This conclusion disagrees with results obtained by Ferry [28] on PMMA. Shear creep deformation up to 5% were fully recoverable although the linear viscoelastic limit was below 1%.

A number of investigators mechanically condition specimen prior to creep testing. The reason is that during the first creep test a certain amount of deformation takes place which does not recover upon removal of the stress. In subsequent creep tests on the same specimen at the same or smaller load there is no such nonrecoverable creep. The stress-strain relationship thus becomes repeatable. The material is therefore considered "mechanically conditioned." Leaderman [22] showed

that the permanent set in fibers disappears when the fiber was steamed under no load and then dried. Thus no real structural change or plasticity was introduced by the conditioning process.

This author fears, however, that a significant volume of the matrix material might be yielded by the very inhomogeneous stress fields caused by the geometrical nature of the composite material. Evidence of such a matrix yielding phenomenon in shear deformation, based on a finite element analysis, was published by Foye [95]. His results shown in Fig. 6.18a give some indication of the progress of the plastic zone boundaries due to shear loading in repeating elements of a graphite-epoxy composite with 50% fiber by volume. Yielding initiates at the interface in an area enclosed by plastic zone boundary number 1. The plastic zone boundaries numbered 2 through 8 correspond to increasing postyielding load levels. Figure 6.18b, on the other hand, shows that in transverse deformation, yielding first occurs at a point in the matrix midway between two adjacent fibers. Foye also showed that initial yielding of the composite during the transverse deformation mode occurs at slightly lower average normal stress levels than the bulk matrix. In the shear deformation mode the composites yielded at much lower average shear stress levels than the bulk matrix.

In conclusion, preconditioning was not made part of the testing program since it was feared that the stress-strain relationship would become repeatable at the expense of changing the matrix phase to an entirely new material in the sense of a plasticity type shakedown model.

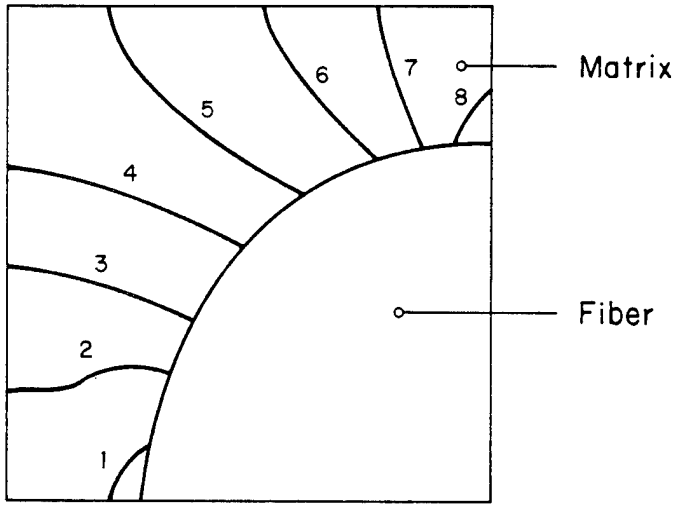

Fig. 6.18a Inhomogeneous Stress Distribution Due to Shear Deformation Due to Shear Deformation After Foye [95].

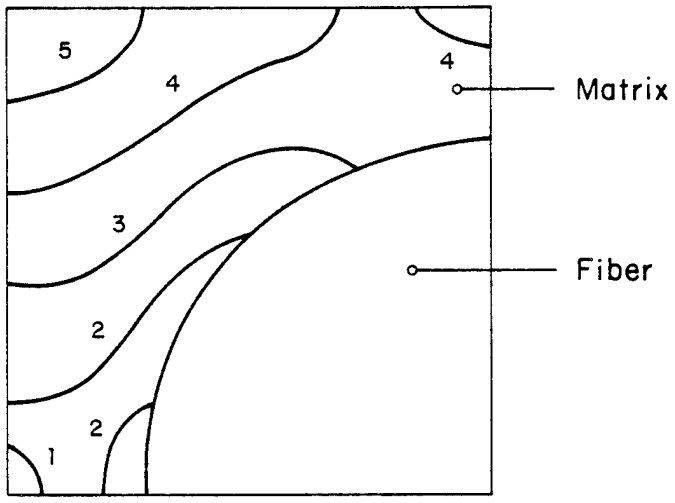

Fig. 6.18b Inhomogeneous Stress Distribution Due to Transverse Deformation After Foye [95].

The creep response in the shear deformation mode was modeled with the power law

$$D(t) = g_o^{(S)} D_o + \frac{g_1^{(S)}\, g_2^{(S)}}{a_\tau^{\,n}} D_1 \cdot t^n \qquad (6.5)$$

The upper index (S) indicates that the nonlinearizing functions are evaluated in the shear mode. Plots of the nonlinearizing functions $g_o^{(S)}$, $g_1^{(S)}$, $g_2^{(S)}$, and a_τ obtained at 246°F as a function of stress are shown in Figs. 6.19a to 6.19d. Similar curves are obtained at higher temperatures. It can also be seen that $g_1^{(S)}$ and $g_2^{(S)}$ vary in such a way with stress level, that their product is nearly unity and equation (6.5) for creep response becomes approximately

$$D(t) \simeq g_o^{(S)}\, D_o + \frac{D_1}{a_\tau^{\,n}}\, t^n \qquad (6.6)$$

6.3.3 Time-Stress Superposition Principle (TSSP)

A very useful viscoelastic concept is that time and stress are equivalent for describing viscoelastic behavior [7]. This is due to the fact that an increased tensile stress shifts the creep spectra towards shorter times as shown in Fig. 6.20a. Thus, as shown in Fig. 6.20b, creep observed for short times at a given stress τ_1 is identical with creep observed for longer times at a lower stress τ_o provided that these data are shifted on a logarithmic time axis. Similarly, portions of the creep curve for $\tau = \tau_o$ can be observed for stresses $\tau = \tau_1, \tau_2, \ldots$, as indicated by the curved segments shown in Fig. 6.20b. These curved segments can then be shifted along the log time axis to construct a composite curve or the sigmoidal master curve applicable for the given stress level τ_o, extending over many decades of time.

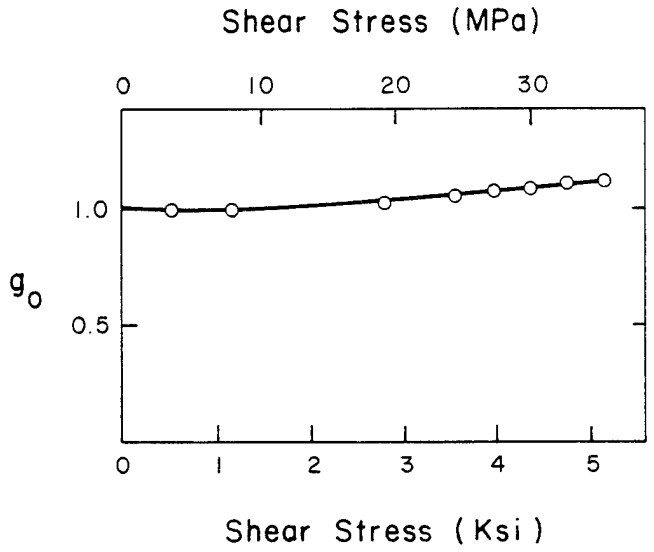

Fig. 6.19a Nonlinear Parameter $g_0(\tau)$.

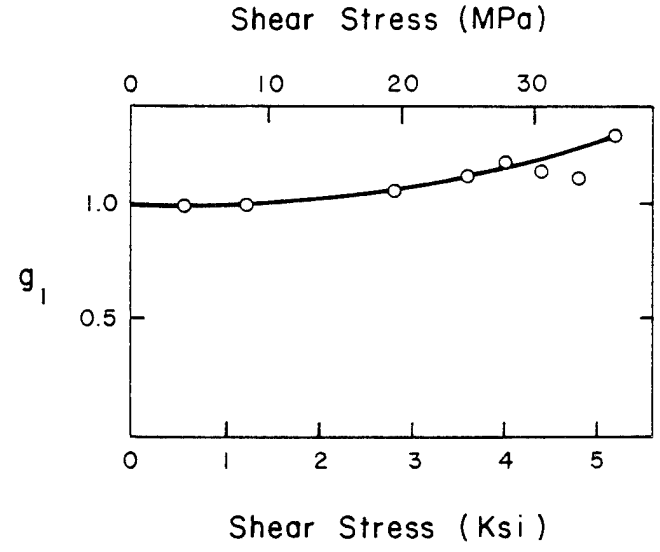

Fig. 6.19b Nonlinear Parameter $g_1(\tau)$.

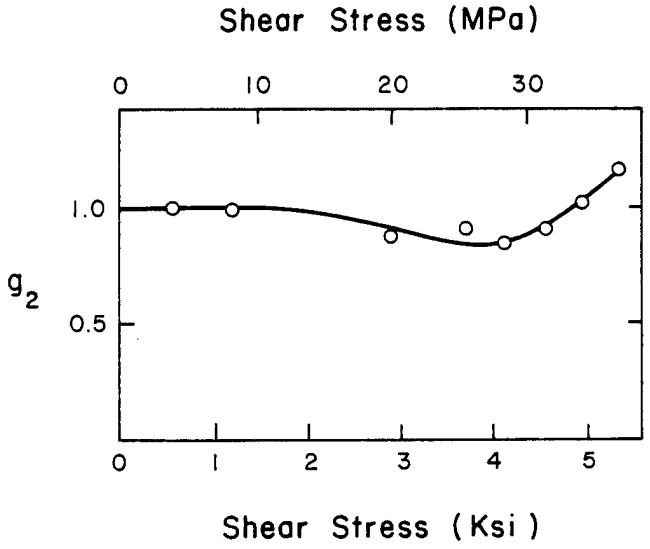

Fig. 6.19c Nonlinear Parameter $g_2(\tau)$.

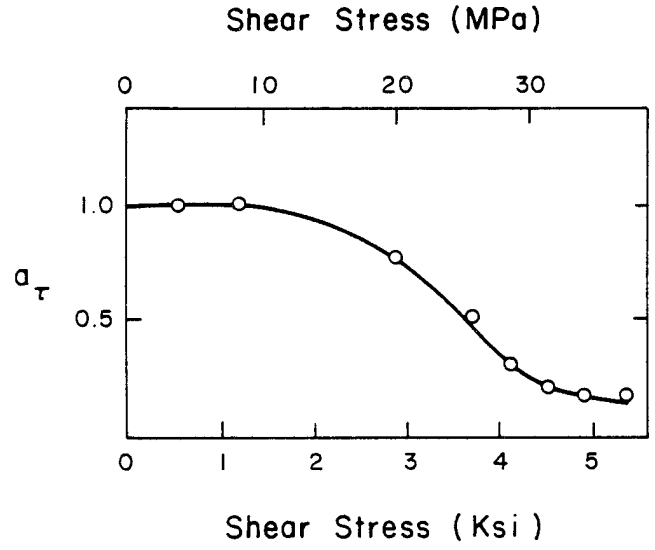

Fig. 6.19d Nonlinear Parameter $a_\tau(\tau)$.

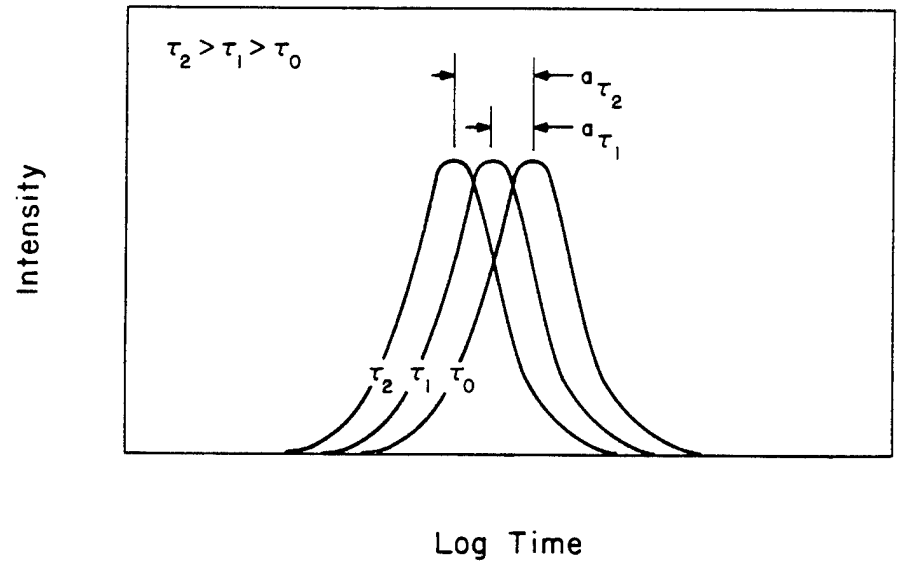

Fig. 6.20a Influence of Stress on Retardation Spectrum.

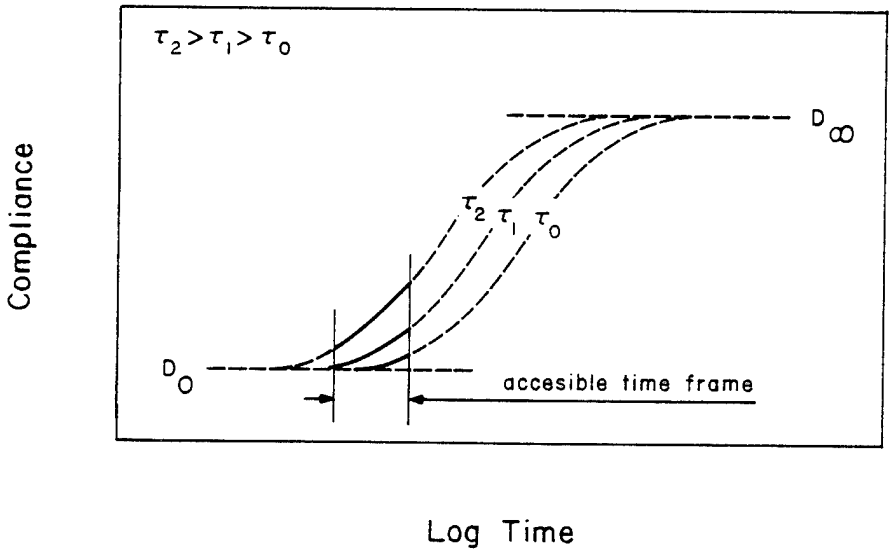

Fig. 6.20b Dependence of Compliance D on log t and Stress τ.

The logarithm of the shift factor a_τ for a particular curved segment is the horizontal shift necessary to allow it to join smoothly into the master curve. Each of the curved segments in Fig. 6.20b can be described by

$$\epsilon = g_o^{(S)} D_o + \frac{g_1^{(S)} g_2^{(S)} C}{a_\tau^n} \tag{6.7}$$

This same equation has a limited capability to represent a master curve using the form,

$$D = g_o^{(S)} D_o + g_1^{(S)} g_2^{(S)} C \left(\frac{t}{a_\tau}\right)^n \tag{6.8}$$

The reason for this limitation is due to the approximate nature of the power law used and was discussed earlier in Chapter 2.

The time-stress-superposition principle (TSSP) described above was used to convert the data of Figs. 6.16a, b, c and d to master curves for each temperature and are given in Figs. 6.21a, b, c and d. Also, equation (6.8) was used to analytically determine each master curve and the resulting shift parameters. The symbols represent the master curves produced graphically while the solid line represents the analytically produced master curve. Comparison of the shift factors found by the two methods are shown in Figs. 6.22a, b and c. A three-dimensional version of these results is shown in Fig. 6.23. As may be observed, excellent agreement was obtained between graphically and analytically produced master curves.

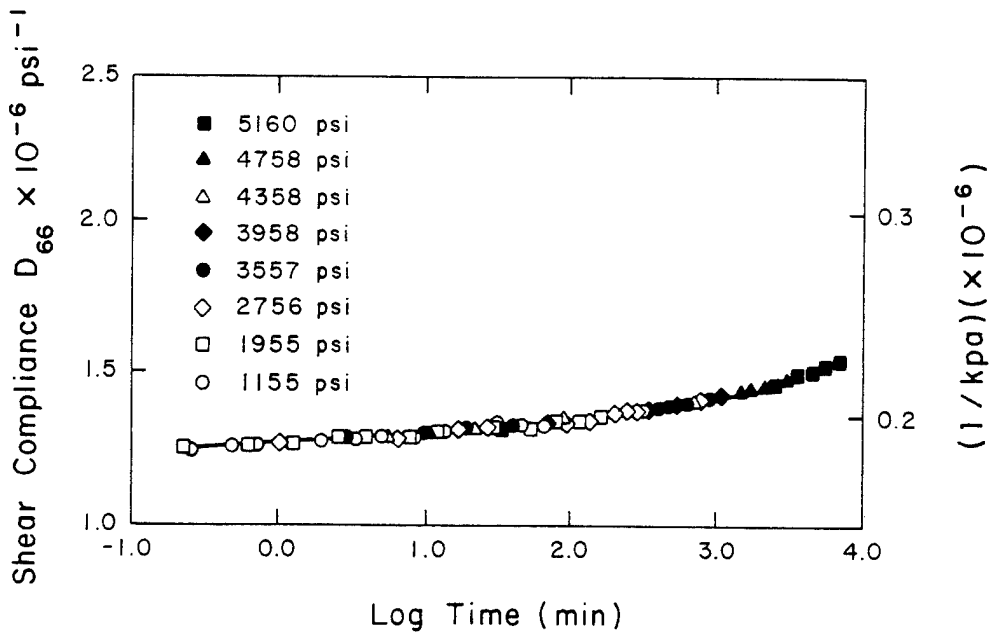

Fig. 6.21a S_{66} Master Curve for T300/934 at 246°F (119°C).

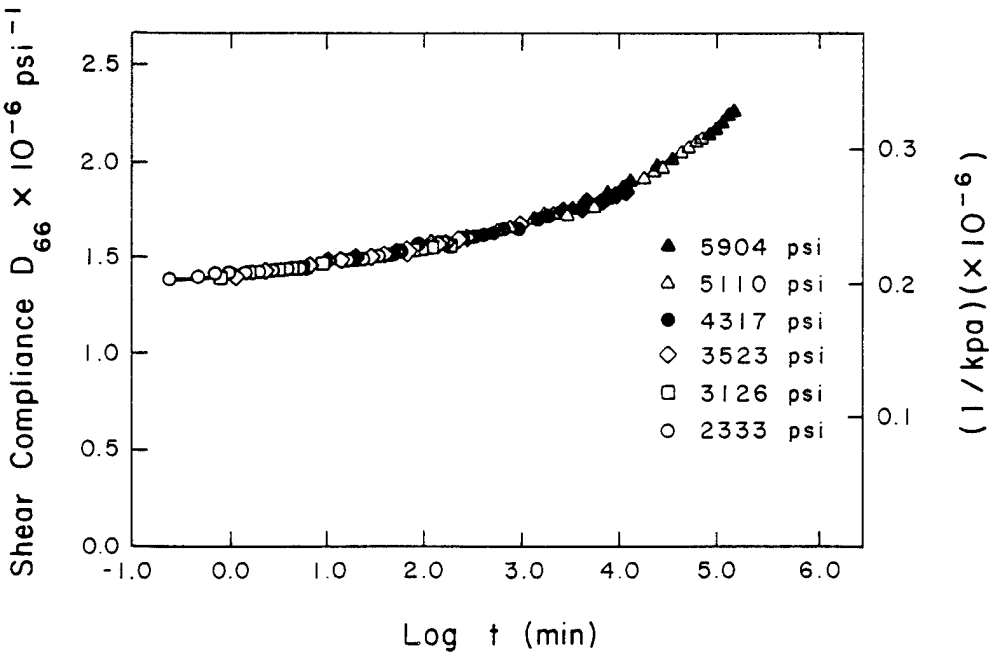

Fig. 6.21b S_{66} Master Curve for T300/934 at 300°F (149°C).

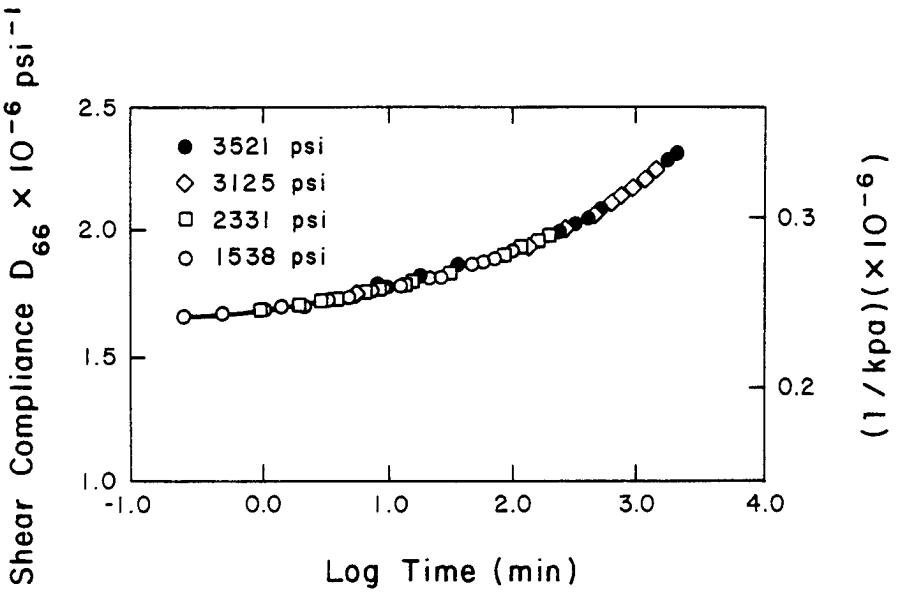

Fig. 6.21c S_{66} Master Curve for T300/934 at 320°F (160°C).

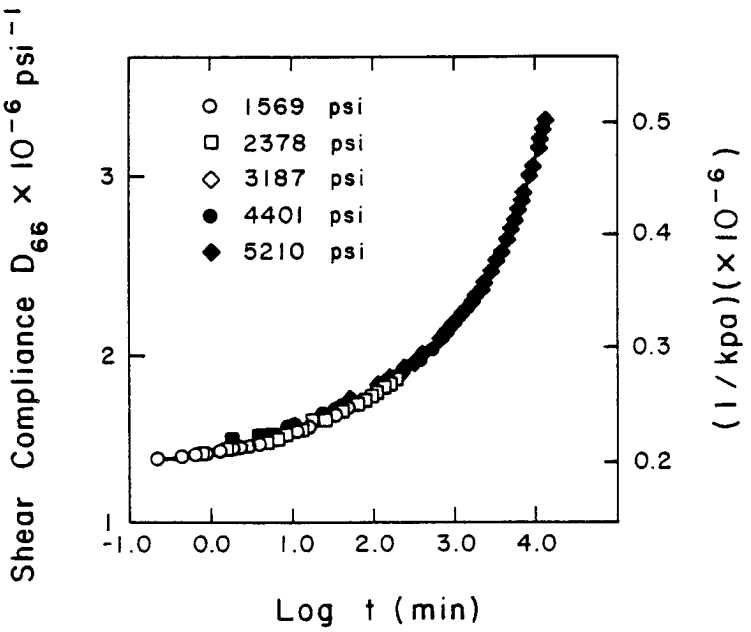

Fig. 6.21d S_{66} Master Curve for T300/934 at 335°F (168°C).

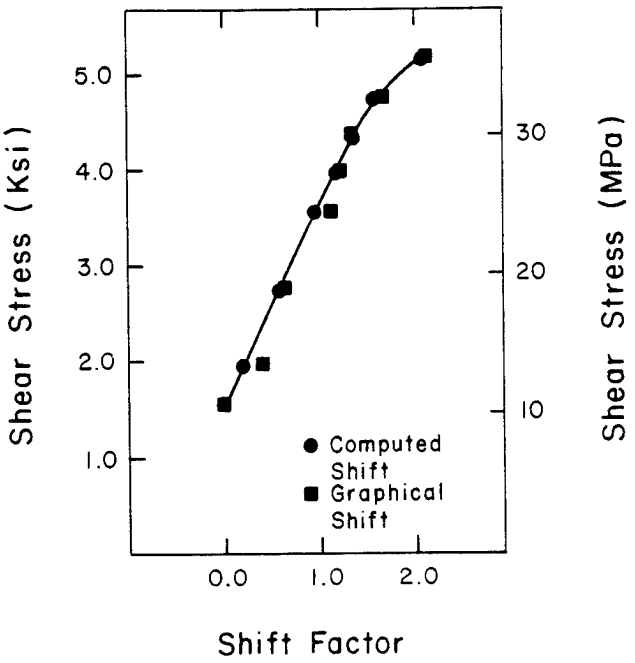

Fig. 6.22a Comparison of Graphical and Analytical Obtained Horizontal Shift Factor .10 deg - off - axis for 246°F (119°C).

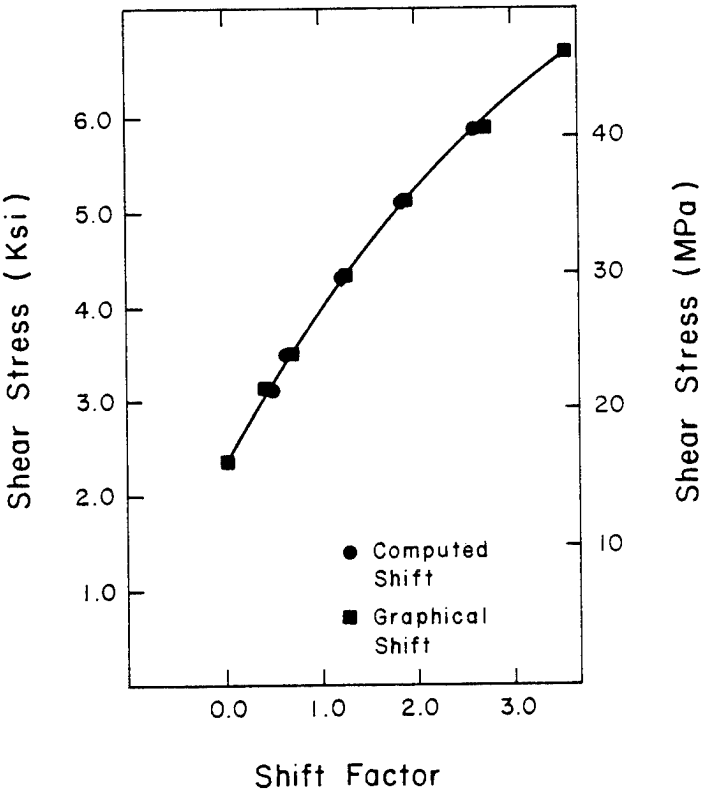

Fig. 6.22b Comparison of Graphical and Analytical Obtained Horizontal Shift Factor .10 deg - off - axis for 300°F (149°C).

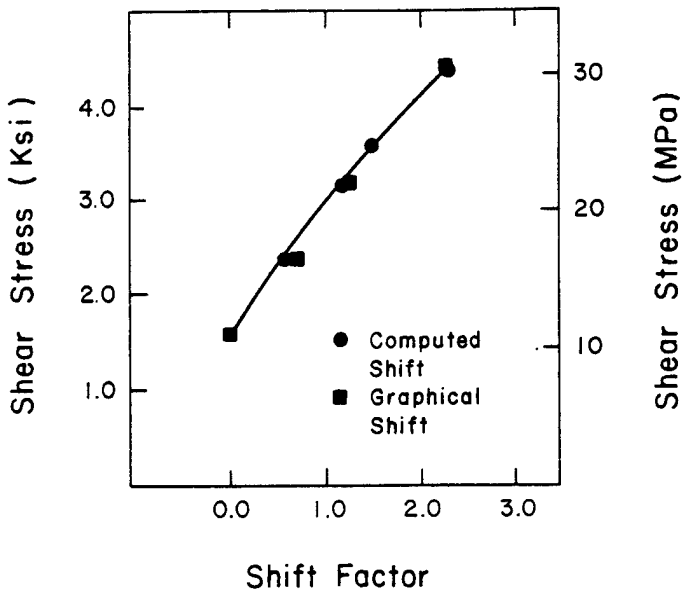

Fig. 6.22c Comparison of Graphical and Analytical Obtained Horizontal Shift Factor . 10 deg - off - axis for 335°F (168°C).

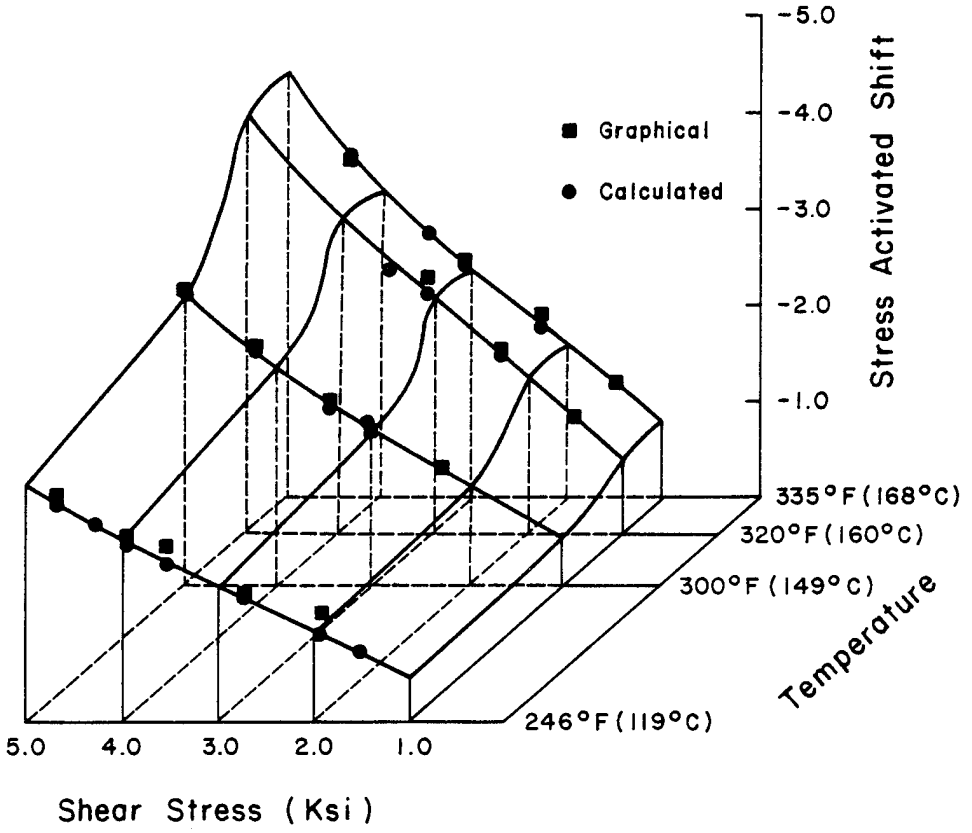

Fig. 6.23 Graphical and Computed Shift Function Surface for T300/934.

Often, a vertical shift as well as a horizontal shift is necessary to produce a smooth master curve. In fact, even a rotation of individual compliance curves may be necessary. The type of shifting needed depends on the behavior of the limiting compliances D_u and D_R as a function of stress as shown schematically in Fig. 6.24. A vertical shift of $D_u^{\tau} - D_u^{\tau_o}$ produces the dotted durve $D_\rho^{\tau}(t)$ which can be superimposed on $D^{\tau_o}(t)$.

A rotation would be necessary when the limiting compliances are affected differently by the stress intensity, i.e., when

$$\frac{D_R^{\tau} - D_u^{\tau}}{D_R^{\tau_o} - D_u^{\tau_o}} \neq 1 \tag{6.9}$$

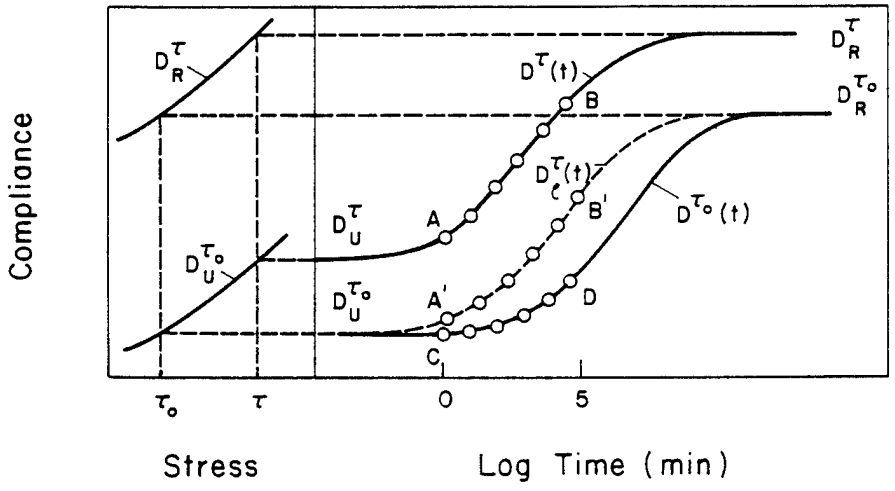

Fig. 6.24 Illustration of the Stress-Shifting-Procedure (Based on McCrum et al. [96]).

In our case, a small vertical shift was found necessary at 246°F. This shift however was nonexistent at higher temperatures as shown in Figs.

6.25a, b and c, where the vertical shift is plotted versus the horizontal shift.

It was thought initially that the true vertical shift $(D_u^{\tau} - D_u^{\tau_o})$, given in Fig. 6.24, was equivalent to $(g_o - 1)D_o$. This however leads to an overprediction due to the fact that the sigmoidal compliance curves change location with increasing stress. The implication is that even when the limiting compliance values are completely insensitive to stress (which turns out to be the case in this investigation) we still would record a g_o value different from unity since the retardation spectrum involves rapid creep on the time scale of microseconds. In conclusion, very accurate short time limiting compliance data is needed to obtain a proper estimate of the true vertical shift.

As a final conclusion, a long time control test remains the only criterion for checking a particular accelerated test method. These long term creep tests are currently being carried out and will dictate the adaptations necessary to achieve a proper mathematical modeling for the prediction of long term properties from short term test results. These final modeling equations should in some way reflect the mechanism of inelastic phenomena operating at the microstructural level.

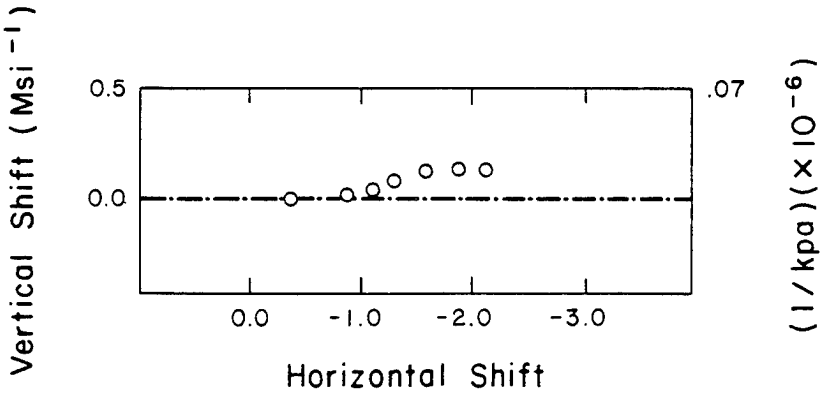

Fig. 6.25a Cross-plot of Horizontal and Vertical Shift at 246 Deg F (119°C)

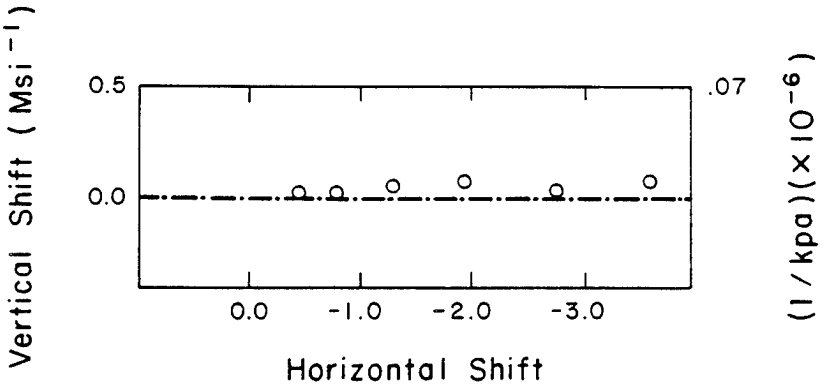

Fig. 6.25b Cross-plot of Horizontal and Vertical Shift at 300 Deg F (149°C)

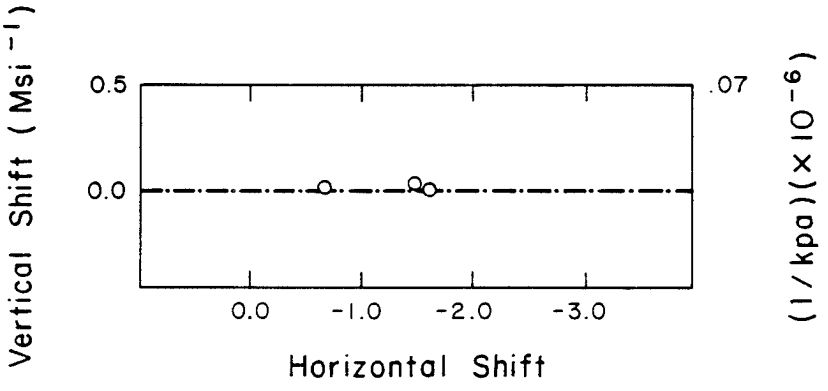

Fig. 6.25c Cross-plot of Horizontal and Vertical Shift at 320 Deg F (160°C)

Chapter 7

EXPERIMENTAL RESULTS AND DISCUSSION ON DELAYED FAILURE AND LAMINATE RESPONSE

7.1 Introduction

The usual concept of elastic deviatoric strain energy in which the Tsai-Hill anisotropic failure criterion is based cannot be carried over directly to viscoelastic materials without modifications to account for dissipation mechanisms. However, a better method to include dissipation as well as the entire history of deformation is the concept of free energy which can be used to define a "critical" stress state at the point of failure. A delayed failure model based upon these concepts was developed in Chapter 4.

The delayed failure model requires information on both creep and on creep rupture. An existing creep rupture data base for $[90]_{8s}$ and $[60]_{8s}$ orientations of T300/934 was available from the work of Griffith [7]. $[90]_{8s}$ creep data is given in Chapter 6. The needed $[60]_{8s}$ creep response to compliment the $[60]_{8s}$ rupture data can be inferred from the $[90]_{8s}$ and $[10]_{8s}$ data given in Chapter 6. However, it was decided to obtain the needed $[60]_{8s}$ creep response from new specimen because inferred response would introduce a hypothetical octahedral stress interaction factor, τ^{m}_{oct}.

7.2 Delayed Failure

7.2.1 Analysis on $[90]_{8s}$ Results

The compliance versus time curve at 320°F (160°C) and 1580 psi (10.88 MPa) (Fig. 6.8) was fitted with a six-element Kelvin model,

using a collocation scheme proposed by Schapery [97]. The resulting compliance D(t) can be expressed as:

$$D(t) = .71 + .041\,[1 - \exp(-t/.01)] + \\ + .041\,[1 - \exp(-t/1)] + .060\,[1 - \exp(-t/10)] \\ + .049\,[1 - \exp(-t/100)] + .164\,[1 - \exp(-t/1000)] \\ + .158\,[1 - \exp(-t/10000)] \times 10^{-6}\ \text{psi}^{-1} \qquad (7.1)$$

Based on this identification scheme, we can use Eqs. (4.9 - 4.11) to calculate the total creep energy, stored free energy and dissipated energy as a function of time as shown in Fig. 7.1. A gradual increase of the total dissipation with time originates from the energy consumption in the subsequent viscous elements. This dissipation has to be subtracted from the total creep energy, which is in this case equal to the potential energy loss of the external loading, in order to obtain the total stored free energy.

An identical evolution of the free energy was also obtained based on the power law parameters (D_0,D_1,n) which made it possible to evaluate Eq. (4.17) as a function of time. This procedure has a definite advantage in that it avoids a collocation scheme.

A comparison of the experimental creep-rupture results and the free energy based prediction shows that very good agreement was obtained as shown in Fig. 7.2. The full line (—■—) represents a given constant free energy line. Thus a creep rupture result is obtained from creep compliance data at the expense of only one additional parameter (w). Earlier attempts, in which we tried to correlate the total creep-energy with creep to rupture data, gave very poor agreement.

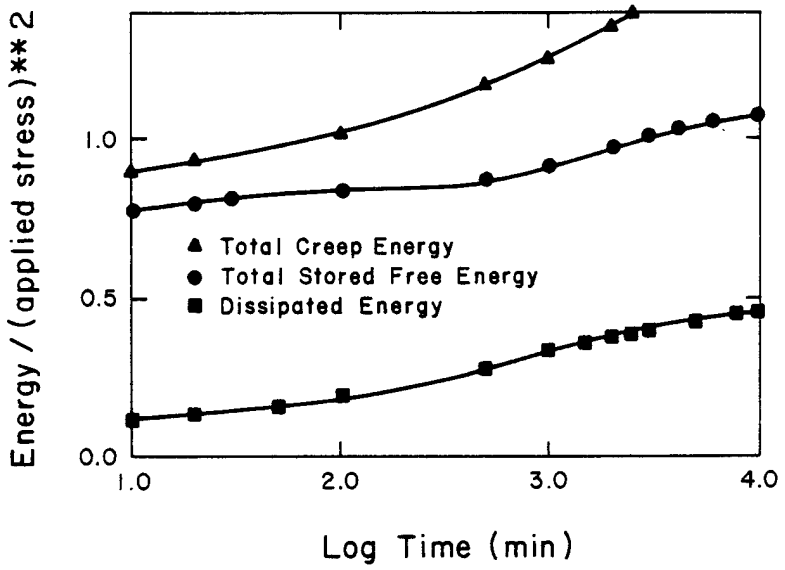

Fig. 7.1 T300/934: Evolution of Total Creep Energy, Total Stored Energy and Dissipated Energy as a Function of Time for $[90]_{8s}$ at 320 deg F (160° C).

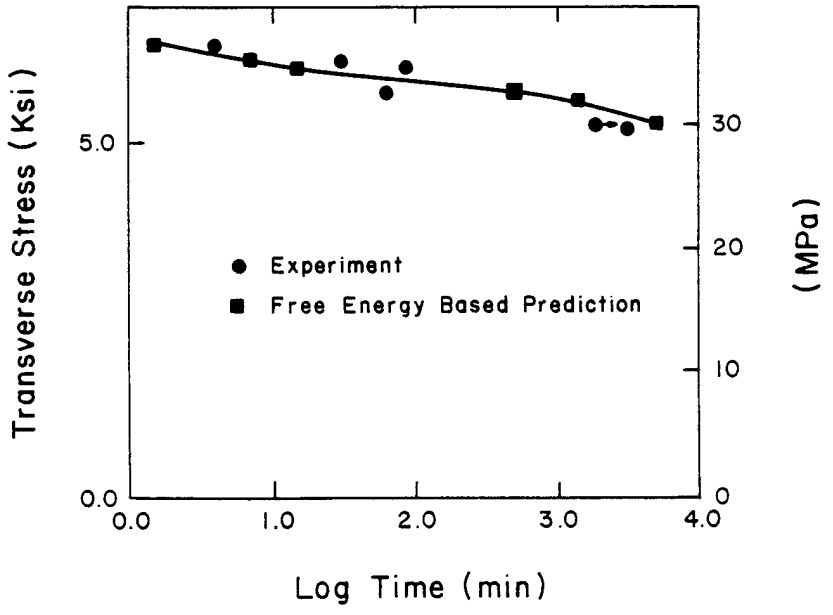

Fig. 7.2 T300/934: Comparison of Free Energy Based Creep to Rupture Prediction with Experimental Results Obtained on $[90]_{8s}$ at 320 deg F.

7.2.2 Analysis of $[60]_{8s}$ Results

Long time creep and creep recovery data were obtained on a 60-deg off axis specimen. The details on postcuring, strain gaging and testing were identical with those already discussed in Chapters 5 and 6.

A plot of the compliance change with log t at a stress level of 72% of ultimate is shown in Fig. 7.3. A result obtained by Griffith [7] on the same orientation but at 55% of ultimate is also shown in this figure. The curvature of these plots is clearly affected by the stress intensity. In addition, however, a rather large vertical shift would be needed to superimpose both curves. This could be due to matrix plasticity, since a rather large permanent deformation remained after creep recovery (Fig. 7.4). Martirosyan [98] gave evidence of such results which are reproduced in Fig. 7.5. The nonrecoverable creep deformation is seen to behave as an increasing-decreasing function with fiber angle. These bell-shaped curves are parameterized by a number that indicates the stress intensity as a fraction of ultimate. Obviously a large nonrecovered strain was observed which varies very nonlinearly with stress intensity.

The creep response curve at 72% of ultimate was again modeled with a six element Kelvin model, with an additional free dashpot in series, as shown in Fig. 7.6.

The free energy at rupture is seen to be constant for delayed failures in excess of 30 min. as shown in Fig. 7.7. Exactly the same free energy evolution with time was found again through the power law approximation. The power law parameters were evaluated, however, after subtraction of the free dashpot contribution.

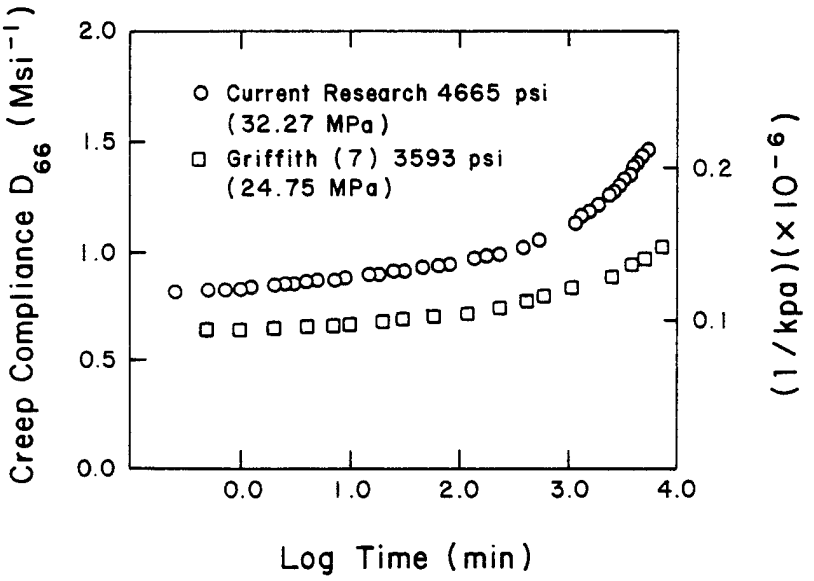

Fig. 7.3 Long Time Creep Compliance of $[60]_{8s}$ T300/934 at 320°F (160°C).

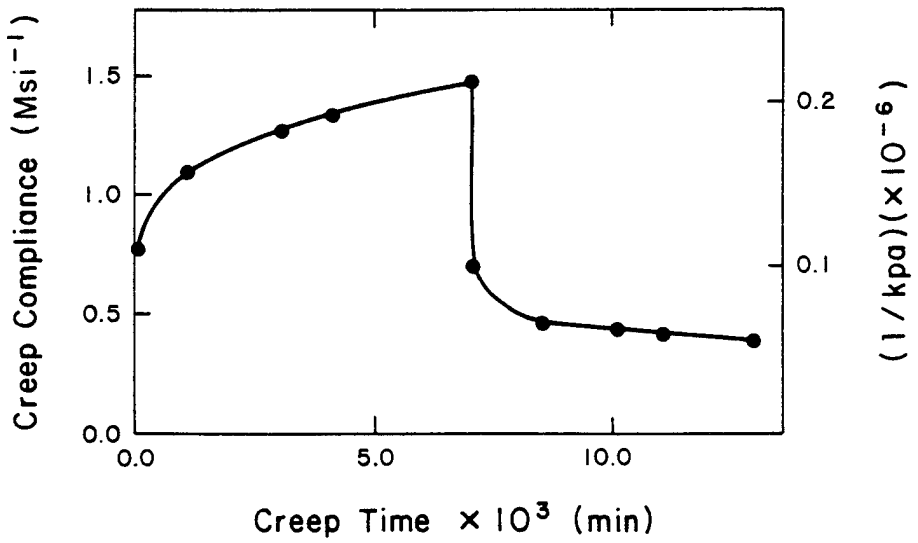

Fig. 7.4 Typical Creep Curve for $[60]_{8s}$ T300/934 at 320°F (160°C).

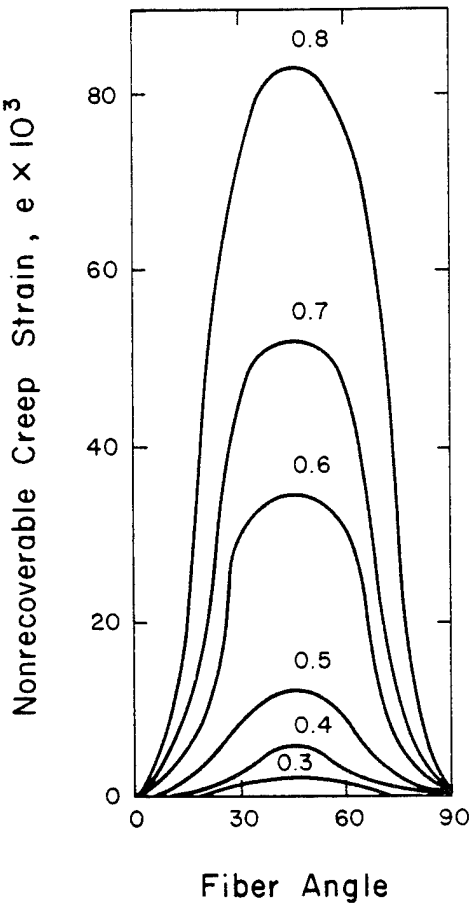

Fig. 7.5 Nonrecoverable Creep of Glasfiber Reinforced Plastic with Respect to Fiber Angle and Percent of Ultimate Stress.

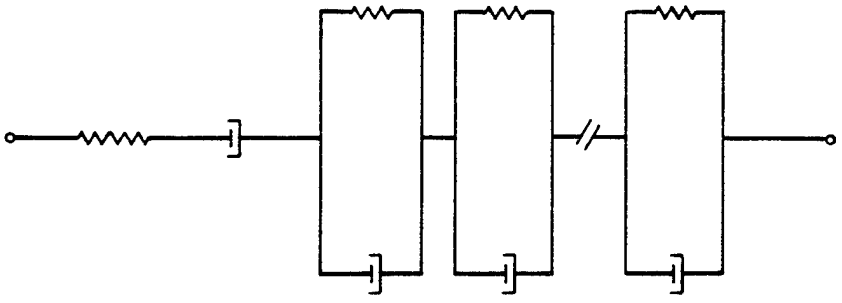

Fig. 7.6 Kelvin Element Used to Model Creep Response for $[60]_{8s}$ at 320°F (160°C).

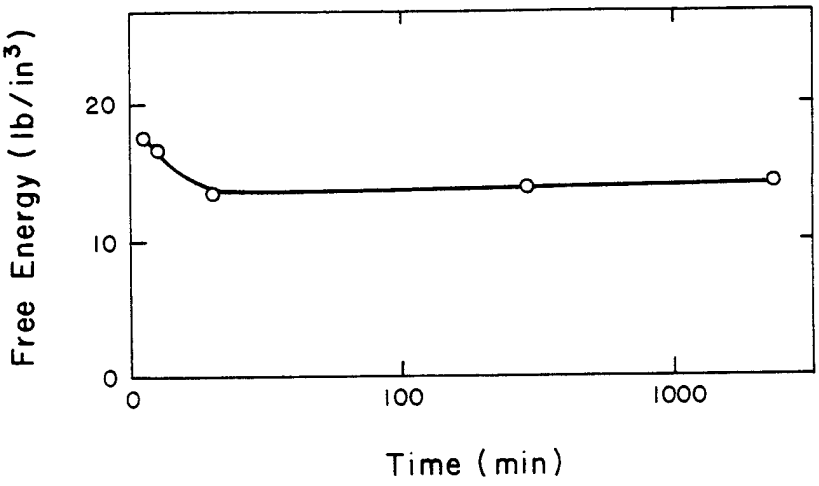

Fig. 7.7 Free Energy at Rupture for $[60]_{8s}$ T300/934 at 320°F (160°C).

A reasonable free energy based creep-rupture prediction was obtained, as seen in Fig. 7.8. Final conclusions however cannot be made yet, due to the limited number of experimental data points which are currently available.

7.3 Creep Response on $[90/\pm45/90]_{2s}$, Compared with Creep response of $[90]_{8s}$ and $[\pm45]_{4s}$ at 320°F (160°C)

It can be expected, that a $[90/\pm45/90]_{2s}$ laminate configuration will operate at a lower creep rate than a $[\pm45]_{4s}$, since the latter contains only two fiber orientations which allows scissoring action as may be visualized in Fig. 7.9. The former contains three fiber orientations and thus a fibre truss network is formed as shown in Fig. 7.9 which prevents scissoring.

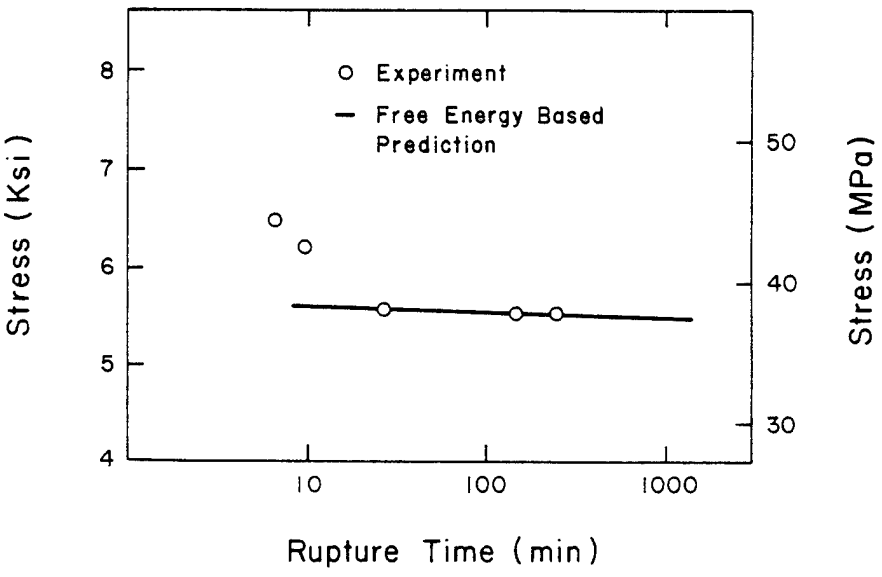

Fig. 7.8 Free Energy at Rupture Predictions for $[60]_{8s}$ T300/934 at 320°F (160°C).

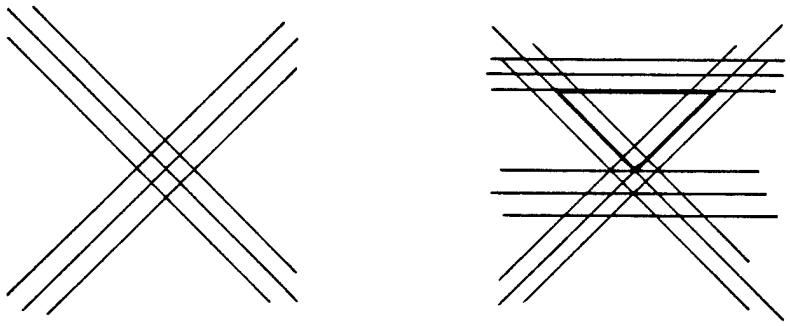

Fig. 7.9 Schematic of [±45] and [90/±45/90] Laminates with Fiber Truss Network in Latter.

Figure 7.10 compares the creep responses of three laminates. It is qualitatively clear that the $[\pm 45]_{4s}$ fiber orientation shows the most transient creep. This can also be quantified when we compare the power law coefficients, D_1, which are a function of stress, as given in Figs. 7.11. A comparison of the $[90/\pm 45/90]_{2s}$ laminate results with those for the $[90]_{8s}$ and $[\pm 45]_{4s}$ laminates reveals that the creep rate for the former is an order of magnitude less than that for the other orientations. The initial compliance however decreased only by 35% as compared to the $[\pm 45]_{4s}$ orientation.

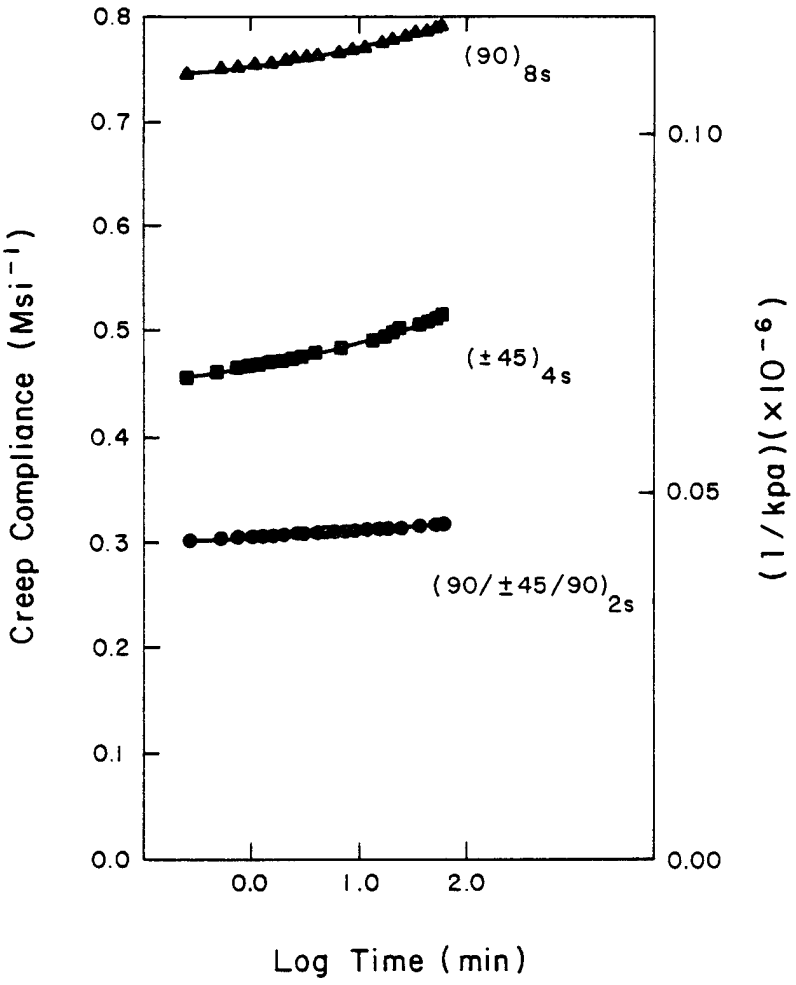

Fig. 7.10 Creep Compliance for Three T300/934 Laminates.

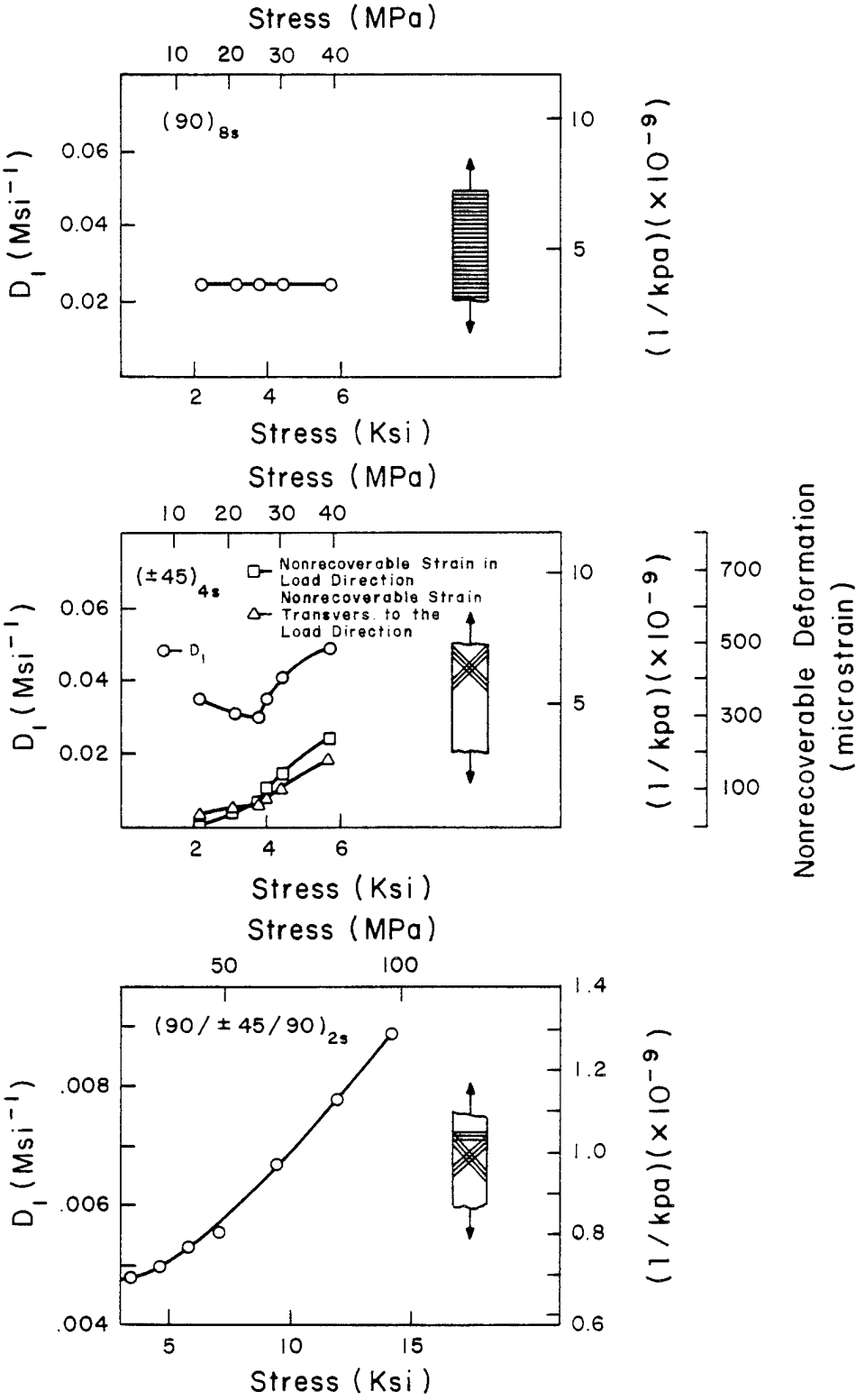

Fig. 7.11 Comparison of the Power Law Coefficient D_1 Obtained for Three Different Laminates at 320°F (160°C)

In conclusion, adding 90's to a ± 45 orientation increases the modulus by only 35% but decreases creep sensitivity by an order of magnitude.

Prior to testing the $[\pm 45]_{4s}$ laminate, we also put a strain gage transverse to the loading direction. This information allows us to obtain the shear compliance [99] which is given by

$$D_{66} = \frac{2(\epsilon_x - \epsilon_y)}{\sigma_x} \tag{7.2}$$

It was observed, however, that $\epsilon_x(t)$ and $\epsilon_y(t)$ had approximately the same magnitude. This led to untolerable large errors and even inconsistencies in the creep recovery data.

7.4 Numerical Prediction of $[90/\pm 45/90]_{2s}$ Laminate Behavior

The incremental nonlinear viscoelastic lamination theory-program, which was written and documented by Dillard [7] during an earlier phase of our research program, was used to generate the creep response of a $[90/\pm 45/90]_{2s}$ laminate.

A comparison of the numerical prediction with the experimental result at 70% of ultimate at 320°F (160°C) is shown, on an expanded scale, in Fig. 7.12. Reasonable agreement between predicted and measured compliance was obtained. Creep rupture-time, however, was even more seriously underpredicted, indicating a basic deficiency of the numerical approach which lies in its inability to reflect the microstructural effects of the laminate. This microstructural behavior was deduced using edge replicas [100], as shown in Fig. 7.13. An

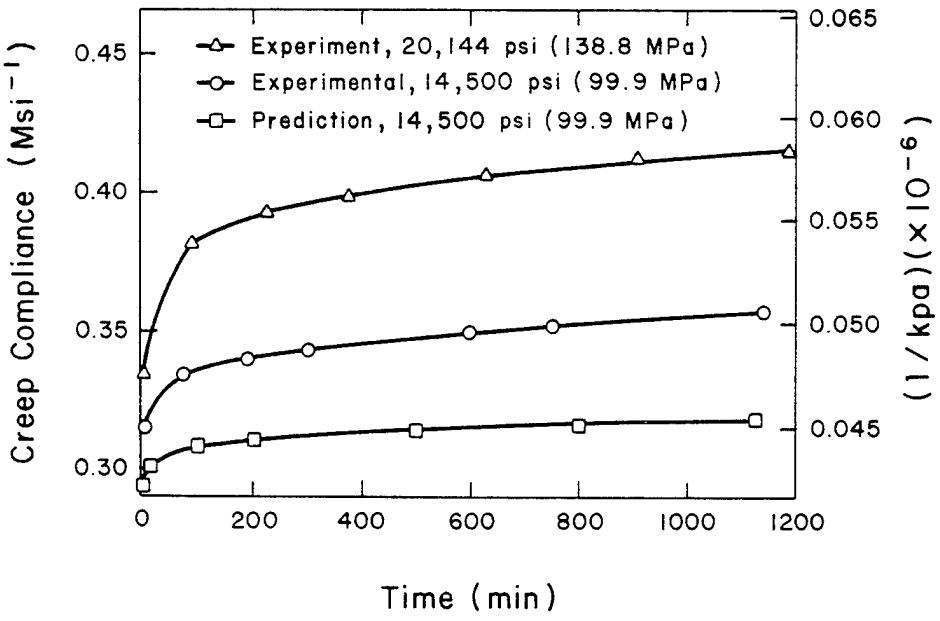

Fig. 7.12 Creep Compliance of a $[90/\pm45/90]_{2s}$ T300/934 Laminate at 320°F (160°C).

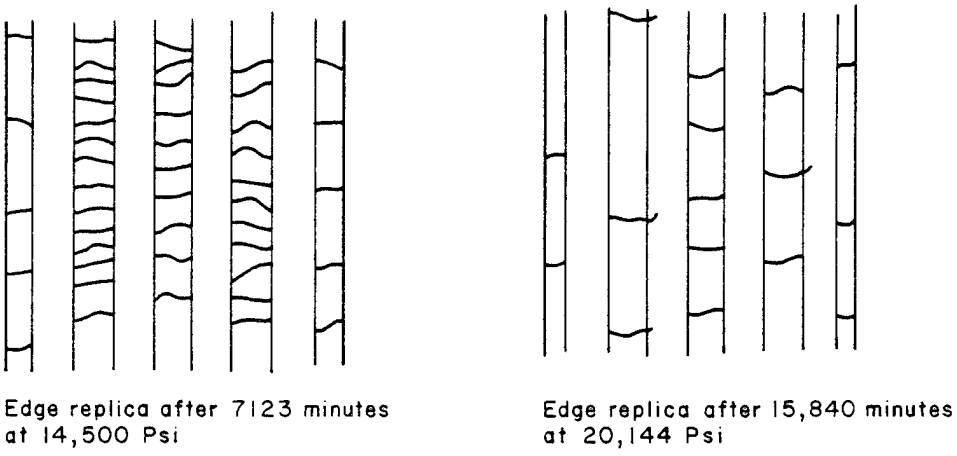

Fig. 7.13 Edge Replicas of $[90/\pm45/90]_{2s}$ Laminate.

attempt to model the stress transfer mechanism involved by means of a shear-lag model [101], which was simple enough for subsequent implementation in the laminate analysis program, turned out to be unsuccessful.

Comparison of the creep response at 97% of ultimate, also as shown in Fig. 7.12, with the response at 70% of ultimate indicates a large vertical shift. The edge replica, obtained after unloading, however, revealed a very different crack spacing between results at the two stress levels. The crack spacing in the 90-deg. oriented lamina is considerably less than in the previous case and some cracking in the 45-deg. oriented lamina became visible at the higher load level.

Figure 7.14 shows the irregularities in the strain reading at the beginning of the creep rupture experiment at 97% of ultimate. This indicates a sequence of events at the microstructural level, which could be deterministic in the selection process of the stress transfer mechanism.

More understanding in this area should be generated, including the answer on the question of whether or not crack healing sets in under certain unloading or strain-recovery conditions.

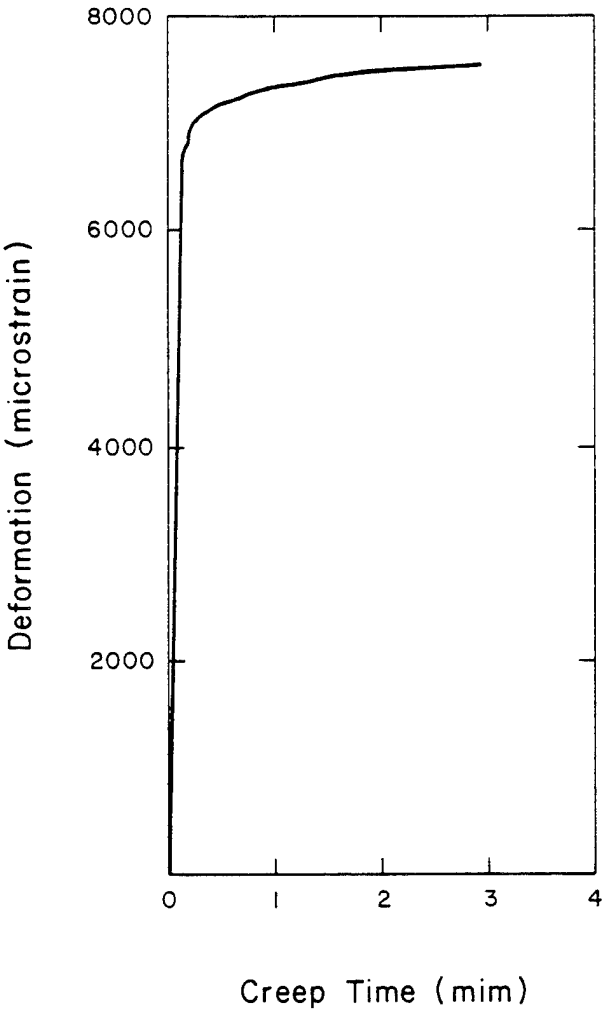

Fig. 7.14 Creep Curve at 97% of Ultimate.

Chapter 8

SUMMARY AND RECOMMENDATIONS FOR FURTHER STUDY

Different constitutive formulations able to model material nonlinearities in viscoelastic systems have been discussed. Nonlinear viscoelasticity models are often quite complicated, creating great experimental difficulties for the determination of material parameters. It was concluded that the approach advocated by Schapery is sufficiently general to account for stress-activated nonlinear behavior in polymers and composites. Particularly the following experimentally observed phenomena were easily modeled:

- An initial elastic creep-recovery which is greater than the initial elastic creep response
- A recovery behavior which is overpredicted by linear viscoelastic considerations (i.e. the actual recovery curve in the nonlinear range is flatter than in the linear range)

Creep and creep-recovery experiments which were carried out on the neat 934-resin did not reveal any stress dependent change in materials response other than plasticity. The analysis of time-dependent response, which is exclusively connected with specifics of the molecular structure revealed the existence of a secondary transition-temperature located between 200 and 250°F (93-121°C).

Essentially the same series of experiments were carried out on the T300/934 graphite-epoxy system. The transverse compliance $D_{22}(t)$ was found to be very stress insensitive. The shear compliance $D_{66}(t)$, on the other hand, turned out to be a sensitive function of stress.

The role of yielding and subyielding of the matrix phase, due to differences in loading path (transverse loading vs. shear loading) was discussed. Two uncoupled equations were fit to the data $D_{22}(t)$ and $D_{66}(t)$ respectively. The calibration of the material parameters $(D_0, C, n, g_0, g_1, g_2, a)$ was done by a computer routine. It is well known however that mathematical models fit data well when used on the stress paths which were applied for parameter calibration purposes. In order to account for stress interaction along general loading paths, the principle of octahedral stress, was borrowed from nonlinear approaches in isotropic viscoelasticity. The validity of this approach however needs to be carefully checked. The power law creep exponent (n), was found to be .23 and independent of stress and temperature. The secondary transition, which was identified in the resin, was also identified in the composite, but at a slightly higher temperature.

Short time data could be shifted graphically into a unique "master curve." The horizontal shift was found to be in very good agreement with the analytical shift ($\log a_\tau$). The vertical shift was very small, and became even nonexistent at higher temperatures. It was shown that vertical shifting is related to the behavior of the limiting compliances. An interesting point in this context is that Urzhumtsev [102] presents evidence that the time-stress-superposition principle, when used to shift short term compliance curves obtained on porous polyurethane is in excellent agreement with a long time control experiment whereas the time-temperature superposition leads to very serious overpredictions of long time compliance data.

It should be noted that no mechanical conditioning was applied, since conditioning should be used to isolate delayed elastic response, which is something that has never been proven for fiber reinforced composites (at least not to this author's knowledge).

Creep compliance data were merged into a free energy-based failure criterion and reasonable creep-rupture predictions were obtained. The creep response of a $[90/\pm45/90]_{2s}$ laminate was found to be an order of magnitude less than the creep response of $[90]_{8s}$ and $[\pm45]_{4s}$, while the modulus increased only by a factor of 1.35. A reasonable creep compliance versus time prediction was obtained by means of a nonlinear viscoelastic laminate analysis program. It is felt, however, that a damage model that operates on the minimechanics level of the problem would give a better agreement than the cumulative damage model which was actually used [9]. Promising ideas in this direction were published recently by Nuismer et al. [103]. They developed a realistic and simple scheme that accounts for influences on the constitutive behavior of given matrix dominated laminas through the lamina-laminate interaction after damage initiation. Another, more fundamental, approach that describes the influence of damage through a continuum vector field has been pursued, within a continuum thermodynamics framework by Talreja [104].

Based on this current research effort, the following recommendations for further study seem appropriate:

- The feasibility of mechanical conditioning, in case of composites, should be thoroughly checked.

- Test programs for boron-epoxy by Cole and Pipes [14] and for graphite polymide by Pindera and Herakovich [15] produced evidence that the octahedral shear stress is not a valid representation of stress mode interaction. Pindera and Herakovich showed that, in order to get access to the actual stress interaction, 3 off-axis tests were needed. An identification of the actual representation for stress mode interaction in case of graphite-epoxy T300/934 would at least give indications on its relative importance with respect to nonlinearities in transverse deformation and shear.

- The free energy based failure criterion together with the Tsai-Hill criterion, could be developed to predict delayed off-axis failure, based on transverse and shear compliances only.

- The necessity of transient temperature tests, in order to isolate the exact vertical shift, and thus obtain maximum predictive power, should be explored.

- Reversibility is always dependent on the choice of a well-defined easily reproducible reference state. In composites, however, initial stresses arise as a result of physio-chemical processes, technological operations and mechanical and thermal incompatibility. The natural state, i.e. a body free of stresses and strains, is nonexistent. The importance of an "eigenstress"-field on the viscoelastic behavior should be checked.

REFERENCES

1. Forsch, H. H. "An Introduction to Advanced Composite Materials", Short Course on Advanced Composite Materials at San Jose State University, Nov. 1982.

2. Ripley, E. L. In "Advanced Approaches to Fatigue Evaluation", Sixth ACAF Symposium, Miami Beach, Florida, May 13-14, 1971.

3. Adamson, M. J. "A Conceptual Model of the Thermal-Spike Mechanism in Graphite/Epoxy Laminates." Presented at ASTM Conference on Long Term Behavior of Composite Laminates. Williamsburg, March 1981.

4. Brinson, H. F., D. H. Morris, and Y. T. Yeow. "A New Experimental Method for the Accelerated Characterization of Composite Materials", Sixth International Conference on Experimental Stress Analysis, Munich, September 18-22, 1978.

5. Yeow, Y. T. "The Time-Temperature Behavior of Graphite Epoxy Laminates", Ph.D. Dissertation, VPI & SU, Blacksburg, VA, 1978.

6. Yeow, Y. T., and Brinson, H. F. "A Comparison of Simple Shear Characterization Methods for Composite Laminates", Composites, pp. 49-55, Jan. 1978.

7. Griffith, W. I. "The Accelerated Characterization of Viscoelastic Composite Materials", Ph.D. Dissertation, VPI & SU, Blacksburg, VA, 1980; also VPI Report VPI-E-80-15, with D. H. Morris and H. F. Brinson, 1980.

8. Brinson, H. F., D. H. Morris, W. I. Griffith, and D. A. Dillard. "The Viscoelastic Response of a Graphite/Epoxy Laminate", Proceedings of International Conference on Composite Structures, Paisley, Scotland, September 1981.

9. Dillard, D. A. "Creep and Creep Rupture of Laminated Graphite/Epoxy Composites", Ph.D. Dissertation, VPI & SU, Blacksburg, VA, 1981; also VPI Report VPI-E-81-3, with D. H. Morris and H. F. Brinson, 1981.

10. Dillard, D. A., Morris, D. H., and Brinson, H. F. "Predicting Viscoelastic Response and Delayed Failures in General Laminated Composites", ASTM Sixth Conference on Composite Materials: Testing and Design, Phoenix, AZ, May 1981.

11. Dillard, D. A., D. H. Morris, and H. F. Brinson. "Creep Rupture of General Laminates of Graphite/Epoxy Composites", Proceedings of 1981 Spring Meeting, SESA, Dearborn, June 1981.

12. Dillard, D. A., and H. F. Brinson. "Nonlinear Creep Compliance of General Laminated Graphite/Epoxy Composites", Proceedings SESA Spring Meeting, Honolulu, HI, May 1982.

13. Brinson, H. F. "Experimental Mechanics Applied to the Accelerated Characterization of Polymer Based Composite Materials", in New Physical Trends in Experimental Mechanics, (J. T. Pindera, ed.), CISM Courses and Lectures, No. 264, 1981.

14. Cole, B. and Pipes, R. "Filamentary Composite Laminates Subjected to Biaxial Stress Fields", AFFDL-TR-73-115, 1974.

15. Pindera, M. J., and Herakovich, C. T. "An endochronic theory for transversely isotropic fibrous composites", Interim report 25, the NASA Virginia Tech Composites Program, 1981.

16. Gradowczyk, M. H. "On the Accuracy of the Green-Rivlin Representation for Viscoelastic Materials", Intern. J. Solids and Struct., 5(8), 873-877, 1969.

17. Green, A. E., Rivlin, R. S. "The Mechanics of Nonlinear Materials with Memory", Arch. Ration. Mech. and Anal., 1(1), pp. 1-21, 1957.

18. Pipkin, A. C. and Rogers, T. G. "A Nonlinear Integral Representation for Viscoelastic Behavior", J. of the Mechanics and Physics of Solids, Vol. 16, p. 59, 1968.

19. Hiel, C. C. Unpublished research, Labo voor Toegepaste mechanika, VUB, 1978-81.

20. Kinder, D. F., and Sternstein, S. S. "A Path Dependent Approach to Nonlinear Viscoelastic Behavior", Trans. Soc. Rheol. 20(1), pp. 119-140, 1976.

21. Koltunov. "The selection of kernels for the solution of problems with account of relaxation and creep", Mekh polim., No. 4, 483, 1966.

22. Leaderman, H. "Elastic and Creep Properties of Filamentous Materials and Other High Polymers", The Textile Foundation, Washington, 1943.

23. Rabotnov, Yu. N. "Some Problems of Creep Theory", Vestnik Mosk. Univ. Matem., Mekh., No. 10, pp. 81-91 (in Russian), 1948.

24. Ferry, J. D. and Stratton, R. A. "The free volume interpretation of the dependence of viscosities and viscoelastic relaxation times on concentration, pressure, and tensile strain", Kollod. Z. 171, pp. 107-111, 1960.

25. Beuche, F. "Rate and Pressure Effects in Polymers and Other Glass Forming Substances", J. Chem. Phys., 36, 1962.

26. O'Reilly, J. M. "The Effect of Pressure on Glass Temperature and Dielectric Relaxation Time of Polyvinyl Acetate", J. Polymer Sci., 57, 1962.

27. Knauss, W. G. and Emri, I. J. "Nonlinear Viscoelasticity Based on Free Volume Consideration", Computers and Structures, 13, pp. 123-128, 1981.

28. Ferry, J. D. "Viscoelastic Properties of Polymers", J. Wiley & Sons, Inc., 1970.

29. Hutter, K. "The Foundations of Thermodynamics, Its Basic Postulates and Implications. A Review of Modern Thermodynamics", Acta Mechanica 27, pp. 1-54, 1977.

30. Coleman, B. D. and Noll, W. "The Thermodynamics of Elastic Materials with Heat Conduction and Viscosity", Arch. Rational. Mech. Anal., 13, pp. 167-178, 1963.

31. Onsager, L. "Reciprocal Relations in Irreversible Processes", I. Phys. Rev., 37(9), 1931.

32. Biot, M. A. "Theory of Stress-Strain Relations in Anisotropic Viscoelasticity and Relaxation Phenomena", J. Appl. Phys., 25(11), pp. 1385-91, 1954.

33. Ziegler, H. "An Attempt to Generalize Onsager's Principle, and Its Significance for Rheological Problems", Zeit. f. ang. Math. u. Phys., 9, pp. 748-63, 1958.

34. Schapery, R. A. "A Theory of Non-Linear Thermoviscoelasticity Based on Irreversible Thermodynamics", Proc. 5th U.S. National Congress of Applied Mechanics, ASME, pp. 511-530, 1966.

35. Valanis, K. C. "Thermodynamics of Large Viscoelastic Deformations", J. Math. Phys. 45, pp. 179-212, 1966.

36. Perzyna, P. "Thermodynamic Theory of Viscoplasticity" in Advances in Applied Mechanics, Vol. 11 (Yih, C. S., ed.), pp. 313-354, New York - London A.P., 1971.

37. Bach, L. "Nonlinear Mechanical Behavior of Wood in Longitudinal Tension", Ph.D. Dissertation, State Univ. College of Forestry at Syracuse Univ., 1965.

38. Landel, R. F. and Fedors, R. F. "Rupture of Amorphous Unfilled Polymers" in Fracture Processes in Polymeric Solids (B. Rosen, ed.), pp. 361-485, 1964.

39. Clauser, J. F. and Knauss, W. G. "On the Numerical Determination of Relaxation and Retardation Spectra for Linearly Viscoelastic Materials", Transactions of the Society of Rheology 12: 1, 143-153, 1968.

40. Schapery, R. A. "Application of Thermodynamics to Thermomechanical Fracture and Girefringent Phenomena in Viscoelastic Media", Journal of Applied Physics, Vol. 35, No. 5, pp. 1451-1465, 1964.

41. Schapery, R. A. "An Engineering Theory of Nonlinear Viscoelasticity with Applications", Int. J. Solids and Struct., Vol. 2, No. 3, 1966.

42. Schapery, R. A. "On a Thermodynamic Constitutive Theory and Its Application to Various Nonlinear Materials", Proc. IUTAM Symposium, East Kilbriole, June, 1968.

43. Schapery, R. A. "Further Development of a Thermodynamic Constitutive Theory and Stress Formulation", A&ES Report No. 69-2, Purdue University, February, 1969.

44. Schapery, R. A. "Viscoelastic Behavior and Analysis of Composite Materials", Chapter 4 in Composite Materials, Vol. 2, G. P. Sandeckyz, Ed. Academic Press, p. 85, 1974.

45. Truesdell, C. and Toupin, R. A. In S. Flugge, Encyclopedia of Physics (Springer-Verlag, Berlin), III/1, p. 700, 1960.

46. Biot, M. "Thermoelasticity and Irreversible Thermodynamics", J. Appl. Physics, Vol. 27, No. 3, March 1956.

47. Onsager, L. "Reciprocal Relations in Irreversible Processes", I Phys. Rev., 37, 4, 405-26, 1931; II. Phys. Rev., 38, 12, 2265-79, 1931.

48. Schapery, R. A. "A Theory of Crack Growth in Viscoelastic Media", Report MM 2764-73-1, March 1973.

49. Lou, Y, C., and Schapery, R. A. "Viscoelastic Characterization of a Nonlinear Fiber-Reinforced Plastic", Journal of Composite Materials, Vol. 5, 1971.

50. Bertolotti, A., Hiel, C. C. and Brinson, H. F. Unpublished research, Experimental Mechanics and Non-Metallic Characterization of Materials Lab, VPI & SU, 1982.

51. Schapery, R. A. and Martin, R. E. "On the Thermal Diffusivity of Filled Elastomers", Mech. Mat. Res. Center Rep. 72-2, Texas A & M Univ., 1972.

52. Weitsman, Y. "On the Thermoviscoelastic Characterization of Adhesives and Composites", Progress in Science and Engineering of Composites, T. Hayashi, K. Kawata and S. Umekawa, eds. ICCM-IV, Tokyo, 1982.

53. Schapery, R. A., Beckwith, S. W. and Conrad, N. "Studies on the Viscoelastic Behavior of Fiber-Reinforced Plastic", Technical Report AFML-TR-73-179, July 1973.

54. Halpin, J. C. and Tsai, S. W. "Effects of Environmental Factors on Composite Materials", AFML-TR-67-423, June 1969.

55. Reiner, M. and Weissenberg, K. "A Thermodynamic Theory of the Strength of Materials", Rheology Leaflet No. 10, pp. 12-20, 1939.

56. Naghdi, P. M. and Murch, S. A. "On the Mechanical Behavior of Viscoelastic-Plastic Solids", Journal of Applied Mechanics, Vol. 30, 1963, p. 327.

57. Crochet, M. J. "Symmetric Deformations of Viscoelastic Plastic Cylinders", Journal of Applied Mechanics, Vol. 33, 1966, pp. 327-334.

58. Hill, R. "Elastic Properties of Reinforced Solids: Some Theoretical principles", J. Mech. Phys. Solids, Vol. II, pp. 357-373, 1963.

59. von Mises, R. "Mechanik der plastischen formanderung von Bristallen", Richard von Mises, Selected Papers, Vol. 1, pp. 251-293.

60. Pagano, N. J. "Distortional Energy of Composite Materials", Journal of Composite Materials, Vol. 9, January 1975, p. 67.

61. Brüller, O. S., Potente, H. and Menges, G. "Energiebetrachtungen zum Kriechverhalten von polymeren", Rheol Acta, 16, 282-290, 1977.

62. Brüller, O. S. and Brand, N. "Voraussage der Dehnung von Kunstoffen bei Zyklischer Be-und Entlastung im linear-Viscoelastischen Bereich. Kunstoffe 67, 9, 1977.

63. Brüller, O. S. and Peutz, D. "Voraussage der Rißbildungs-grenze beim Kriechen von amorphen polymeren", Kautschuk + Gummi Kunstoffe, Heft 5, 30, Jahrg 1977 Seiten 295-299.

64. Brüller, O. S. "On the Damage Energy of Polymers in Creep", Polymer Engineering and Science, January 1978, Vol. 18, No. 1.

65. Brüller, O. S. and Schmidt, H. H. "On the Linear Viscoelastic Limit of Polymers--Exemplified on Poly(methyl Methacrylate)", Polymer Engineering and Science, September 1979, Vol. 19, No. 12.

66. Brüller, O. S. "Energy-Related Failure of Thermoplastics", Polymer Engineering and Science, Feb. 1981, Vol. 21, No. 3.

67. Brüller, O. S. and Reichelt, B. "Beschreibung des Nichtlinearen Verhaltens von Kunstoffen unter Belastung mit Konstanter Dehngeschwindigkeit", Rheol Acta 20, 240-246, 1981.

68. Brüller, O. S. "Das Versagen von Polymeren unter Belastung mit Konstanten Dehngeschwindigkeiten", Rheol Acta 20, 548-552, 1981.

69. Zhurkov, S. N. "Das problem der festigkeit fester korper", Zeitschrift fur physikalische Chemie (Leipzig), 213, p. 183, 1960.

70. Roylance, D. and Wang, S. S. "Penetration Mechanics of Textile Structures: Influence of Non-Linear Viscoelastic Relaxation", Polymer Engineering and Science, Mid-November, 1978, Vol. 18, No. 14.

71. Williams, M. L., De Vries, K. L. and Roylance, D. K. "An Experimental Investigation of Some Models of Polymer Fracture", Internat. Journal of Fracture Mechanics, 7 p. 197, 1974; AMR 25 (1972) Rev. 3703.

72. Williams, M. L. and De Vries, K. L. "An EPR Investigation of Newly Formed Fracture Surfaces", Sagamore Army Materials Research Conference Proceedings: Surfaces and Interfaces II, Syracuse University Press, 1968.

73. Regel, V. R., Savitskii, A. V., and Sanfirova, T. P. "Temperature-Forte Dependence of Lifetime of Composites", Polymer Mechanics, Vol. 12, No. 6, Nov-Dec (1976), 876-882.

74. McCullough, R. L. Concepts of Fiber Resin Composites. Dekker, N.Y., 1971.

75. Hancox, N. L. "The Effects of Flaws and Voids on the Shear Properties of Carbon Fiber Reinforced Plastics." J. Mater. Sci. 12, 884, 1977.

76. Yang, P., Carlsson, L. and Sternstein, S. S. "Dynamic-Mechanical Response of Graphite/Epoxy Composite Laminates and Neat Resin", paper submitted for publication in Polymer Composites, Sept. 15, 1981.

77. Petrie, S. E. B. "Enthalpy Relaxation in Organic Glasses." In Polymeric Materials Relationships Between Structure and Mechanical Behavior, edited by E. Baer and S. V. Radcliffe (American Society for Metals, Metal Park, Ohio), Chap. 2, 1975.

78. Petrie, S. E. B. "The Effect of Excess Thermodynamic Properties Versus Structure Formation on the Physical Properties of Glassy Polymers", Physical Structure of the Amorphous State, edited by G. Allen and S. E. B. Petrie. Marcel Dekker, Inc., 1977.

79. Keenan, J. D., Seferis, J. C. and Quinlivan, J. T. "Effect of Moisture and Stochiometry on the Dynamic Mechanical Properties of a High-Performance Structural Epoxy", Journal of Applied Polymer Science, Vol. 24, 2375-2387, 1979.

80. Morgan, R. J. and O'Neal, J. E. "Effect of Epoxy Monomer Crystallization and Cure Conditions on Physical Structure, Fracture Topography, and Mechanical Response of Polyamide Cured Bisphenol-A-Diglicidyl Ether Epoxies", J. Macromol. Sci. Phys. B15 (1) 139, 1978.

81. Bell, J. P. and McCarvill, W. T. "Surface Interaction Between Aluminum and Epoxy Resin", J. Appl. Polym. Sci. 18, 2243, 1974.

82. Deisai, R. and Whiteside, J. B. "Effect of Moisture on Epoxy Resins and Composites", Advanced Composite Materials - Environmental Effects, ASTM STP 658, J. R. Vinson, ed., pp. 2-20, 1978.

83. Hahn, H. T. and Tsai, S. W. "Nonlinear Elastic Behavior of Unidirectional Composite Laminae", J. Composite Materials, vol. 7, January 1973, p. 102.

84. Isaksson, A. "Creep Rates of Eccentrically Loaded Test Pieces." Transactions of the Royal Institute of Technology, No. 110, Stockholm, Sweden, 1957.

85. Sims, David F. "Viscoelastic Creep and Relaxation Behavior of Laminated Composite Plates." Dissertation, Southern Methodist University, May 21, 1972.

86. Aklonis, J. J. and Tobolsky, A. V. "Stress Relaxation and Creep Master Curves for Several Monodisperse Polystyrenes." J. Appl. Phys., 36, 3983, 1965.

87. Whitney, J. M. "Elastic Moduli of Unidirectional Composites with Anisotropic Filaments", J. Composite Materials, 1967.

88. Ishikawa, T., et al. "Elastic Moduli of Carbon-Epoxy Composites and Carbon Fibers", J. Composite Materials, Vol. 11, 1977, pp. 332-344.

89. Thompson, T. E. "Carbon Fiber Modification", NASA CR 166201, 1978.

90. Bulavs, F. Ya., Auzukalns, Ya. V. and Skudra, A. M. "Deformative Characteristics of Plastics Reinforced with High-Modulus Anisotropic Fibers", Mekhanika Polimerov, No. 4, 1972, pp. 631-639.

91. Hashin, Z. "Analysis of Properties of Fiber Composites with Anisotropic Constituents", Journal of Applied Mechanics, Vol. 46, 1979, pp. 543-550.

92. Gauchel, J. V. "The Viscoelastic Behavior of Epoxy-Glass Composites." Doctor of Science Thesis, Washington Univ., St. Louis, January 1972.

93. Chamis, C. C. and Sinclair, J. H. "10° Off-Axis Tensile Test for Intralaminar Shear Characterization of Fiber Composites", NASA TN D-8215, 1976.

94. Pagano, N. J. and Halpin, J. C. "Influence of End Constraint in the Testing of Anisotropic Bodies", J. Composite Materials, Vol. 2, No. 1, p. 18.

95. Foye, R. L. "Theoretical Post-Yielding Behavior of Composite Laminates. Part I - Inelastic Micromechanics", Journal of Composite Materials, Vol. 7, April 1973, p. 178.

96. McCrum, W. G., Read, B. E. and Williams, G. Anelastic and Dielectric Effects in Polymeric Solids. John Wiley & Sons, 1967.

97. Schapery, R. A. "Approximate Methods of Transform Inversion for Viscoelastic Stress Analysis", Proc. 4th U.S. Natl. Congr. Appl. Mech., ASME, 1962, p. 1075.

98. Martirosyan. "Transient Creep of Glass-Reinforced Plastics", Polymer Mechanics, 1, No. 2, 38, 1965.

99. Rosen, B. W. "A Single Procedure for Experimental Determination of the Longitudinal Shear Modulus of Unidirectional Composites", J. Comp. Mat. 6, 552, 1972.

100. Reifsnider, K. L. and Talug, A. "Characteristic Damage States in Composite Laminates", Proc. of Workshop on Composite Materials Research, Duke Univ., Oct. 17-18, 1978.

101. Vasil'ev, V. V., Dudchenko, A. A. and Elpat'evskii, A. N. "Analysis of the Tensile Deformation of Glass Reinforced Plastics", Mekhanika Polimerov 1, 144-147, 1970.

102. Urzhumtsev, Yu. S. "Prediction of the Deformation and Fracture of Polymeric Materials", Mekhanika Polimerov, No. 3, pp. 498-514, May-June 1972.

103. Nuismer, R. J. and Tan, S. C. "The Role of Matrix Cracking in the Continuum Constitutive Behavior of a Damaged Constitutive Ply", Proc. of the IUTAM Symposium on Mechanics of Composite Materials, Z. Hashin and C. T. Herakovich, eds.

104. Talreja, R. "A Continuum Mechanics Characterization of Damage in Composite Materials", VPI Internal Report, 1983.

105. Hoff, N. J., "Mechanics Applied to Creep Testing." The William M. Murray Lecture 1958, Society for Experimental Stress Analysis, Murray Lectures 1953-1967. B. E. Rossi, editor. 1968.

APPENDIX A

Cure Procedure for T300/934 Composite Panels

1. Vacuum bag - insert lay-up into autoclave at room temperature.
2. Apply full vacuum. (A minimum of 25 inches of Hg.) Hold for 30 minutes at room temperature.
3. Maintain full vacuum throughout entire cycle.
4. Raise temperature to 250 F (+5. - 10 F) at 2 ± 5 F per minute.

*5. Hold at 250 F (+5. - 10 F) for 15 ± 5 minutes, apply 100 psi (+5. - 0 psi).

*6. Hold at 250 F (+5. - 10 F) and 100 psi (+5. - 0 psi) for 45 ± 5 minutes.

*7. Raise temperature to 350 F (+10. - 0 F) at 2 ± 5 F per minute.

*8. Hold at 350 F (+10. - 0 F) for two hours ± 15 minutes.

*9. Cool under pressure and vacuum to below 175 F.

---

*Pressure was 85 psi.

Curing Procedure for Resin Panel #1

1. Resin heated until fluid and poured into heated mold.
2. Mold vacuum bagged and inserted into autoclave.
3. Full vacuum applied and held 30 min.
4. Raise temperature to 250 F (+5. -10 F) at 2 ± 5 F per minute.
5. Hold at 250 F (+5 -10 F) for 15 ± 5 minutes. Apply 100 psi (+5 - 0)
6. Hold at 250 F (+5 -10 F) and 100 psi (+5 - 0 psi) for 45 ± 5 min.
7. Raise temperatuer to 350 F (+10 -0 F) at 2 ± 5 F per minute.
8. Hold at 350 F (+10 -0 F) for two hours ± 15 minutes.
9. Cool under pressure (85 psi) and vacuum to below 175 F.

Fabrication Procedure for Resin Panel #2

1. Mold heated to 200 F.
2. Resin heated to 160 F and degassed in bell jar for 5 minutes.
3. Degassed resin poured into one corner of tilted and heated mold. Air gun used to keep mold warm.
4. Resin then cured in oven with same schedule as prepreg tape, i.e. steps 4-9 above.

The Curing Procedure for Resin Panel #3

934 Resin Cure Procedure - Solution Form

1. Break off chunks of solid (cold) resin.
2. Place in beaker of acetone or methyl ethyl keytone.
3. Slowly warm and stir solution up to 80°F (26°C) and until all resin is dissolved to taffy consistency.
4. Pour into teflon coated bread pan and place in vacuum oven. Heat to 150°F (66°C) under full vacuum. Observe until bubbles cease (about 2 hours).
5. Remove from vacuum oven and put in 212°F (100°C) oven over night (roughly 3:00 p.m. - 7:00 a.m.).
6. Remove from oven in morning.
7. Put in oven at 325°F - 350°F (163°C - 177°C) for two (2) hours.
8. Turn off oven and allow to cool gradually.

APPENDIX B

$$G = F - Q_m\, q_m \tag{B.1}$$

with

$$F = F(q_m, q_r, T)$$

and

$$Q_m = \frac{\partial F}{\partial q_m}$$

Thus

$$G = G(Q_m, q_r, T) \tag{B.2}$$

$$dG = \frac{\partial F}{\partial T}\, dT + \frac{\partial F}{\partial q_r}\, dq_r + \frac{\partial F}{\partial q_m}\, dq_m - Q_m\, dq_m - q_m\, dQ_m \tag{B.3}$$

$$dG = \frac{\partial F}{\partial T}\, dT + \frac{\partial F}{\partial q_r}\, dq_r + (-q_m)\, dQ_m \tag{B.4}$$

$$dG = \frac{\partial G}{\partial T}\, dT + \frac{\partial G}{\partial q_r} + \frac{\partial G}{\partial Q_m}\, dQ_m \tag{B.5}$$

(B.4) and (B.5) $\rightarrow$

$$\frac{\partial G}{\partial q_r} = \frac{\partial F}{\partial q_r} \tag{B.6}$$

$$\frac{\partial G}{\partial T} = \frac{\partial F}{\partial T} \tag{B.7}$$

$$q_m = -\frac{\partial G}{\partial Q_m} \tag{B.8}$$

$$= -\rho\, \frac{\partial G}{\partial Q_m}$$

APPENDIX C

INFLUENCE OF EXCENTRIC LOAD APPLICATION [105]

Suppose that the load F is applied with a small excentricity e. This causes not only the homogeneous stress state which we intended to produce, but also the bending moment F•e as is shown in Fig. C.1.

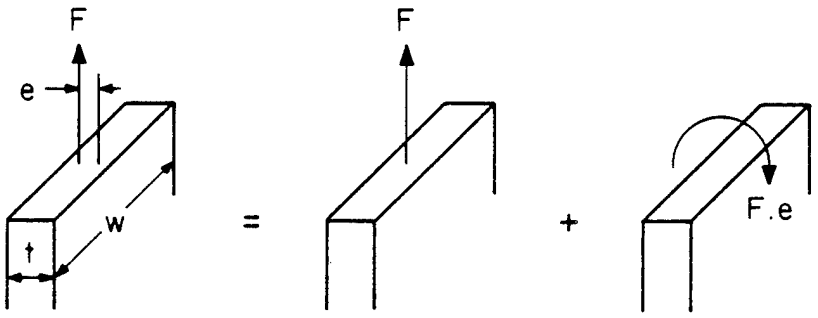

Fig. C.1 Superposition of Normal Stress and Bending Due to Excentric Load Application

The stress, at the gage location σ_{GL} can then be written as,

$$\sigma_{GL} = \frac{F}{w \cdot t} + \frac{F \cdot e}{\frac{w \cdot t^2}{6}}$$

$$= \sigma_u \left[1 + 6 \cdot \frac{e}{t}\right]$$

with $\sigma_u = \frac{F}{wt}$, the uniform stress, which we intended to apply.

1. Report No.	2. Government Accession No.	3. Recipient's Catalog No.
NASA CR-3772		

4. Title and Subtitle	5. Report Date
The Nonlinear Viscoelastic Response of Resin Matrix Composite Laminates	July 1984
	6. Performing Organization Code
7. Author(s)	8. Performing Organization Report No.
C. Hiel, A.H. Cardon, and H.F. Brinson	VPI-E-83-6
	10. Work Unit No. T-4241
9. Performing Organization Name and Address	11. Contract or Grant No.
Department of Engineering Science and Mechanics Virginia Polytechnic Institute and State University Blacksburg, VA 24061	NCC2-71
	13. Type of Report and Period Covered
12. Sponsoring Agency Name and Address	Contractor Report
National Aeronautics and Space Administration Washington, D.C. 20546	14. Sponsoring Agency Code 505-33-21

15. Supplementary Notes

Point of Contact: Howard G. Nelson, MS: 230-4, Ames Research Center, Moffett Field, CA 94035 415-965-6137 or FTS-448-6137

16. Abstract

A review of possible treatments of nonlinear viscoelastic behavior of materials is presented. A thermodynamic based approach, developed by Schapery, is discussed in detail and is used as the means to interpret the nonlinear viscoelastic response of a graphite epoxy laminate, T300/934.

Test data to verify the analysis for Fiberite 934 neat resin as well as transverse and shear properties of the unidirectional T300/934 composited are presented.

Long time creep characteristics as a function of stress level and temperature are generated. Favorable comparisons between the traditional, graphical and the current analytical approaches are shown.

A free energy based rupture criterion is proposed as a way to estimate the life that remains in a structure at any time.

17. Key Words (Suggested by Author(s))	18. Distribution Statement
Time-temperature-stress superposition, Creep, Relaxation, Accelerated testing, Life prediction.	Unclassified - unlimited STAR Category - 24

19. Security Classif. (of this report)	20. Security Classif. (of this page)	21. No. of Pages	22. Price*
UNCLASSIFIED	UNCLASSIFIED	152	A08

*For sale by the National Technical Information Service, Springfield, Virginia 22161 NASA-Langley, 1984